

Technical Report

TR-13-04

The potential for cold climate conditions and permafrost in Forsmark in the next 60,000 years

Jenny Brandefelt, Jens-Ove Näslund
Svensk Kärnbränslehantering AB

Qiong Zhang
Department of Meteorology, Stockholm University

Juha Hartikainen
School of Engineering, Aalto University

May 2013

Svensk Kärnbränslehantering AB
Swedish Nuclear Fuel
and Waste Management Co
Box 250, SE-101 24 Stockholm
Phone +46 8 459 84 00



ISSN 1404-0344

SKB TR-13-04

ID 1378383

The potential for cold climate conditions and permafrost in Forsmark in the next 60,000 years

Jenny Brandefelt, Jens-Ove Näslund
Svensk Kärnbränslehantering AB

Qiong Zhang
Department of Meteorology, Stockholm University

Juha Hartikainen
School of Engineering, Aalto University

May 2013

Preface

This document contains information on possible future timings of the occurrence of permafrost in the Forsmark region. The information is of relevance for the analysis of long-term repository safety in e.g. SKB's safety assessment SR-PSU. In particular, the information will be used in the report "Climate and climate-related issues for the safety assessment SR-PSU" and in the "SR-PSU Main report".

Stockholm, May 2013

Jens-Ove Näslund

Person in charge of the SKB climate programme

Summary

This report presents results of a study devoted to extend the current knowledge of the climate in Sweden in the next ~60,000 years (60 ka). Specifically, the potential of cold climate and permafrost development in south-central Sweden, and in the Forsmark region, over this time horizon was investigated.

The climate system is an interactive system consisting of five major components: the atmosphere, the hydrosphere, the cryosphere, the land surface and the biosphere, forced or influenced by various external forcing mechanisms, of which the most important is the Sun. Also the direct effect of human activities on the climate system is considered an external forcing. The latitudinal and seasonal distribution of incoming solar radiation (insolation) varies on millennial time scales due to variations in the Earth's orbit and axial tilt. These variations, together with variations in the atmospheric CO₂ concentration, are viewed as two main factors in determining the climate variation between interglacial (warmer) and glacial (colder) climates.

Summer insolation at high northern latitudes is at a minimum 17 ka and 54 ka after present (AP). These periods were therefore identified as potential future periods of cold climate conditions in high northern latitudes in general and in south-central Sweden in particular. Due to human emissions of carbon to the atmosphere, the atmospheric CO₂ concentration is currently 392 ppmv (2011 AD), a substantial increase as compared to the range of atmospheric CO₂ concentrations of 180–295 ppmv found in ice cores for the last 400 ka. The future atmospheric CO₂ concentration is determined by i) future human carbon emissions to the atmosphere, ii) possible emissions due to feedbacks in the climate system, and iii) by the global carbon cycle.

To investigate the potential of cold climate conditions in south-central Sweden in the next 60 ka the future air temperature in Forsmark was estimated based on simulations with an Earth system model of intermediate complexity (EMIC) and a state-of-the-art Earth System Model (ESM). To span the possible combinations of future orbital variations and possible future atmospheric CO₂ concentrations, three sets of simulations were performed. The first set consists of a suite of EMIC simulations performed for the future periods of minimum summer insolation at high northern latitudes (17 ka and 54 ka AP) with the atmospheric CO₂ concentration varying in the range 180–400 ppmv. These are equilibrium simulations with constant forcing conditions. The second set consists of two EMIC simulations with constant atmospheric CO₂ concentration of 200 or 400 ppmv respectively and insolation variations for the full period from the present to 61 ka AP. The third set of simulations consists of two ESM equilibrium simulations with insolation for 17ka and 54ka AP and atmospheric CO₂ concentration set to 200 ppmv and 180 ppmv respectively. This set was used, in combination with published results from climate model inter-comparisons, to estimate the uncertainty in the EMIC results due to the simplified model formulation.

The annual average bias-corrected air temperature at 2 m height (T_{2m}) at Forsmark (with respect to observations) varies from 0.96°C to 5.3°C (1.6°C to 5.7°C) in the EMIC simulations for orbital year 17 ka AP (54 ka AP) when the atmospheric CO₂ concentration is varied from 180 ppmv to 400 ppmv. The insolation difference between orbital year 17 ka AP and 54 ka AP results in a difference in the annual average Forsmark T_{2m} of c. 0.3°C–1.2°C with a tendency towards larger differences for lower atmospheric CO₂ concentration. These results indicate that the future atmospheric CO₂ concentration is more important than insolation variations for future climate in Forsmark in the next 60 ka.

The ESM simulations reveal significant inter-model differences in the simulated climate, specifically in the regional climate, in line with earlier inter-comparison studies. Annual average Forsmark T_{2m} is 5.9°C and 7.7°C colder than the pre-industrial in the ESM simulations for 17 ka AP and 54 ka AP respectively. These values are 3.9°C and 4.4°C, respectively, lower than in the corresponding EMIC simulations.

The climate models used in the present study do not include glacier and ice sheet dynamics, which presents a potential warm bias in the simulated climate. Comparison of the results presented here to earlier studies of future climate evolution with EMICs that include ice sheet dynamics indicate a potential bias on the order of 5°C in the results presented here. The uncertainties in the simulated Forsmark T_{2m} due to future glacier and ice sheet growth, inter-model differences, internal variability and future greenhouse gas concentrations are estimated. The collective uncertainty is taken to be larger for orbital year 54ka AP, reflecting two factors. Firstly, inter-model differences generally increase when the difference between the simulated climate state and the present climate increases. Secondly, several earlier studies indicate that ice sheet growth may occur in 40 ka to 50 ka AP if the atmospheric CO_2 concentration reaches pre-industrial or lower values.

To analyse the potential of permafrost development in the Forsmark region in south-central Sweden, the bias-corrected T_{2m} from the EMIC simulation with the coldest climate was used as input to a site-specific 2D permafrost model for Forsmark. In accordance with previous permafrost simulations for Forsmark, the permafrost model is set up under assumption of dry climate conditions and dry surface conditions to promote permafrost at the site. A number of sensitivity simulations are further performed to investigate the potential of frozen ground when the uncertainties in simulated Forsmark T_{2m} are taken into account.

Under the assumptions made in this study, it is concluded that frozen ground (ground temperature of 0°C) cannot be excluded at c. 60 m and c. 110 m depth at 17 ka AP or at 54 ka AP. Furthermore, it is concluded that it is very unlikely to get ground temperature of -3°C or less, relevant for analysis of freezing of concrete repository structures, at c. 60 m and c. 110 m depth at 17 ka AP, but that this possibility cannot be excluded at 54 ka AP. The main reason for the different conclusions for the two time periods is the expected slow decrease in atmospheric CO_2 concentration.

Contents

1	Introduction	9
1.1	Background	9
1.1.1	Earth's climate evolution until 2100 AD	10
1.1.2	Earth's climate evolution until 10 ka AP	10
1.1.3	Earth's climate evolution on a 100 ka timescale	11
1.2	Objectives	16
2	Methodology	17
2.1	Selection of time periods and forcing conditions	17
2.2	Earth system modelling	17
2.2.1	The Earth system model of intermediate complexity LOVECLIM	17
2.2.2	The climate system model CCSM4	18
2.3	Forcing conditions for earth system modelling	19
2.3.1	Orbital solar forcing	19
2.3.2	Greenhouse gases	20
2.3.3	Aerosols	22
2.3.4	Ice sheets and glaciers	22
2.3.5	Sea level, coastlines, topography and bathymetry	22
2.3.6	Vegetation	22
2.4	Earth system model simulations	23
2.4.1	Pre-industrial control climate	23
2.4.2	Future climate	24
2.5	Permafrost modelling	26
2.5.1	Forcing conditions and input data for permafrost modelling	27
2.5.2	Sensitivity to model formulation improvement	28
2.6	Observations for climate model evaluation	28
2.7	Spatial interpolation	29
2.8	Bias correction	30
2.8.1	LOVECLIM bias for Uppsala	30
2.8.2	CCSM4 bias for Uppsala	33
3	Results and discussion	35
3.1	Equilibrium simulations for 17 ka AP and 54 ka AP	35
3.1.1	Simulated global climate	35
3.1.2	Simulated Forsmark climate	45
3.1.3	Sensitivity to atmospheric CH ₄ concentration	50
3.2	Transient EMIC simulations	51
3.2.1	Simulated global climate	51
3.2.2	Simulated Forsmark climate	53
3.3	Uncertainty in climate model results	54
3.4	Permafrost modelling	56
3.4.1	Initialization and initial state	57
3.4.2	The 54 ka AP period	57
3.4.3	Sensitivity to Forsmark T _{2m}	57
3.4.4	Sensitivity to model formulation	61
4	Potential for permafrost – synthesis	63
5	Summary and conclusions	65
	Acknowledgements	67
	References	69
Appendix A	Deliverables and data format for input- and output data stored in data base at SKB	73
Appendix B	Glossary	75

1 Introduction

1.1 Background

Swedish Nuclear Fuel and Waste Management Company (SKB) is responsible for the management of spent nuclear fuel and radioactive waste generated within the Swedish nuclear power program. SKB plan to submit an application to extend the existing geological repository for low- and intermediate-level radioactive waste in Forsmark (Figure 1-1). An important document for the application is the assessment of long-term repository safety. The geological repository shall keep radiotoxic material separated from man and environment for very long periods of time, up to 100,000 years (100 ka). The repository safety performance is dependent on e.g. the risk for freezing and intrusion of saline water – factors that are controlled by the presence of ice sheets, permafrost and changes in sea level/shoreline elevation. Thus to assess repository safety, knowledge of the future evolution of Earth's climate is of primary importance. This study aims at giving a review of the current knowledge about the future evolution of Earth's climate on this time scale and to contribute to the knowledge based on new simulations with an Earth system model of intermediate complexity (EMIC) and an Earth system model (ESM). Specifically, the study aims at investigating the potential for a cold climate and permafrost development in south-central Sweden during the next 60 ka.

The main processes affecting repository safety functions in a cold and relatively dry climate is the aggradation and degradation of permafrost and the related maximum depth of perennially frozen ground, as well as the associated changes in ground water flow. The evolution of permafrost is a complex process affected by many factors such as presence of water bodies, snow cover, vegetation, topography, thermal and physical properties of soil, bedrock and groundwater. However the main factor affecting permafrost development is the temperature climate (e.g. Hartikainen et al. 2010). In the present study a 2D permafrost model has been employed to assess the potential for permafrost development in south-central Sweden given by the climate simulated with the climate models.

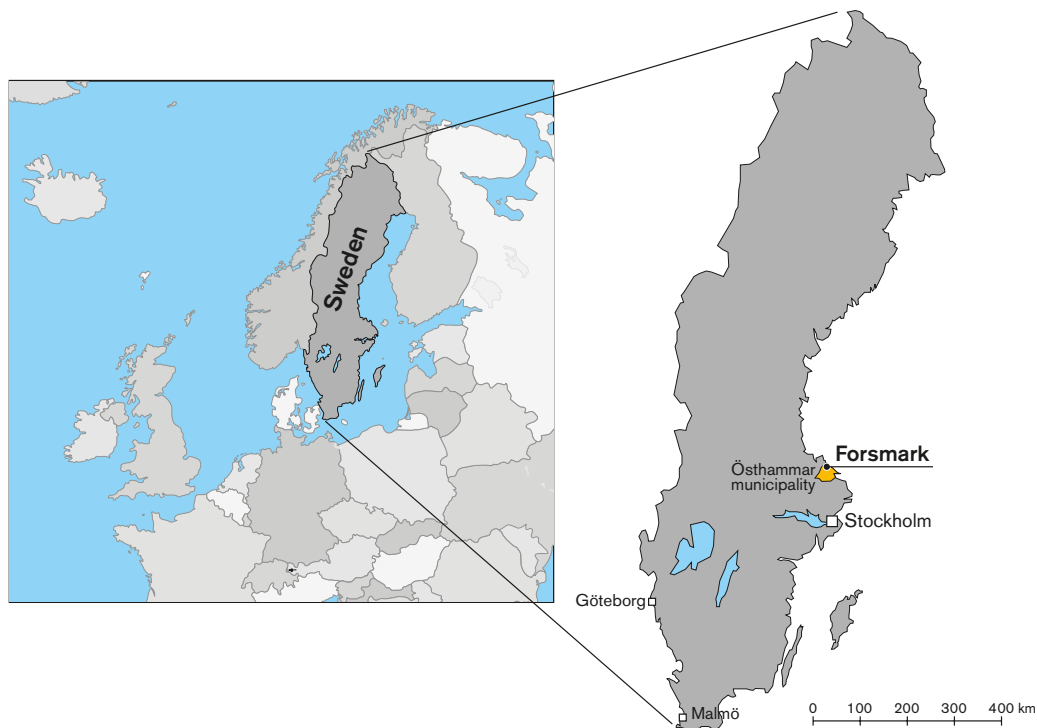


Figure 1-1. Geographical location of Forsmark.

A review of the current knowledge on Earth's future climate evolution in the coming ~100 ka is given below. Projections of future climate evolution are obtained using models of varying complexity ranging from Earth System Models (ESMs), Atmosphere-Ocean General Circulation Models (AOGCMs), Earth System Models of Intermediate Complexity (EMICs) to Simple Climate Models (SCMs). In general terms, the range from ESMs to SCMs involves decreasing complexity of the model physics and dynamics of the different components of the climate system as compared to the real world, as well as decreasing spatial and temporal model resolution. The computational cost of state-of-the-art ESMs and AOGCMs prevent use of these models for modelling of more than a few centuries-millennia. The review of the future projected climate evolution is divided into different timescales based on the complexity of the models used.

The timing of the next glacial inception and subsequent maximum glaciation has been investigated using a variety of models. These studies are of relevance to the present study, since glaciation in this region is likely to be preceded by a cold climate with potential for permafrost development. The review formed basis for the design of the present modelling study.

1.1.1 Earth's climate evolution until 2100 AD

Global and annual average near-surface air temperature is expected to increase in the current century due to increasing atmospheric greenhouse gas concentrations (Meehl et al. 2007). Future climate change on this timescale is assessed using a hierarchy of models, ranging from AOGCMs and EMICs to SCMs. These models are forced with atmospheric concentrations of greenhouse gases and other constituents derived from various emissions scenarios ranging from non-mitigation scenarios to idealised long-term scenarios (IPCC 2000). The multi-model global annual average near-surface air temperature (SAT) warming for 2090 to 2099 AD relative to 1980 to 1999 AD for a low, medium and high CO₂ emission scenario ranges from 1.8°C to 3.4°C (Meehl et al. 2007). The geographical patterns of projected SAT warming show the greatest temperature increases over land and at high northern latitudes and less warming over the Southern Ocean and the North Atlantic Ocean. The multi-model annual average SAT warming for 2090 to 2099 relative to 1980 to 1999 in south-central Sweden ranges from 2.5°C to 3.5°C for the different SRES scenarios (Meehl et al. 2007).

1.1.2 Earth's climate evolution until 10 ka AP

Recent studies with coupled climate-carbon cycle models have shown that the century-scale global mean temperature response to CO₂ emissions is independent of the emissions pathway (Eby et al. 2009, Zickfeld et al. 2009). Further, it has been demonstrated that global mean temperature remains approximately constant for several centuries after cessation of CO₂ emissions (e.g. Solomon et al. 2009). These results can be generalized to show that the instantaneous global temperature response is proportional to cumulative carbon emissions (Matthews et al. 2009).

To estimate the future climate evolution, the atmospheric concentration of CO₂ must be determined. Archer et al. (2009) assessed the range of possibilities for the long-term fate of fossil CO₂ in the atmosphere, ocean, and terrestrial biosphere by means of a model inter-comparison project including nine models. CO₂ is released instantaneously in a climate with pre-industrial atmospheric concentrations in a pulse of 1,000 and 5,000 Pg (10¹⁵ g) carbon respectively and the global carbon cycle evolution 10 ka into the future was simulated. For comparison, humankind has already released ~300 Pg carbon and the entire reservoir of fossil fuel, predominantly coal, totals ~5,000 Pg carbon. After 10 ka, 8–19% (10–33%) of the emissions remained in the atmosphere following the 1,000 Pg (5,000 Pg) carbon initial pulse.

The NSF Committee on Stabilization Targets for Atmospheric Greenhouse Gas Concentrations (2011) discuss the evolution of Earth's climate beyond the next few centuries. They combine results from Archer et al. (2009) with IPCC (2007) derived climate sensitivities to determine a range of very long-term warming. They find that after 10 ka, 0.5–1.3°C (2.5–7.5°C) of warming remained following a 1,000 Pg (5,000 Pg) carbon initial pulse. They conclude that in all cases, the warming decays very little between 5 ka and 10 ka, and in fact the warming remaining after 10 ka would take 100 ka or more to recover under the slow action of silicate weathering processes, even in the absence of destabilizing long-term Earth System feedbacks (such as release of methane by destabilization of clathrates stored in permafrost or in sea-floor sediments).

1.1.3 Earth's climate evolution on a 100 ka timescale

Geological archives show that Earth's climate has evolved from warm (interglacial) to cold (glacial) periods characterized by extensive ice sheets in the high northern latitudes and permafrost conditions in ice-free high-latitude regions. For the past ~800 ka interglacials have occurred every 80 to 120 ka. To illustrate these variations, a proxy for global ice volume and atmospheric CO₂ concentration, as measured in Antarctic ice cores, are displayed in Figure 1-2. The ~100 ka timescale in the glacial/interglacial cycles is commonly attributed to control by variations in the Earth's orbit that influence the incoming solar radiation at northern high latitudes ("Milankovitch forcing"). The variations in the Earth's orbit include variations in the eccentricity of the Earth's orbit, the obliquity (i.e. the tilt of the Earth's axis of rotation), and in the precession of the equinoxes, with dominant frequencies at about one cycle per 100 ka (eccentricity), 41 ka (obliquity) and 21 ka (precession). The most obvious similarity to the ~100 ka timescale of the glacial/interglacial cycles is that of eccentricity. The variation in incoming solar radiation (insolation) associated with the eccentricity cycle is however far too small to explain the large amplitude cycle in ice sheet volume. It has been suggested that the insolation variation associated with eccentricity can be amplified by feedbacks in the climate system such as ice sheets (Imbrie and Imbrie 1980), the ocean circulation (Imbrie et al. 1993) and the carbon cycle (Shackleton 2000). More recently, Huybers and Wunsch (2005) suggested that the timing of deglaciation is determined by the obliquity cycle such that the climate state skips one or two obliquity beats before deglaciating, thus giving durations of either ~80 or ~120 ka. This suggestion fits better with the data of e.g. Winograd et al. (1992), who find that the duration of the most recent four glacial cycles recorded in the vein calcite of Devils Hole, Nevada, were approximately 79 ka, 85 ka, 113 ka and 128 ka.

Support for the suggestion that deglaciation occurs every two or three obliquity cycles is given by Drysdale et al. (2009). They present a new speleothem-based North Atlantic marine chronology that shows that the penultimate glacial termination (Termination II) commenced 141 ka ± 2.5 ka before the present, too early to be explained by Northern Hemisphere summer insolation but consistent with changes in Earth's obliquity. They show that glacial terminations I (~18 to 9 ka ago) and II are separated by three obliquity cycles and that they started at near-identical obliquity phases.

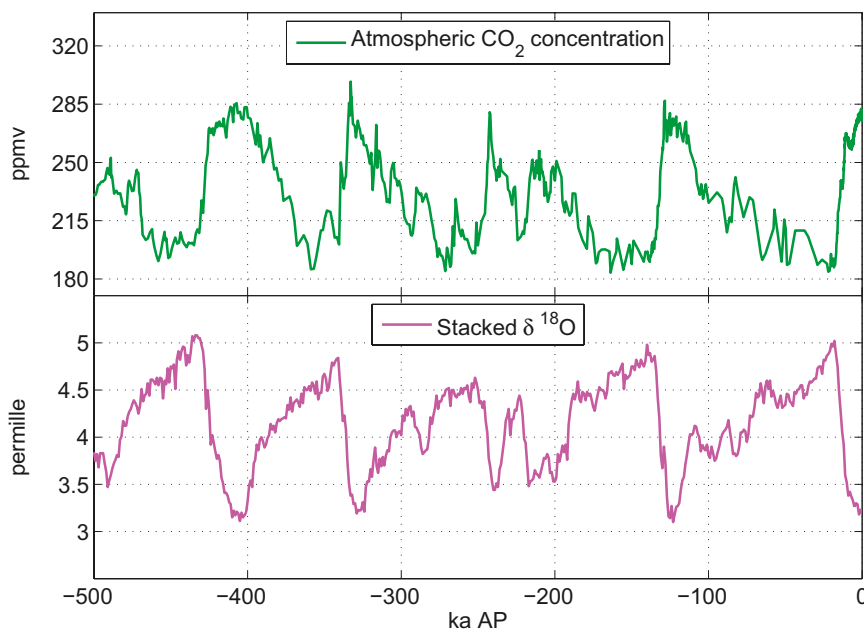


Figure 1-2. CO₂ composite record (ppmv; upper panel) (Lüthi et al. 2008). High values of CO₂ correspond to a warmer climate (interglacial state). The LR04 stack (Lisiecki and Raymo 2005) of 57 benthic $\delta^{18}\text{O}$ records (permille; lower panel); the $\delta^{18}\text{O}$ is a proxy for the global volume of ice. High values of $\delta^{18}\text{O}$ correspond to a colder climate (glacial state).

A number of modelling studies have been performed to enhance understanding of the physical mechanisms associated with deglaciation and glaciation. Studies with so called EMIC models that include simplified descriptions of the main components of the climate system, i.e. atmosphere, ocean, sea ice, ice sheets and sometimes vegetation indicate that the combination of seasonal and latitudinal variations in insolation, the “Milankovitch forcing”, and glacial-interglacial atmospheric CO₂ variations give a reasonable agreement between simulated and reconstructed glacial cycles (e.g. Ganopolski et al. 2010, Loutre and Berger 2000). For reference, June insolation at 60°N and obliquity is displayed for the period 130 ka BP to 100 ka AP in Figure 1-3. The variation in atmospheric CO₂ concentration, as recorded in ice cores, is also displayed for the period 130 ka BP to the present. The present day atmospheric CO₂ concentration of 392 ppmv (2011 AD) is included in this curve.

Based on different modelling studies, several suggestions regarding the climate dynamics of glacial inception, i.e. the transition from an interglacial to a glacial period, have been made. These have pointed towards the importance of including amplifying feedbacks due to vegetation, the oceans, sea ice, and the polar surface energy balance. Mysak (2008) gives a review of modelling studies of glacial inception.

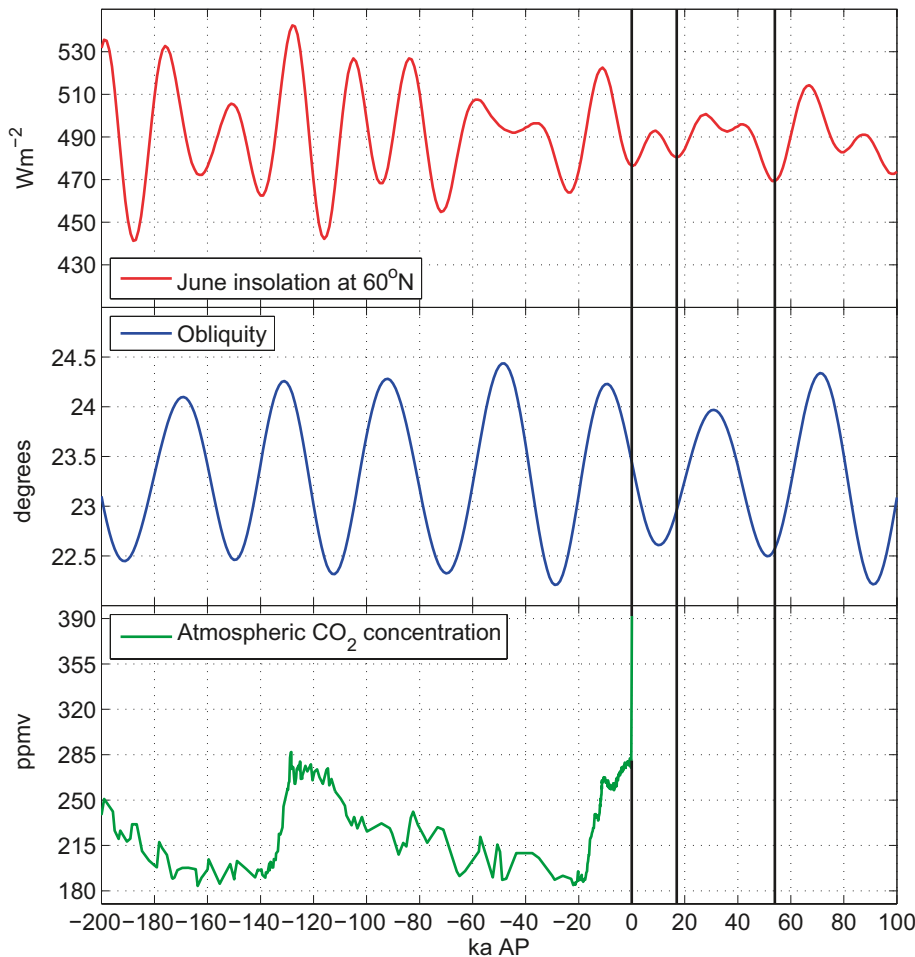


Figure 1-3. Insolation at 60°N in June (Wm⁻²; upper panel) and obliquity (degrees; middle panel) for the period 130 ka BP to 100 ka AP (Berger 1978). Data downloaded from <ftp://ftp.ncdc.noaa.gov/>. Atmospheric CO₂ concentration as recorded in Antarctic ice cores (ppmv; bottom panel) (Lüthi et al. 2008), the present day (2011 AD) concentration is also included. Vertical black lines are drawn at the present (0 ka) and for the two future periods of minimum June insolation at 60°N at 17 ka AP and 54 ka AP.

The last glacial cycle

Several different EMICs have been employed to simulate the last glacial cycle (last ~120 ka) (e.g. Berger and Loutre 2010, Ganopolski et al. 2010). Forced by known variations in insolation due to variations in the Earth's orbital parameters and greenhouse gas concentrations from ice core measurements, these models simulate the climate evolution of the last glacial cycle, as recorded in natural archives, reasonably well.

Recently, Smith and Gregory (2012) performed a number of transient climate simulations of the last 120 ka using a low-resolution version of a comprehensive AOGCM. The rate of change of the forcing conditions (atmospheric greenhouse gas concentrations, seasonal and latitudinal varying insolation, ice sheet topography) was increased by a factor of 10 in their experiments. Smith and Gregory (2012) found that the simulated long-term temperature changes on Antarctica were in good agreement with reconstructions derived from ice-core data, as is variability on timescales longer than 10 ka. Last Glacial Maximum (LGM) cooling on Greenland is reasonably well simulated, although their simulations, which lack ice sheet meltwater forcing, do not reproduce the abrupt, millennial scale climate shifts seen in Northern Hemisphere climate proxies or their slower Southern Hemisphere counterparts.

As computing power increases, several studies with comprehensive AOGCMs have been performed to improve the understanding of glacial inception (e.g. Vettoretti and Peltier 2004 2011). In a recent study, Jochum et al. (2012) compare the difference in snow accumulation associated with the difference in orbital forcing between the present day and 115 ka BP in two simulations with a comprehensive AOGCM. They conclude that, contrary to studies with older versions of the same and other AOGCMs, the difference in orbital forcing is sufficient to produce snow accumulation comparable to that inferred from reconstructions for the last glacial inception.

The coming 100–200 ka

For the coming ~100–200 ka, climate models are forced with the known future variations in insolation due to variations in the Earth's orbital parameters (Berger and Loutre 1991) and different hypothesized atmospheric CO₂ concentrations. For all models, the event of glaciation is crucially dependent on the atmospheric level of CO₂. In the following, published studies of Earth's climate in the coming 100–200 ka are briefly described, with a focus on the timing of glacial inception and maximum Northern Hemisphere ice volume. These studies are of relevance to the present study of the potential for permafrost in south-central Sweden, since glaciation in this region is likely to be preceded by a cold climate with potential for permafrost development. The results are summarized in Table 1-1 and Figure 1-4.

Loutre and Berger (2000) simulated the coming 130 ka with the Louvain-la-Neuve two-dimensional Northern Hemisphere climate model (LLN 2-D NH) forced by future variations in orbital parameters and a number of different constant atmospheric CO₂ concentrations. They found that, in their model, glaciation occurs 50 ka into the future in simulations with CO₂ concentration lower than 280 ppmv, whereas for CO₂ concentrations above this value glaciation is postponed beyond 50 ka into the future. For CO₂ concentrations lower than 220 ppmv glaciation inception was found to be imminent.

Berger and Loutre (2002) simulated the period 200 ka BP to 130 ka AP with the LLN 2-D NH model forced by future variations in orbital parameters and three different scenarios for future atmospheric CO₂ concentration; constant concentration of 210 ppmv, constant concentration of 280 ppmv, and an anthropogenic scenario with the concentration reaching 750 ppmv in 200 years from now and decreasing to 280 ppmv in 1,000 years from now. In accordance with Loutre and Berger (2000), they found that glacial inception is imminent in the 210 ppmv scenario, whereas glacial inception occurs after ~50 ka in the 280 ppmv and the anthropogenic scenarios.

The BIOCLIM project (Texier et al. 2003) simulated the coming 200 ka with two EMICs, MoBidiC (an improved version of the LLN model) and CLIMBER-GREMLINS, forced by variations in orbital parameters and prescribed time-varying atmospheric CO₂. They found that the two EMICs responded quite differently to the imposed forcing conditions. MoBidiC produced ice sheets over North America from the start of the simulation when CO₂ was kept constant at 280 ppmv, whereas CLIMBER-GREMLINS produced no glaciation until after 50 ka AP. Under this scenario none of the models produced ice sheets over Fennoscandia during the next 100 ka.

Table 1-1. Review of the timing of first Northern Hemisphere (NH) glacial inception and maximum NH ice volume. Note that glacial inception in this context indicates growth of NH ice to substantially larger volume than at present, which can result in periglacial or glacial climate conditions in south-central Sweden depending on the extent of a Fennoscandian ice sheet.

Authors, model	Atmospheric CO ₂ concentration (ppmv)	Total cumulative emissions (Pg C)	Timing of first NH glacial inception (ka AP)	Timing of maximum NH ice volume (ka AP)
Loutre and Berger (2000)	210		0	~61
LLN 2-D NH	220		0	~22, ~62
	230		~40	
	240–270		~50	~60
	280, 290		>130	
Berger and Loutre (2002)	210		0	~60, ~100
LLN 2-D NH	280		~50	~60, ~100
	750→280		~50	~60, ~100
Texier et al. (2003) MoBidiC	280		0	~120
Texier et al. (2003) CLIMBER-GREMLINS	280		~50	~200
Archer and Ganopolski (2005) CLIMBER-2	280		~50	
		300	~50	
		1,000	~130	
		5,000	>500	
Cochelin et al. (2006)	≤270		0	~100
McGill Paleoclimate Model	280, 290		50	>100
	≥300		>100	
Crucifix and Rougier (2009)	Naturally varying		40	60
Pimenoff et al. (2011) CLIMBER-2	280		0	~20, ~60
	400		~50	~60

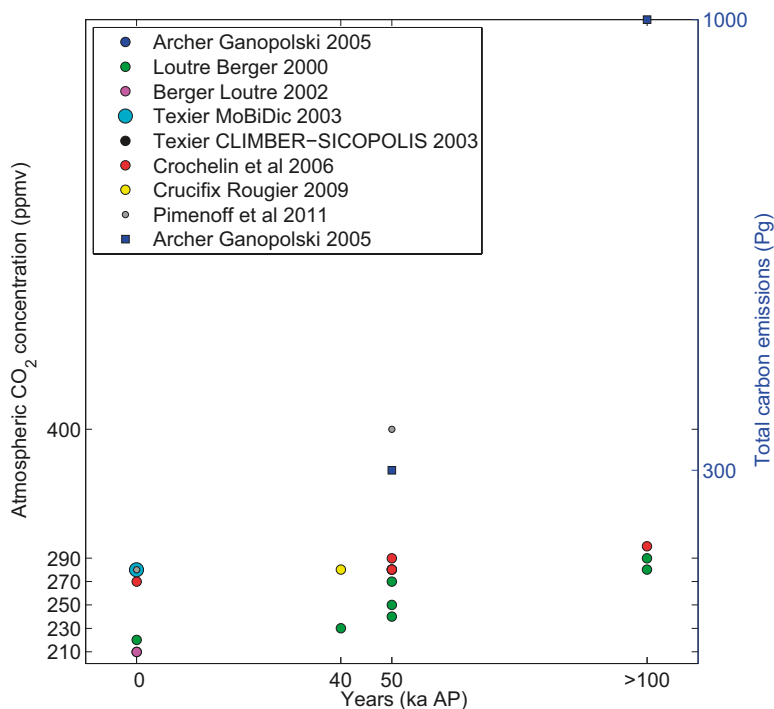


Figure 1-4. Approximate timing of glacial inception (years ka AP) and atmospheric CO₂ concentration (ppmv) in the studies summarized in Table 1-1 (circles and asterisk). Approximate timing of glacial inception and total carbon emissions (squares).

Based on simulations with the EMIC CLIMBER-2, forced with future insolation variations and a constant atmospheric CO₂ concentration, Archer and Ganopolski (2005) predicted that a carbon release from fossil fuels or methane hydrate deposits of 5,000 Pg carbon could prevent glaciation for the next 500 ka. For cumulative emissions of 300 Pg and 1,000 Pg carbon, glacial inception occurs after ~50 ka and ~130 ka respectively. Archer and Ganopolski (2005) point out that for an atmospheric CO₂ concentration of 280 ppmv, a slight shift in the model parameters can easily tip the simulation to onset of glaciation now rather than in 50 ka.

Cochelin et al. (2006) simulated the coming 100 ka with the McGill Paleoclimate Model (MPM) forced by variations in orbital parameters and prescribed atmospheric CO₂. Their model produced three types of evolution for the ice volume: an imminent glacial inception (low CO₂ levels), a glacial inception in 50 ka (CO₂ levels of 280 or 290 ppmv), or no glacial inception during the next 100 ka (CO₂ levels of 300 ppmv and higher).

Crucifix and Rougier (2009) utilize a three-dimensional stochastic system to investigate the timing of the next glacial inception. The system simulates ice volume, atmospheric CO₂ concentration and deep-ocean temperature forced by the variations in insolation at 65°N at summer solstice. Their inference takes the form of a data assimilation of paleo proxy data and the model parameters are trained to match the past record. As stated by the authors, if phenomenological models are to be used to predict actual climate system behaviour, then we must take very careful account of the uncertainty introduced by their limitations. Their provisional results indicated that without anthropogenic intervention (i.e. only natural processes) peak glacial conditions would occur in 60 ka AP, with glacial inception starting at 40 ka AP. Predictability by their model after that point is said to be poor.

Pimenoff et al. (2011) employ the CLIMBER-2 model with SICOPOLIS to study the future evolution of climate in Olkiluoto, the site selected for the Finnish repository for spent nuclear fuel. They simulated the coming 120 ka with a constant atmospheric CO₂ concentration of 280 ppmv and 400 ppmv respectively. The climate evolution differs substantially between these two experiments, with an immediate glaciation occurring in the 280 ppmv experiment as opposed to very restricted glaciation during the coming 120 ka in the 400 ppmv experiment. The insolation minimum at about 17 ka AP causes a large ice sheet over northern Fennoscandia in the 280 ppmv scenario as opposed to only some ice in the Scandinavian mountain range in the 400 ppm scenario. The following insolation minimum at about 54 ka AP produces an extensive ice sheet in the 280 ppmv scenario as opposed to a small ice sheet from the Scandinavian mountain range to Finnish Lapland and parts of Northern Ostrobothnia in the 400 ppmv scenario. In the 400 ppmv scenario, the mean temperatures at Olkiluoto are warmer than at present for most of the time. An exception is the insolation minimum at about 54 ka AP, where the mean temperatures are about the same as at present.

Vettoretti and Peltier (2011) investigated the impact of isolation, greenhouse gas forcing and ocean circulation changes on glacial inception with the AOGCM CCSM3. Based on the seasonal and latitudinal distribution of insolation, they argue that MIS 11, ~420 ka BP, is a good analogue for the present interglacial. They simulate the climate for orbital year 10 ka AP, when obliquity is at a minimum and eccentricity is low. They conclude that this period is favorable for the full onset of the next glacial cycle if atmospheric greenhouse gas concentrations have reached pre-industrial or lower levels.

Tzedakis et al. (2012a) determine the natural length of the current Holocene interglacial. They argue that MIS 19c, ~780 ka BP, is a good analogue to the present interglacial. Assuming that ice growth mainly responds to insolation and CO₂ forcing, this analogy suggests that the end of the current interglacial would occur within the next 1,500 years, if atmospheric CO₂ concentrations did not exceed 240 ± 5 ppmv. Tzedakis et al. (2012b) demonstrate the importance of obliquity, rather than summer insolation at high northern latitudes, for the timing of glacial inception. They conclude that glacial inception always takes place when obliquity is decreasing and never after the obliquity minimum. The phasing of precession and obliquity appear to influence the persistence of interglacial conditions over one or two insolation peaks, leading to shorter (~13 ka) and longer (~28 ka) interglacials (Tzedakis et al. 2012b). The onset of interglacials, on the other hand, occurs within 2 ka of the summer insolation maximum at high northern latitudes.

The latter two studies are not included in Table 1-1, but should be taken as an indication of the uncertainty in the current knowledge of the occurrence of the next Northern Hemisphere glaciation.

1.2 Objectives

The long-term safety for the SFR repository for low and intermediate-level waste in Forsmark is analysed within the SR-PSU safety assessment.

The main objective of the present study is to support climate scenario descriptions and selections for the SR-PSU safety assessment by investigating the potential for permafrost development during the next 60 ka at the Forsmark site, south-central Sweden.

The main factor affecting permafrost development at the Forsmark site is the conditions at the ground surface, of which the air temperature is the most important (Hartikainen et al. 2010). To assess the potential for permafrost in south-central Sweden, an EMIC and a state-of-the art ESM have been utilized to simulate possible future climate in the next 60 ka. In a subsequent step, the results of the climate model simulations were used as input to a site-specific 2D permafrost model simulation.

Any results of modelling are associated with uncertainty as to representativity of the model in describing, in this case, the Earth's climate evolution. For instance, Vavrus et al. (2011) recently tested the influence of model resolution on glacial inception using a coupled atmosphere – slab ocean version of the CCSM3 (Community Climate System Model, version 3). They found that lowering greenhouse gas concentrations from recent to lower values generates much more extensive glacial inception when using a high resolution compared to a lower resolution simulation. To estimate the uncertainty in the results presented in this report, the model results are compared against several datasets, e.g. observations of the present climate and other modelling studies of the present century climate evolution (Solomon et al. 2009), to other modelling studies of the future ~3–10 ka (Eby et al. 2009, Mikolajewicz et al. 2007) and to studies of the next 100–200 ka (Cochelin et al. 2006, Loutre and Berger 2000, Pimenoff et al. 2011, Texier et al. 2003).

2 Methodology

2.1 Selection of time periods and forcing conditions

As described in Section 1 previous studies with EMICs (e.g. Loutre and Berger 2000, Ganopolski et al. 2010) have shown that the last glacial cycle can be simulated in reasonable agreement with climate proxy data using a combination of variations in the latitudinal and seasonal distribution of insolation due to variations in the Earth's orbital parameters and glacial-interglacial atmospheric CO₂ variations. Following these studies, periods with a potential for cold climate in south-central Sweden in the next 60 ka are identified. The identification is based on the available literature on future greenhouse gas concentrations (Archer et al. 2009, Eby et al. 2009, Moss et al. 2010) and variations in the Earth's orbital parameters (Berger and Loutre 2002).

Summer insolation at high northern latitudes is at a minimum 17 ka AP and 54 ka AP (see Figure 1-3). These periods were therefore identified as potential future periods of cold climate conditions in high northern latitudes in general and in south-central Sweden in particular. Due to human emissions of carbon to the atmosphere, the atmospheric CO₂ concentration is currently 392 ppmv (2011 AD), a substantial increase as compared to the range of atmospheric CO₂ concentrations of c. 180–295 ppmv found in ice core records for the last 800 ka (see Figure 1-2). The future atmospheric CO₂ concentration is determined by future human emissions of carbon to the atmosphere, and by the global carbon cycle. A review of the current knowledge on the future atmospheric CO₂ concentration is given in Section 2.3.2 below.

To span the possible combinations of future orbital variations and possible future atmospheric CO₂ concentrations, a suite of EMIC and ESM simulations were performed. The earth system models used in this study are described in Section 2.2. Further, forcing and boundary conditions used in the study are described and justified in Section 2.3. Initial conditions, forcing and boundary conditions used in the different simulations is described in Section 2.4.

To analyse the potential of permafrost in the region surrounding Forsmark, given the simulated future air temperature, ground- and bedrock temperatures are modelled with a 2D thermo-hydro-chemical model of permafrost and perennially frozen ground. This model is described in Section 2.5 along with conditions and settings used in these simulations.

2.2 Earth system modelling

EMICs are designed to represent the different components of the climate system, but at a lower computational cost than ESMs or AOGCMs. Typically, EMICs are run at coarser horizontal and vertical resolution and in many cases without directly modelling the atmospheric dynamics. In this study, ensembles of simulations were required to estimate the uncertainty in the results. Further, modelling of long time periods (60 ka for the transient runs) was needed. Therefore, an EMIC rather than an ESM was utilized for the majority of the climate simulations. The EMIC LOVECLIM (version 1.2) was used in this study. This model has an advantage as compared to other EMICs that it includes simplified atmospheric dynamics (quasi-geostrophic 3-level model). One disadvantage as compared to some other EMICs is that the version utilized here does not include an interactive ice sheet model, an important part of the climate system.

To test the sensitivity of the results of the EMIC simulations, two simulations with a state-of-the-art AOGCM have also been performed.

2.2.1 The Earth system model of intermediate complexity LOVECLIM

We used the 3D coupled EMIC LOVECLIM 1.2 (Driesschaert et al. 2007, Goosse et al. 2010). In this study, we only use three coupled components, namely the atmospheric ECBilt and oceanic CLIO components, and the vegetation module VECODE. ECBilt is a quasi-geostrophic, T21 spectral model, with three vertical levels (Opsteegh et al. 1998). Due to its spectral resolution

corresponding to a coarse horizontal resolution of $\sim 5.6^\circ \times 5.6^\circ$, its surface topography is simplified. Its parameterisation scheme allows for fast computing and includes a linear long-wave radiation scheme. ECBilt contains a full hydrological cycle, including a simple bucket model for soil moisture over continents, and computes synoptic variability associated with weather patterns. Precipitation falls in the form of snow when surface air temperatures fall below 0°C . CLIO is a primitive-equation 3D, free-surface ocean general circulation model coupled to a thermo-dynamical and dynamical sea-ice model (Goosse and Fichefet 1999). CLIO has a realistic bathymetry, a $3^\circ \times 3^\circ$ horizontal resolution and 20 vertical levels. In order to bring precipitation amounts in ECBilt-CLIO closer to observations, a negative precipitation-flux correction is applied over the Atlantic and Arctic Oceans. This flux is reintroduced in the North Pacific. The climate sensitivity of LOVECLIM to a doubling of atmospheric CO_2 concentration is 1.8°C , associated with a global radiative forcing of 3.8W m^2 (Driesschaert 2005). The dynamical terrestrial vegetation model VECODE computes the surface fraction of each land grid cell covered by herbaceous plants, trees and desert fractions (Brovkin et al. 1997) and is coupled to ECBilt through the surface albedo (Driesschaert 2005). LOVECLIM produces a reasonably realistic modern climate (Driesschaert 2005) and an LGM climate generally consistent with data (Roche et al. 2007). Nevertheless, in a control climate forced with pre-industrial boundary conditions, a systematic warm bias of annual mean surface air temperatures of globally about 2°C compared to a 1971–2000 climatology is found in the model (Driesschaert 2005).

Equilibrium climate sensitivity (ECS) is defined as the global equilibrium surface-air-temperature change in response to instantaneous doubling of atmospheric CO_2 concentration. The ECS is 1.7°C for LOVECLIM (Driesschaert 2005), which is low as compared to the ECS of $2.0\text{--}4.5^\circ\text{C}$ for the AOGCMs in IPCC AR4 (Randall et al. 2007) and the ECS of $2.1\text{--}4.7^\circ\text{C}$ for the AOGCMs in CMIP5.

2.2.2 The climate system model CCSM4

The NCAR Community Climate System Model version 4 (CCSM4) is a fully coupled ocean-atmosphere-land-sea-ice model that may be employed for the simulation of past, present and future climates (Brandefelt et al. 2011, Gent et al. 2011). The atmosphere component of the version employed in the present work is an atmospheric general circulation model with a finite volume core and a horizontal grid with a resolution of $\sim 2^\circ$ (Neale et al. 2011, unpublished manuscript). The atmosphere has 26 vertical levels from the surface to approximately 2 hPa. The land component is the Community Land Model version 4 (CLM4), which uses the same horizontal resolution as the atmosphere component (Lawrence et al. 2011). The ocean component is based on the Parallel Ocean Program version 2 (Smith et al. 2010), which has a horizontal resolution of $\sim 1^\circ$. There are 60 depth layers in the vertical (vs. 25 depth layers in the previous version CCSM3). The sea ice module is the Community Ice Code version 4 (Hunke and Lipscomb 2008), which employs the same horizontal grid as the ocean module. Compared to the previous version CCSM3, CCSM4 includes several significant developments and improvements, including carbon-nitrogen cycling, a much improved representation of atmospheric deep convection, a new freeze-dry scheme for polar low clouds, an improved representation for surface runoff and frozen soil, an improved parameterization for near-surface oceanic eddies, new parameterizations for sub-meso scale mixed layer eddies and ocean overflows, and a new radiative transfer scheme for sea ice/snow (Gent et al. 2011). These changes improve the model representations of the frequency of ENSO variability (Neale et al. 2008), of polar cloud cover (Vavrus and Waliser 2008), of the penetration of the North Atlantic meridional overturning circulation (Danabasoglu et al. 2012), of land water storage (Lawrence et al. 2011), and of the Arctic sea ice concentration and its trend (Gent et al. 2011). For example, the ENSO power spectrum in CCSM4 is now comparable to the observed 2–7 yr period (Gent et al. 2011), whereas it is dominated by variability at ~ 2 yr period in CCSM3 and its precursors (Collins et al. 2006, Peltier and Solheim 2004). As a further example, the Antarctic bottom water (AABW) transport in CCSM4 is approximately 8 Sv, which is in much better agreement with observations and much weaker than in CCSM3 (~ 16 Sv) (Danabasoglu et al. 2012). An ensemble of twentieth-century simulations produces a good match to the observed September Arctic sea ice extent from 1979 to 2005 (Gent et al. 2011). The CCSM4 ensemble mean increase in globally averaged surface temperature between 1850 and 2005 is larger than the observed increase by about 0.48°C . This is consistent with the fact that CCSM4 does not include a representation of the indirect effects of aerosols, although other factors may come into play. The CCSM4 still has significant biases, such as the mean precipitation distribution in the tropical Pacific Ocean, too much low cloud in the Arctic, and the latitudinal distributions of shortwave and longwave cloud forcings (Gent et al. 2011).

Further a warm bias is found in annual average near surface temperature over land, with a maximum of more than 5°C in eastern Europe and central Eurasia (Gent et al. 2011).

The ECS is 3.1°C for CCSM4 when run at the same resolution as in the present study (Bitz et al. 2012), which is close to the average of the ECS of 2.0–4.5°C for the AOGCMs in IPCC AR4 (Randall et al. 2007) and the ECS of 2.1–4.7°C for the AOGCMs in CMIP5.

2.3 Forcing conditions for earth system modelling

2.3.1 Orbital solar forcing

As described in Section 2.1, potentially cold periods are identified based on minima in June insolation at high northern latitudes (65°N). In the next 60 ka, minima in this parameter are found 17 ka AP and 54 ka AP (see Figure 1-3; Berger and Loutre 2002). The insolation as a function of latitude and month of the year is displayed in Figure 2-1 for the present day (0 ka AP), and the difference between future periods of minimum June insolation at high northern latitudes (17ka AP and 54 ka AP) and the present. June insolation at high northern latitudes is at a minimum also at present day and, although at a minimum, this region will receive more insolation at 17 ka AP than at the present.

Minima in the June insolation at high northern latitudes are not coincident with minima in the obliquity (see Figure 1-3). Minimum obliquity, indicative of potential for glacial inception (e.g. Huybers and Wunsch 2005), occurs around 10 ka AP and around 51 ka AP. For comparison the difference between future periods of minimum obliquity (10 ka AP and 51 ka AP) and maximum obliquity (31 ka AP) and the present are also displayed in Figure 2-1. The potential for cold climate conditions in Forsmark in the periods of low obliquity is evaluated with a set of LOVECLIM simulations as described in Section 2.4. It should however be noted that the climate models used in this study do not include the feedback of glacier and ice sheet dynamics needed for glacial inception.

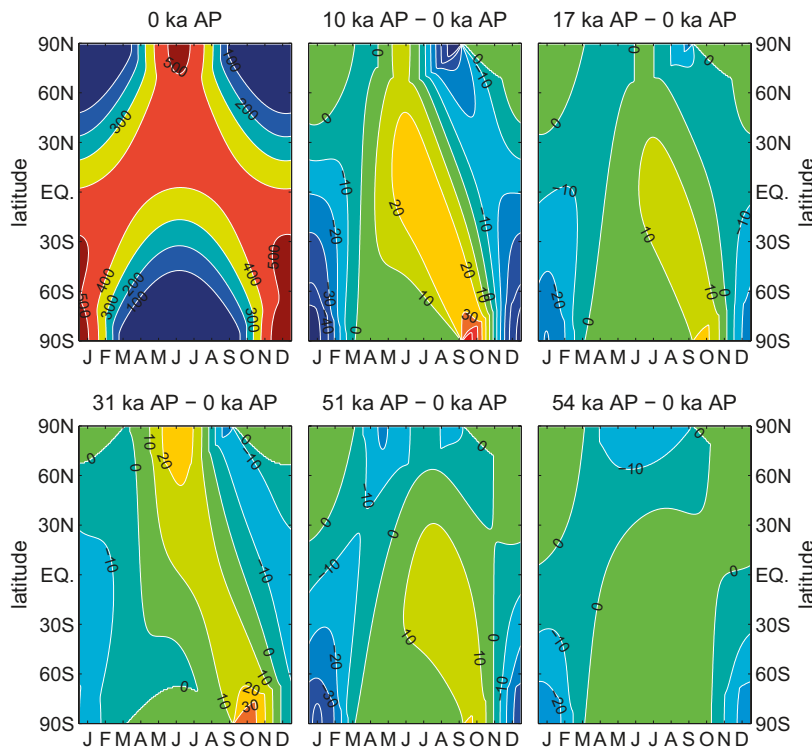


Figure 2-1. Insolation (Wm^{-2}) as a function of latitude and month of the year at present (0ka AP; upper left panel). The difference in insolation between 10 ka AP (upper middle panel), 17 ka AP (upper right panel), 31 ka AP (lower left panel), 51 ka AP (lower middle panel) and 54 ka AP (lower right panel) and the present (0 ka AP). Insolation calculated following Berger (1978).

2.3.2 Greenhouse gases

Contrary to the future seasonal and latitudinal distribution of insolation, which is known, future atmospheric greenhouse gas concentrations are highly uncertain. Future anthropogenic carbon emissions can be estimated using global carbon cycle models in combination with assumptions on future human carbon emissions. The estimates are uncertain though, both due to uncertainty in global carbon cycle and in the future socio-economic development that forms the basis for the human carbon emission scenarios.

To set the range of atmospheric CO₂ concentrations used in this study into perspective, a review of the current knowledge on the future atmospheric CO₂ concentration under the influence of man-made emissions is given here.

After anthropogenic carbon emissions have stopped, the future atmospheric concentration will depend on the total cumulative emissions up to that point in time and on the processes that act to decrease the concentration (e.g. Zickfeld et al. 2012). Thus to assess the future atmospheric CO₂ concentration we need to assess 1) the total cumulative carbon emissions or maximum atmospheric CO₂ concentration and 2) the timescale for the removal of atmospheric CO₂.

Total cumulative carbon emissions

Archer (2005) modelled the future fate of total emissions of 300–5,000 Pg carbon based on the present knowledge of the processes that remove CO₂ from the atmosphere. He concludes that 17–33% of the fossil fuel carbon is expected to still reside in the atmosphere 1 ka from now, decreasing to 10–15% at 10 ka AP, and 7% at 100 ka AP. Archer's calculations do however not account for the natural atmospheric CO₂ variability that drive the glacial/interglacial and shorter-term climate cycles, see below.

Archer et al. (2009) performed a review and model inter-comparison of the atmospheric lifetime of fossil fuel CO₂ as predicted by nine different carbon cycle models and EMICs. Cumulative emissions of 1,000 and 5,000 Pg carbon were added in the models. For comparison, humankind has up to now released c. 300 Pg carbon and will surpass 1,000 Pg carbon cumulative release under business-as-usual projections before the end of the century. The entire remaining fossil fuel reserve totals c. 5,000 Pg carbon. The initial atmospheric CO₂ concentration in the model simulations is 280 ppmv. Archer et al. (2009) concluded that the models agree that 20–35% of the CO₂ remains in the atmosphere after equilibration with the ocean (200–2,000 years). Further, they concluded that neutralization by CaCO₃ draws the airborne fraction down further on timescales of 3 to 7 ka. After 10 ka of integration following the 1,000 Pg (5,000 Pg) carbon initial pulse, 8–19% (10–33%) of the emissions remained in the atmosphere. These results are summarized in Table 2-1.

Table 2-1. Atmospheric CO₂ concentration as a function of time as given by Archer et al. (2009). The numbers were taken from a figure and are approximate. The concentration given for 10 ka AP is the minimum of the different models included in the inter-comparison. Numbers in italic were calculated here under the assumption of the same decrease until 10 ka AP as in the 1,000 Pg C experiments.

Total cumulative carbon emissions (Pg C)	Maximum atmospheric CO ₂ concentration (ppmv)	Atmospheric CO ₂ concentration 10 ka AP (ppmv)
300	392	289
590	560	302
1,000	750	318
5,000	2,700	520

Timescale for removal of atmospheric CO₂

After 10 ka in the model simulations presented by Archer et al. (2009), the atmospheric CO₂ concentration is decreasing at a slow rate determined by the removal rate of atmospheric CO₂ by silicate weathering. Archer et al. (2009) concluded that the decrease to pre-industrial levels at this rate could take tens, or even hundreds, of thousands of years. The experiments analysed by Archer et al. (2009) are based on the assumption of continued human-induced emissions of carbon to the atmosphere. The absolutely most pessimistic assumption (for the possibility of permafrost growth in south-central Sweden) would be to assume that anthropogenic emissions are reduced to zero today and that the atmospheric concentration would start to decrease from the present level of 392 ppmv. This corresponds to total cumulative emissions of ~300 Pg carbon as compared to the 1,000 and 5,000 Pg carbon cumulative emissions used in the experiments presented by Archer et al. (2009). Assuming that the atmospheric CO₂ concentration would decrease at the same rate as for fastest decreasing model for 1,000 Pg carbon cumulative emissions in Archer et al. (2009), 8% of the fossil fuel carbon (i.e. the CO₂ in excess of the preindustrial concentration of 280 ppmv) would remain in the atmosphere after 10 ka in this bounding case. The atmospheric CO₂ concentration would thus be c. 289 ppmv at 10 ka AP.

It is important to note that the carbon cycle models used by Archer et al. (2009) do not include the natural variations of the atmospheric CO₂ concentration, as pointed out by Archer (2005). He suggests that “one might simply imagine natural variations of order 30% superimposed upon the projections here [of future fossil fuel CO₂], by analogy to past perturbations about a steady baseline pCO₂ value”. For an atmospheric CO₂ concentration close to or below the pre-industrial 280 ppmv, the results of different studies range from predicting an imminent glacial inception to glacial inception 40–60 ka into the future (Table 1-1). Current knowledge of glacial-interglacial climate system dynamics thus leads us to the conclusion that ice sheet build up cannot be excluded under a similar to present latitudinal and seasonal insolation distribution and atmospheric CO₂ concentrations around or below 280 ppmv. Specifically, Vettoretti and Peltier (2011) investigate the potential for glacial inception at 10 ka AP, when obliquity is at a minimum. They conclude that this period is favorable for the full onset of the next glacial cycle if atmospheric greenhouse gas concentrations have reached pre-industrial or lower levels.

For comparison, the rapid decrease of the atmospheric CO₂ concentration found in ice core data during the last glacial inception (Figure 1-2) is estimated. The atmospheric CO₂ concentration is decreased from interglacial levels of c. 275 ppmv around 115.4 ka BP to c. 228 ppmv around 108.0 ka BP, i.e. c. 47 ppmv CO₂ in 7.4 ka or c. 6.4 ppmv CO₂ per ka.

In summary, we conclude that atmospheric CO₂ concentrations at or below pre-industrial levels cannot be excluded after 10 ka AP if human emissions of CO₂ were reduced to zero in the near future. This improbable scenario can be regarded as a bounding case for the possibility of permafrost conditions in south-central Sweden. Under more realistic scenarios for future anthropogenic carbon emissions, the atmospheric CO₂ concentration would be at or above 300 ppmv at 10 ka AP (Archer et al. 2009).

Atmospheric greenhouse gas concentration used in this study

Due to the uncertainty in the future atmospheric CO₂ concentration, a range of atmospheric CO₂ concentrations has been used in this study. The range used here, 180–400 ppmv, represents the range of atmospheric CO₂ concentrations of c. 180–295 ppmv found in ice core records for the last 800 ka (see Figure 1-2) up to the current atmospheric CO₂ concentration of 392 ppmv (2011 AD).

Atmospheric CH₄ and N₂O concentrations are set to represent 19th century concentrations of 760 ppbv and 270 ppbv respectively. In the LOVECLIM simulations, CH₄ was erroneously set to 650 ppbv. The consequence of this is investigated in Section 3.1.3.

2.3.3 Aerosols

Aerosols are an integral part of the atmospheric hydrological cycle and the atmosphere's radiation budget, with many possible feedback mechanisms that are not yet fully understood (Stevens and Boucher 2012). The most easily understood interaction between aerosols and climate is the direct effect, i.e. scattering and absorption of shortwave and thermal radiation. Interactions with the hydrological cycle, and additional impacts on the radiation budget, occur through the role of aerosols in cloud microphysical processes, as aerosol particles act as cloud condensation nuclei and ice nuclei. The suite of possible impacts of aerosols through the modification of cloud properties is called 'indirect effects'. Since future projections of the atmospheric aerosol burden only exist for the coming few centuries, atmospheric aerosol concentrations are not varied in the present study. The concentrations are kept at the same level as in the respective pre-industrial climate simulation.

2.3.4 Ice sheets and glaciers

Due to computational expense, direct modelling of land ice (ice sheets and glaciers) dynamics has not been included in the Earth system models used in the present study. Ice sheets and glaciers are set at their pre-industrial extent and topography in all simulations. When the climate simulated by the models favours build up or reduction of these ice masses, the models do not capture this evolution. In such cases the lack of dynamical glaciers and ice sheets introduces a warm or cold bias to the simulated global average climate due to the neglect of the cooling effect of the ice sheet albedo. Further, ice sheet albedo and topography would have an influence on the atmospheric large-scale circulation and thus influence e.g. the regional climate in Scandinavia.

Pausata et al. (2011) present a suite of coupled model simulations designed to investigate both the separate and combined influences of the main changes in boundary conditions (greenhouse gases, ice sheet topography and ice sheet albedo) for the Last Glacial Maximum (LGM; 21 ka BP) and the effect these changes have on the mean state and variability of the atmospheric circulation. They find that ice sheet topography accounts for most of the simulated circulation difference between the LGM and the pre-industrial climate. The potential effect on south-central Swedish climate cannot be determined directly from these results since the LGM ice sheet covered this region. The effect can however be estimated from their results by considering land areas away from the direct effect of the Fennoscandian LGM ice sheet in their simulations. In such areas, the annual average near-surface air temperature decrease is 2–5°C with respect to the pre-industrial climate, due to the Laurentide and Fennoscandian ice sheet topography and albedo. In the present study, this is taken as an upper bound on the effect of the neglect of land ice dynamics.

2.3.5 Sea level, coastlines, topography and bathymetry

The sea level, coastlines, continental topography and bathymetry is kept constant at pre-industrial conditions in all simulations. Substantial shrinking or growth of the continental ice sheets would produce substantial sea level rise or fall. In the event of beginning ice sheet growth in North America, the global sea level will decrease. In the last glacial inception around 115 ka BP, global sea level decreased by 40–60 m in 5–10 ka (Lambeck et al. 2002, Waelbroeck et al. 2002). This resulted in isolation of the Baltic Sea from the Atlantic Ocean and decreased depth and areal extent. Due to the coarse resolution of both climate models, a sea level change (increase or decrease) of up to 10–20 meters would not substantially influence the coastline in the model. The actual effect of such a sea level change on the local climate in coastal areas may however be significant, resulting in a more maritime climate in the case of sea level rise and a more continental climate in case of sea level fall.

2.3.6 Vegetation

The treatment of vegetation differs between the models used in this study. LOVECLIM includes a simple vegetation model that adjusts the vegetation in interaction with the simulated climate. CCSM4 uses constant (pre-industrial; 1850 AD) vegetation. This model however includes a carbon-nitrogen cycle model.

2.4 Earth system model simulations

The simulations performed with the two Earth system models are described in the following. All simulations performed with each model were started from the same initial conditions. For LOVECLIM, the initial conditions were taken from the restart files distributed with the model. These represent a pre-industrial climate. For CCSM4, the initial conditions were taken from restart files from NCAR's official CMIP5 simulation of pre-industrial climate at the same resolution used in the present study. The simulated climate needs time to adjust to the changes in forcing conditions (Brandefelt and Otto-Bliesner 2009), therefore the initial 1,000 model years are regarded as the equilibration period for all simulations.

To facilitate comparison to observations and bias-correction of the air simulated air temperature, T_{2m} as simulated in LOVECLIM and CCSM4 is chosen for the analysis.

2.4.1 Pre-industrial control climate

The pre-industrial climate of the 18th and 19th century was used as a reference, or control, climate in this study. This period is characterized by minor variations in atmospheric greenhouse gas concentrations and is therefore often represented by climate model simulations with constant forcing and boundary conditions.

The pre-industrial climate was simulated with the appropriate forcing and boundary conditions for this period as defined by the respective modelling centre or group (i.e. distributed with each model). This choice facilitates comparison to other studies with the same models.

LOVECLIM

The pre-industrial climate simulated with LOVECLIM is determined based on simulations of the climate evolution for the period 1000–2000 AD. For comparison to observations, the period 1751–1850 AD was chosen from these simulations and observations (see Section 2.6). In order to assess the impact of internal variability on the simulated climate for this period, a three-member initial value ensemble was set up. The climate simulations were forced by observed variations in the atmospheric concentrations of CO₂, CH₄ and N₂O displayed in Figure 2-2. The simulations were started from a pre-industrial climate simulated with LOVECLIM and provided with the model. The initial calendar year of the simulations was set to 500, 600 and 800 AD such that each simulation started with slight differences in the atmospheric greenhouse gas concentrations in order to produce an ensemble of different realisations of the climate. The small ensemble size is deemed sufficient for the purpose of calculating 100-year average monthly mean T_{2m} , since inter-decadal and decadal variability associated with e.g. El Niño – Southern Oscillation and the Atlantic Multi-decadal Oscillation will partly be averaged out. The remaining differences between the three simulations were used to estimate the uncertainty in the average pre-industrial annual cycle in LOVECLIM. The monthly averages for each month of the year averaged over years 1751–1850 AD of these simulations was used to determine the pre-industrial climate simulated by LOVECLIM. The average atmospheric greenhouse gas concentrations for 1751–1850 AD used in this simulation were; CO₂=281 ppmv, CH₄=756 ppbv, N₂O=272 ppbv.

As described in the first paragraphs of Section 2.4.1, the pre-industrial climate is often represented by long simulations with constant forcing and boundary conditions. For comparison of the applied methodology to this methodology, a constant forcing and boundary condition simulation was also performed with LOVECLIM. In this simulation the atmospheric greenhouse gas concentrations were set according to the PMIP2 protocol to: CO₂=280 ppmv, CH₄=760 ppbv, N₂O=270 ppbv. The model was integrated for 3,000 model years and the average of the last 2,000 model years was determined. The comparison is discussed in Section 2.8.1.

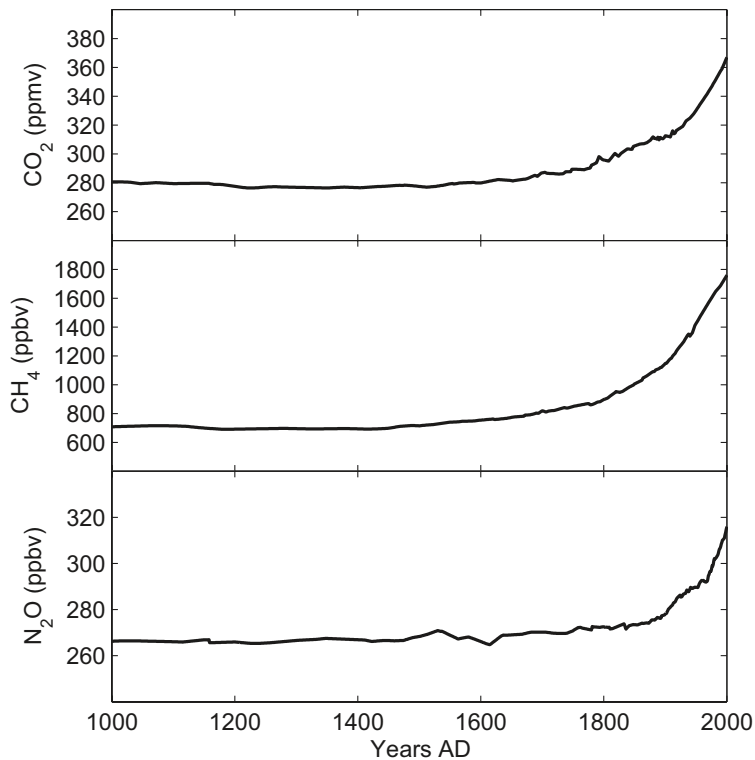


Figure 2-2. Observed atmospheric greenhouse gas concentrations used in the LOVECLIM simulation of the recent past climate (1000–2000 AD).

CCSM4

A multi-millennial simulation of pre-industrial climate, performed within a previous project, was used here to determine the pre-industrial climate simulated with CCSM4. This simulation was started from a 500-model-year CCSM4 simulation performed at NCAR with constant forcing and boundary conditions representing a pre-industrial climate. The last 1,000 model years of this c. 2,400 model-year simulation were used here. The atmospheric greenhouse gas concentrations used in this simulation represent year 1850 AD; CO₂=285 ppmv, CH₄=792 ppbv, N₂O=276 ppbv.

2.4.2 Future climate

The future climate simulations performed within this study were set up with forcing and boundary conditions identical to the respective pre-industrial climate simulation for each model, except for atmospheric greenhouse gas concentrations and the insolation distribution at the top of the atmosphere. The atmospheric greenhouse gas concentrations were set to CH₄=760 ppbv and N₂O=270 ppbv following the PMIP2 protocol for pre-industrial control simulations. It is assumed here that the small concentration differences as compared to the respective pre-industrial simulations are insignificant for the simulated climate. For CH₄, a lower value of 650 ppbv was erroneously used in the LOVECLIM simulations. The effect of this difference is analysed in a set of sensitivity experiments described in Section 3.1.3.

To span the possible combinations of future orbital variations and atmospheric CO₂ concentrations, a suite of EMIC and ESM simulations were performed with the models described in Section 2.2. All the Earth system model simulations performed are listed in Table 2-2.

Table 2-2. The Earth system model simulations performed. For explanations, see section 2.2 and 2.3.

Simulation label	Orbital year (ka AP)	Atmospheric CO ₂ concentration (ppmv)	Earth system model	Simulation type
LC_PI_1, LC_PI_2, LC_PI_3	0	280	LOVECLIM	Transient historical
LC_17k_180, ..., LC_17k_400	17	180, 200, 240, 280, 320, 360, 400	LOVECLIM	Equilibrium
LC_54k_180,, LC_54k_400	54	180, 200, 240, 280, 320, 360, 400	LOVECLIM	Equilibrium
LC_0k_61k_200	0–61	200	LOVECLIM	Transient
LC_0k_61k_400	0–61	400	LOVECLIM	Transient
CM_PI	0	280	CCSM4	Equilibrium
CM_17k_200	17	200	CCSM4	Equilibrium
CM_54k_180	54	180	CCSM4	Equilibrium

Equilibrium simulations for 17 ka AP and 54 ka AP

Firstly, the climate in the future periods of minimum summer insolation at high northern latitudes at 17 ka and 54 ka AP was analysed in a set of simulations with the latitudinal and seasonal insolation distribution set following Berger (1978) for each of the periods (see Figure 2-1) and the atmospheric CO₂ concentration set to a constant value in the range 180–400 ppmv. For each future period (17 ka AP and 54 ka AP), seven LOVECLIM simulations with different atmospheric CO₂ concentration were performed. Further, one CCSM4 simulation was performed for each of the two future periods.

For the CCSM4 simulations an atmospheric CO₂ concentration of 200 ppmv was chosen to represent the lowest possible concentration for the 17 ka AP period based on the discussion in Section 2.3.2. For the 54 ka AP period, an atmospheric CO₂ concentration of 180 ppmv was chosen to represent the lowest concentration found in ice-core records. The model was integrated for a total of 1,590 and 1,660 model years respectively in CM_17k_200 and CM_54k_180. The CCSM4 simulations were used to exemplify the uncertainty in the simulated future climate due to inter-model differences.

The LOVECLIM simulations were integrated for a total of 3,000 model years and the average climate for the last 2,000 model years was used in the analysis. The CCSM4 simulations were integrated for c. 1,600 model years and the average climate for the last 300 model years was used for the analysis.

Transient simulations 0 ka AP – 61 ka AP

Secondly, the climate evolution in the next 61 ka was analysed in a set of two LOVECLIM simulations. The purpose of this set of simulations was to test the presumption that the periods of minimum summer insolation at high northern latitudes (17 ka and 54 ka AP) will give the coldest climate in south-central Sweden during this ~60 ka long future period. Further, the potential for cold climate conditions in Forsmark in the future periods of low obliquity was also evaluated as described in Section 2.3.1. It should however be noted that the climate models used in this study do not include the feedback of glacier and ice sheet dynamics needed for glacial inception.

In this set of simulations the atmospheric CO₂ concentration was set to a constant value of 200 and 400 ppmv respectively. The insolation distribution was set following Berger (1978) for each year from 1 ka BP (before present) until 61 ka AP.

2.5 Permafrost modelling

The present study made use of an improved version of the 2D thermo-hydro-chemical model of permafrost and perennially frozen ground that was used for the so-called SR-Site safety assessment a repository for spent nuclear fuel (Hartikainen et al. 2010). The 2D model domain was set up in the same way as in Hartikainen et al. (2010), and covers a 15 km long and 10 km deep vertical cross-section of the Forsmark site (Figure 2-3). The profile crosses the SFR repository which is the main focus for the present study. The permafrost model includes mathematical expressions for freezing and thawing of saline groundwater-saturated bedrock. The bedrock is considered as an elastic porous medium and the groundwater as an ideal solution of water and ionic solvents. The model is based on the principles of continuum mechanics, macroscopic thermodynamics and the theory of mixtures being capable of describing heat transfer, freezing of saline water, groundwater flow and deformations of bedrock. The freeze-out and transport of solutes is also included in the model. A detailed model description is given by Hartikainen et al. (2010). The improvement made to the model since the study by Hartikainen et al. (2010) is described in the following.

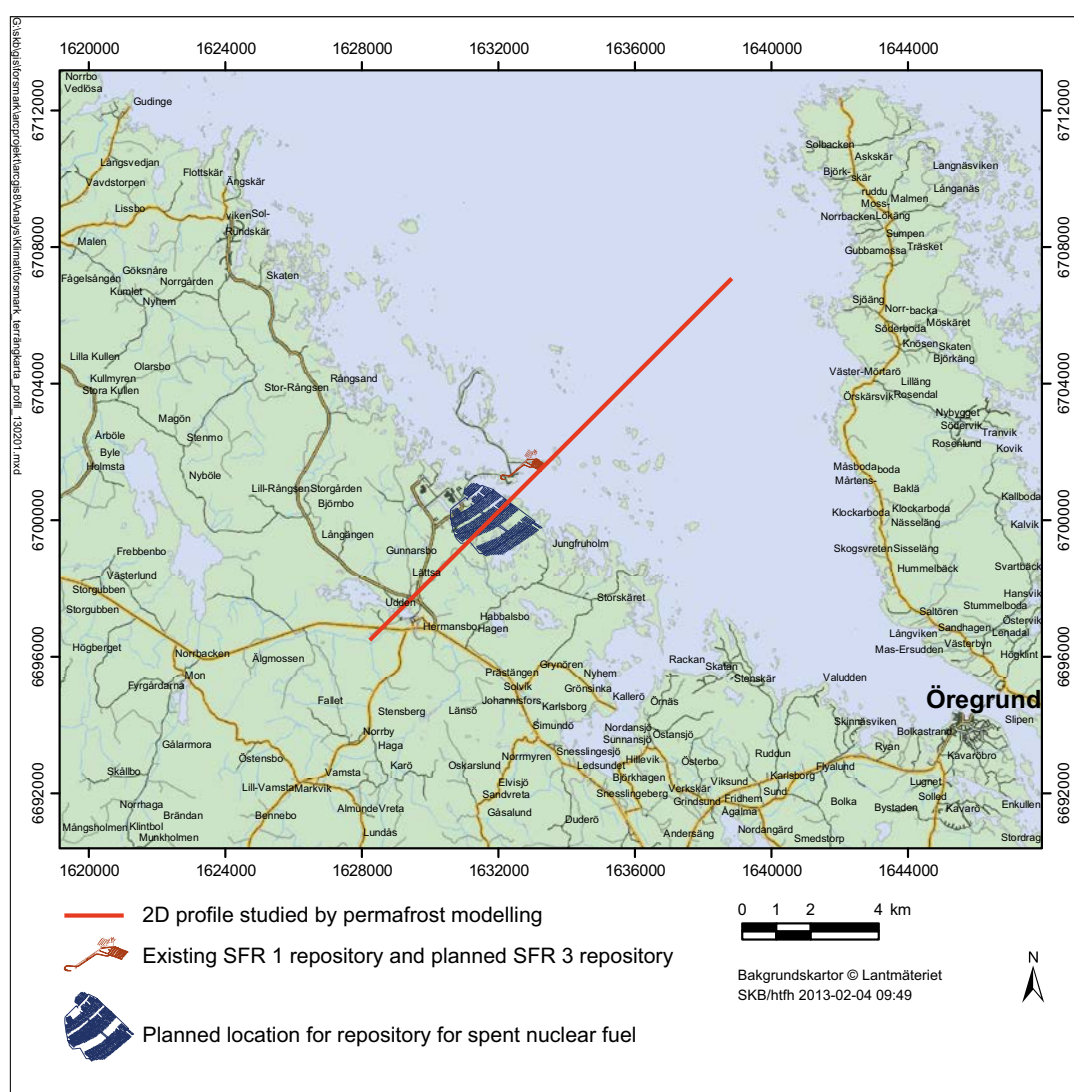


Figure 2-3. Geographical map for the 2D permafrost model domain and the SFR repository in Forsmark.

The improved version of the permafrost model includes seasonal freezing and thawing of the ground. Inter-annual variations in ground surface temperature are now expressed in terms of the monthly mean ground surface temperatures, T_s , which are determined by the monthly mean 2-m air temperatures, T_a , the freezing n -factor, n_{fr} , and thawing n -factor, n_{th} , as

$$T_s = \begin{cases} n_{fr}T_a, & T_a < 0^\circ\text{C} \\ n_{th}T_a, & T_a \geq 0^\circ\text{C} \end{cases} \quad (2-1)$$

The n -factors are statistical relations between the annual mean 2-m air temperature and annual mean ground surface temperature (Lunardini 1978). Values for the n -factors used in this study are given in Table 2-7 in Hartikainen et al. (2010).

The improvement allows for the thermal offset, i.e. a decrease, in the annual mean ground temperature profile due to seasonal freezing and thawing of ground (Goodrich 1978). The offset can be several degrees depending on the amount of freezing water in ground, and may in cases lead to development of perennially frozen ground in locations where the annual mean air temperature is above 0°C .

2.5.1 Forcing conditions and input data for permafrost modelling

Sub-surface properties and conditions

To capture the most important factors and parameters affecting the development of permafrost and frozen ground at the Forsmark site, detailed site-specific sensitivity analyses were previously performed considering surface and subsurface conditions (SKB 2010). Factors of importance, and analysed in the sensitivity studies, were air temperatures and the influence of surface covers such as snow, vegetation and water bodies. The bedrock conditions analysed in the sensitivity experiments were geothermal heat flow and thermal properties of the bedrock (thermal conductivity and diffusivity). Various combinations of the above parameters were also analyzed, including worst-case combinations most favourable for permafrost growth. In addition, the influence of convective heat transfer was also studied. The uncertainty in each of the parameters analysed in the sensitivity experiments was mainly obtained from the detailed site investigation programme that has been conducted for the Forsmark site, see Hartikainen et al. (2010) and references therein. The sensitivity simulations carried out with the 2D permafrost model are presented in (Hartikainen et al. 2010, section 5.2) and in (SKB 2010, section 3.4.4).

In the present study, thermal conductivity and thermal diffusivity are set to the mean values given in Table 2-1 and Table 2-2 in Hartikainen et al. (2010). The uncertainty associated with these parameters is taken from Hartikainen et al. (2010). The geothermal heat flow is also set to the mean value given in Table 2-3 in Hartikainen et al. (2010). The uncertainty associated with these parameters is taken from Hartikainen et al. (2010).

The initial state of subsurface conditions, in terms of groundwater salinity field and soil distribution, is identical to that described in Hartikainen et al. (2010) corresponding to the present-day situation.

The planned SFR 3 repository for short-lived low- and intermediate-level nuclear waste does not produce heat. In contrary to Hartikainen et al. (2010), the heat production from the planned nearby repository for spent nuclear fuel in Forsmark is therefore *not* included in the current simulations. This is a pessimistic assumption in terms of permafrost development and freezing, since the exclusion of heat from a nuclear waste repository may result in somewhat lower bedrock temperatures (Hartikainen et al. 2010, section 5.2).

Surface properties and conditions

The uncertainty in future precipitation and surface conditions is taken into account by assuming conditions that in the previous studies (Hartikainen et al. 2010) were shown to be the most favourable for permafrost growth, i.e. a *dry climate* with *dry surface conditions*. For more detailed definitions of these states, see Hartikainen et al. (2010).

According to Glacial Isostatic Adjustment (GIA) simulations, there is a remaining isostatic uplift from the last glaciation of around 70 m (SKB 2010, section 4.5.2). In the permafrost simulations performed for the 54 ka AP period, this is taken into account by assuming the sea level to be 65 m below the present. In this situation, no Baltic Sea water bodies exist within the permafrost model domain.

Near-surface air temperature

The monthly mean air temperature at 2 m height (T_{2m}) in Forsmark, derived from one of the LOVECLIM climate model simulations, is used as input to the permafrost model. The sensitivity of the permafrost modelling to uncertainties in the climate model results is further analysed based on a number of sensitivity simulations with the permafrost model. Forsmark T_{2m} is spatially interpolated from a coarse grid (see Section 2.7) and bias-corrected to account for the climate model deficiencies (see Section 2.8).

2.5.2 Sensitivity to model formulation improvement

The sensitivity of the results to the improvements made in the new version of the permafrost model was investigated. Thus, the results of the new version of the permafrost model, described in Section 2.5, were compared to experiments with identical forcing and boundary conditions performed with the old version of the model (described by Hartikainen et al. 2010). The results are discussed in Section 3.4.4.

2.6 Observations for climate model evaluation

The climate simulated with the LOVECLIM and CCSM4 climate models is compared to available observations to assess the bias in the simulated climate. Since near-surface air temperature is the only climate model variable utilized for the permafrost modelling, the comparison to observations is limited to the T_{2m} .

To assess the simulation of the recent past climate the CRU TS 3.1 monthly gridded global land air temperature dataset from the Climate Research Unit (CRU) at the University of East Anglia (Mitchell and Jones 2005) is used. The CRU data was created by statistical interpolation from station observations to a regular terrestrial grid at a half-degree spatial resolution. This data set covers the period 1901–2009 AD.

Since the effect of increasing atmospheric aerosol concentrations since industrialisation is not taken into account in our simulations, the accuracy of the simulated climate is best assessed with data from a period prior to industrialisation. Direct observations of T_{2m} in Uppsala located within 50 km distance of Forsmark in south-central Sweden, covering the period 1722 AD to the present, are therefore utilized (http://www.smhi.se/hfa_coord/nordklim/).

2.7 Spatial interpolation

Global climate modelling is computationally expensive and the horizontal and vertical resolution of the simulated climate is therefore relatively low. The horizontal resolution of the LOVECLIM and CCSM4 models used in this study is c. 5.6° in latitude x 5.6° in longitude and 1.9° in latitude x 2.5° in longitude respectively. This spacing between gridpoints corresponds to c. 310 km and c. 122 km at 60°N respectively. The coarse resolution has two important implications for the simulated climate; 1) regional/local details of the climate are not described by the climate models and 2) the best estimate of the simulated climate in a specific location such as Forsmark must be assessed by interpolation or downscaling. In interpolation, only information from the low-resolution climate model simulation is used. The two most commonly used downscaling methods have traditionally been statistical and dynamical downscaling. In statistical downscaling, a model is developed for the region of interest, which statistically relates large-scale climate variables to regional and local variables under known conditions; then the output of a global climate model is input to this statistical model to approximate the corresponding regional and local climate. In dynamical downscaling, a regional climate model (RCM) is integrated over the region of interest, constrained by a global climate model at the lateral model domain boundaries. This method is computationally expensive and commonly used for comparison of a historical and a future period of one or a few decades. The added value of dynamical downscaling was recently questioned by Racherla et al. (2012), who compared dynamical downscaling with spatially interpolated AOGCM results for two decades in the 20th century. They found that the regional climate model improves upon the simulation of the climate change between the two decades, but only modestly so.

In the present study, dynamical downscaling is not used due to the computational cost. Instead, a simple type of statistical downscaling is performed. Spatial interpolation is combined with a bias correction to account for the lack of regional and local details in the global climate model results as described in Section 2.8.

The monthly mean Forsmark T_{2m} is obtained from climate model output and from the CRU data set using inverse distance weighting. Thus, the monthly mean Forsmark T_{2m} is obtained as a inverse distance weighted average of the four closest grid points. This interpolation is performed for the complete time series of monthly mean T_{2m} from CRU, LOVECLIM and CCSM4. For comparison, the observed T_{2m} in Uppsala (http://www.smhi.se/hfa_coord/nordklim/) and CRU T_{2m} (Mitchell and Jones 2005) spatially interpolated to Uppsala are displayed in Figure 2-4. The comparison is performed for years 1901–2000 AD, since CRU data is not available prior to 1901. The annual mean T_{2m} is 0.3°C higher in the interpolated CRU data than the observed. The monthly mean Uppsala T_{2m} derived from CRU data is 0.1°C to 0.6°C higher than the observed Uppsala T_{2m} . This difference exemplifies the error introduced using spatial interpolation.

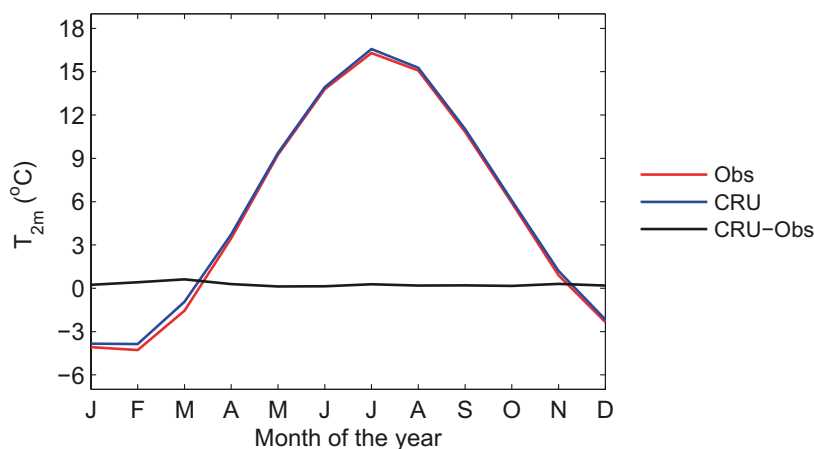


Figure 2-4. Monthly average T_{2m} ($^\circ\text{C}$) in Uppsala, averaged over years 1901–2000 AD, in the observations (red line; http://www.smhi.se/hfa_coord/nordklim/) and in CRU data spatially interpolated to Uppsala (blue line; Mitchell and Jones 2005). The difference between CRU data and the observations is also shown (black line).

2.8 Bias correction

Although both climate models used in this study produce a reasonably realistic modern climate, systematic biases exist between the simulated regional climate and the observed. The bias is due to the combination of incomplete knowledge of some of the physical processes, such as e.g. cloud formation, simplified parameterizations of unresolved physical and dynamical processes (e.g. precipitation and cloud formation, small-scale motions) and incomplete knowledge and unresolved boundary conditions (e.g. topography, bathymetry, land-sea distribution). Further, spatially interpolated variables are biased due to lack of detail in the coarse resolution global model results as discussed in the previous section.

The bias can be assessed for the recent past climate and for variables with a moderate spatial and temporal variability for which observations are available. It is probable that this bias is dependent on the state of the climate system, such that it would differ between, e.g., a simulation of the recent past and a simulation of the LGM climate. Due to lack of data, such climate state dependence in the bias is difficult to assess since validation data is only available for the last few decades to centuries. Therefore, in studies of the response of the simulated climate to changes in boundary and forcing conditions, such as e.g. in the latest IPCC report (Meehl et al. 2007), the bias is assumed (to first order) to be independent of the climate state. This strategy is adopted also in the present study. The bias is calculated separately for the LOVECLIM and CCSM4 models.

The bias is assessed from simulations of the pre-industrial (1751–1850 AD) climate. Since CRU data is only available starting in 1901 AD, the Uppsala station data is used to determine the bias in simulated T_{2m} in the Forsmark region. Further, the bias in the Forsmark region is determined for the location of Uppsala (59.86°N, 17.63°E) rather than Forsmark (60.41°N, 18.21°E). CRU data is used to illustrate the geographical distribution of the bias in the simulated climate.

2.8.1 LOVECLIM bias for Uppsala

For LOVECLIM, the bias in T_{2m} is assessed based on the comparison of the small initial value ensemble of three simulations described in Section 2.4.1 and the station data from Uppsala.

The bias calculation is performed for the period 1751–1850 AD, chosen to represent a pre-industrial period with relatively constant atmospheric greenhouse gas concentrations and small impact of anthropogenic aerosol emissions.

The evolution of the annual average, summer (June–August) and winter (December–February) T_{2m} in Uppsala in the three LOVECLIM simulations and the Uppsala station data is displayed in Figure 2-5 for the period 1751–1850. The variability in the simulated climate is smaller than in the observed, the standard deviation of annual average T_{2m} in Uppsala is 0.47°C in the LOVECLIM simulations as compared to 0.92°C in the Uppsala station data (both calculated for the period 1751–1850). Maximum (minimum) variability occurs in February (September) in the station data with standard deviation of monthly average T_{2m} 3.3°C (1.3°C) respectively. Maximum (minimum) variability occurs in April (July) in the LOVECLIM simulations with standard deviation of monthly average T_{2m} of 2.0°C (0.78°C) respectively. This difference between observed and simulated variability is explained by the low resolution of the model which cannot capture the regional variability. This bias is not corrected for.

The monthly mean T_{2m} in Uppsala in the three LOVECLIM simulations and in the Uppsala series, averaged over the period 1751–1850, is displayed in Figure 2-6. The ensemble average of the three LC_PI simulations for Uppsala T_{2m} is determined for each month of the year. This ensemble average ($\text{LOVECLIM}_{\text{UPPSALA}}$) is used to determine the monthly mean bias in Uppsala ($\text{BIAS}_{\text{LOVECLIM}}$) as

$$\text{BIAS}_{\text{LOVECLIM}} = \text{LOVECLIM}_{\text{UPPSALA}} - \text{OBSERVATIONS}_{\text{UPPSALA}}$$

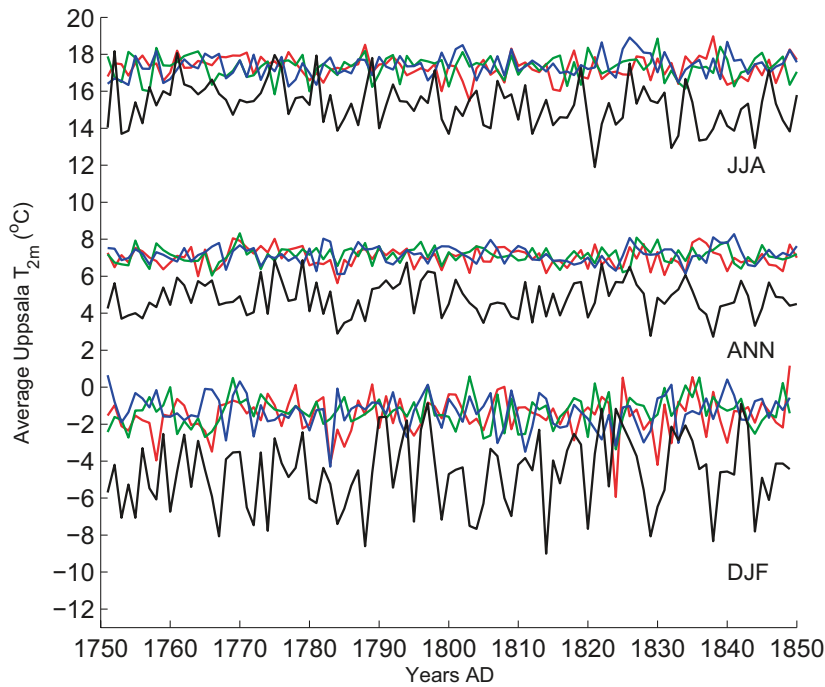


Figure 2-5. Annual average (ANN), June–August (JJA) and December–February (DJF) T_{2m} (°C) in Uppsala in the ensemble of three LOVECLIM simulations (red, blue and green) and in the Uppsala station data (black) for the period 1751–1850 AD. The LOVECLIM data in the figure is not bias-corrected.

The annual average bias is +2.3°C with a maximum of +4.4°C in March and a minimum of –0.2°C in September (Figure 2-6). To account for the bias, the monthly mean bias ($BIAS_{LOVECLIM}$) is subtracted from the LOVECLIM simulated T_{2m} interpolated to Forsmark in all simulations presented in this report.

As described in Section 2.4.1, a long equilibrium simulation of pre-industrial climate with constant forcing and boundary conditions was also performed with LOVECLIM. For comparison, monthly mean T_{2m} in Uppsala in this simulation is also displayed in Figure 2-6. The annual mean difference in Uppsala T_{2m} between the LC_PI ensemble and the equilibrium pre-industrial climate simulation is 0.13°C. The maximum absolute difference of 0.53°C occurs in October. These differences in the simulated annual cycle can be compared to the differences among the three LC_PI ensemble-members. The monthly mean Uppsala T_{2m} difference between the warmest simulation and the coldest simulation is therefore determined for each month of the year. This difference varies in the range 0.049°C to 0.50°C with the largest difference found in February with an annual average difference of 0.14°C. Based on this comparison, it is concluded that the average annual cycle is not significantly different in the LC_PI ensemble average as compared to the equilibrium pre-industrial simulation. Further, it is concluded that the uncertainty in the monthly average T_{2m} bias is less than 1°C.

The bias in T_{2m} in LOVECLIM varies with location and season. The global land temperature bias for LOVECLIM, determined as the difference between LOVECLIM simulated T_{2m} and CRU observations for the period 1901–1950 AD, is shown in Figure 2-7. A warm bias is found over northern mid- and high latitude continents all year around, and a cold bias is found in mountainous and desert regions.

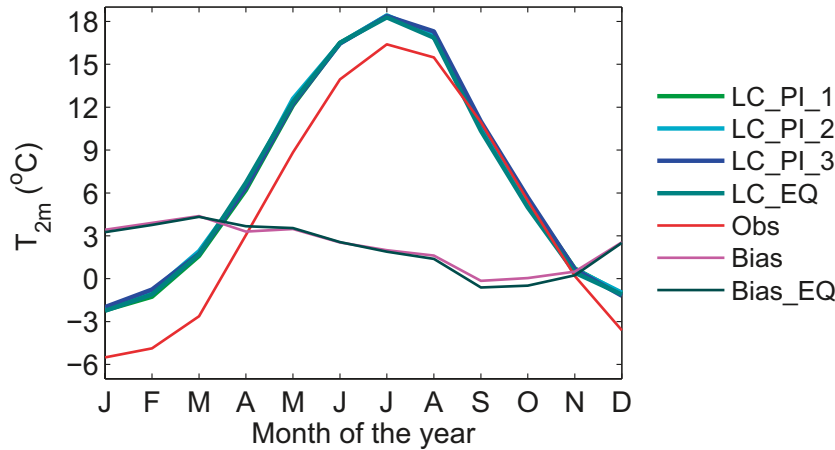


Figure 2-6. Monthly average T_{2m} ($^{\circ}\text{C}$) in Uppsala in the three pre-industrial LOVECLIM simulations (green, cyan and blue) and in the observations from Uppsala (red) averaged over the period 1751–1850 AD. The bias in the monthly average T_{2m} in Uppsala in the pre-industrial LOVECLIM simulations, i.e. the difference between the LOVECLIM ensemble average and the observations from Uppsala, is also shown (magenta). For comparison, monthly average T_{2m} ($^{\circ}\text{C}$) in Uppsala in the equilibrium pre-industrial LOVECLIM simulation (dark green) and the associated bias, i.e. the difference between this simulation and the observations from Uppsala, is also shown (thin dark green).

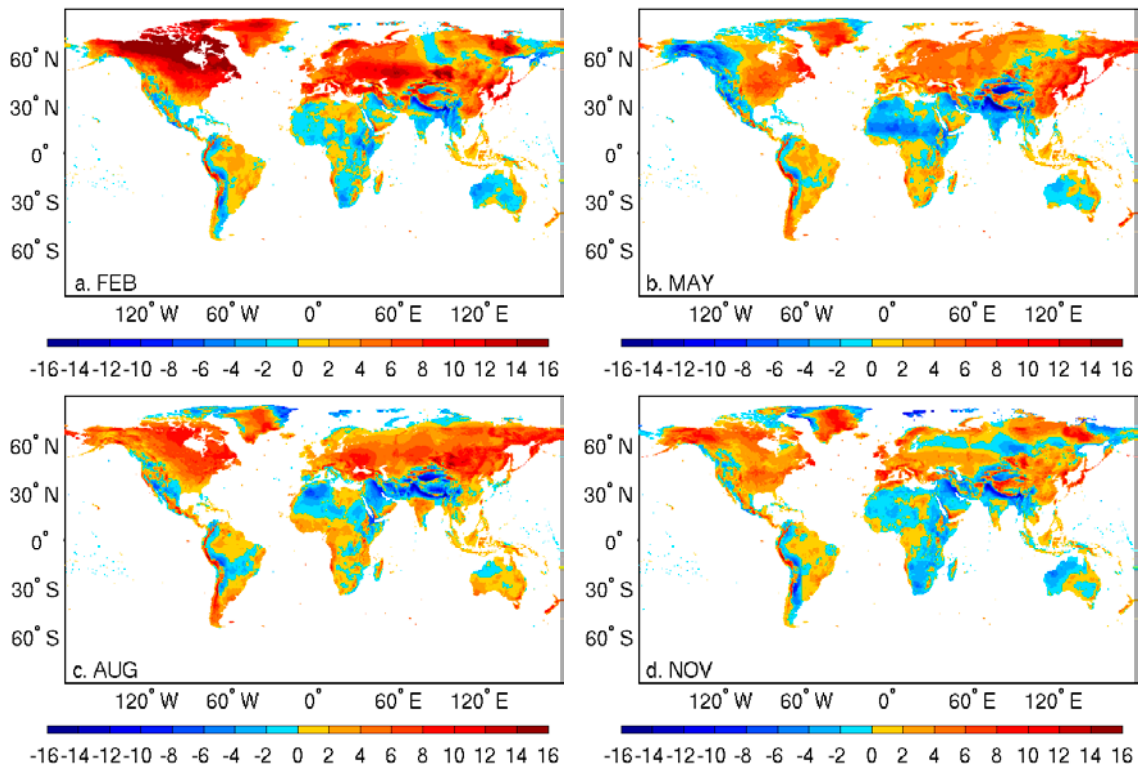


Figure 2-7. The difference between the LOVECLIM simulated T_{2m} ($^{\circ}\text{C}$) and CRU observations for a) February, b) May, c) August and d) November for the period 1901–1950 AD. The LOVECLIM data was interpolated to the CRU $0.5^{\circ} \times 0.5^{\circ}$ latitude-longitude grid.

2.8.2 CCSM4 bias for Uppsala

For CCSM4, the bias in T_{2m} is assessed based on the comparison of a 2,000 year simulation of pre-industrial climate and the station data from Uppsala for the period 1751–1850 AD. The climate simulation was run at the same resolution as the simulations of the two future periods and with all forcing and boundary conditions (atmospheric greenhouse gas concentrations, aerosol concentrations, orbital parameters) set to be representative of 1850 AD. This simulation is a continuation of a simulation run at NCAR for 500 model years (Gent et al. 2011), and the last 1,000 years are analysed to determine the simulated mean climate and climate variability.

The evolution of the annual average, summer and winter T_{2m} in Uppsala in the last 1,000 years of the CCSM4 pre-industrial climate simulation is displayed in Figure 2-8. Due to higher resolution and more sophisticated descriptions of parameterized processes, CCSM4 simulates the variability in better agreement with the observations than LOVECLIM. The standard deviation of annual average T_{2m} in Uppsala is 0.92°C in the CCSM4 simulation (calculated for the last 1,000 years of the simulation) which is the same as in the Uppsala station data (calculated for the period 1751–1850). Maximum (minimum) variability occurs in February (September) in the station data with standard deviation of monthly average T_{2m} 3.3°C (1.3°C) respectively. Maximum (minimum) variability occurs in February (September) in the CCSM4 simulations with standard deviation of monthly average T_{2m} of 2.8°C (1.3°C) respectively.

The annual cycle of T_{2m} (i.e. monthly averages) in Uppsala in the pre-industrial CCSM4 simulation, averaged over 1,000 model years, and in the observed Uppsala series, averaged over the period 1751–1850 AD, is displayed in Figure 2-9. The annual average bias is $+0.95^{\circ}\text{C}$ with a maximum of $+2.38^{\circ}\text{C}$ in January and a minimum of -0.35°C in June (Figure 2-9). The bias in the annual cycle simulated in Uppsala is determined as

$$\text{BIAS}_{\text{CCSM4}} = \text{CCSM4}_{\text{UPPSALA}} - \text{OBSERVATIONS}_{\text{UPPSALA}}$$

To account for the bias, the annual cycle bias ($\text{BIAS}_{\text{CCSM4}}$) is subtracted from the CCSM4 simulated T_{2m} interpolated to Forsmark in all simulations presented in this report.

To estimate the uncertainty in the monthly average T_{2m} bias, the simulated annual cycle is calculated for ten consecutive 100-year periods. For each month of the year, the maximum monthly average difference between any 100-year period and the 1,000 year average was determined. The maximum difference varies in the range 0.52 – 0.96°C . This maximum difference, also displayed in Figure 2-9, is taken as a measure of the uncertainty in the simulated monthly average T_{2m} .

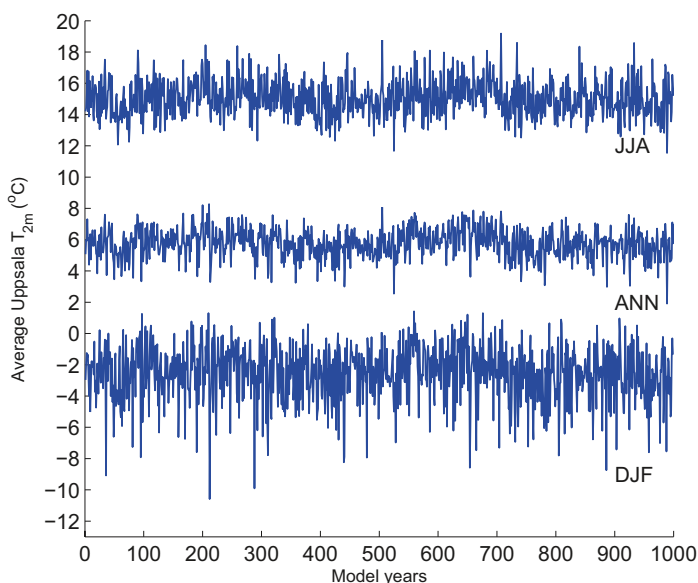


Figure 2-8. Annual average (ANN), June–August (JJA) and December–February (DJF) T_{2m} ($^{\circ}\text{C}$) in Uppsala in the pre-industrial CCSM4 simulation. Note that the simulation was run with constant boundary and forcing conditions, thus describing the internal climate variability under these conditions, but not the climate evolution. The data in the figure is not bias-corrected.

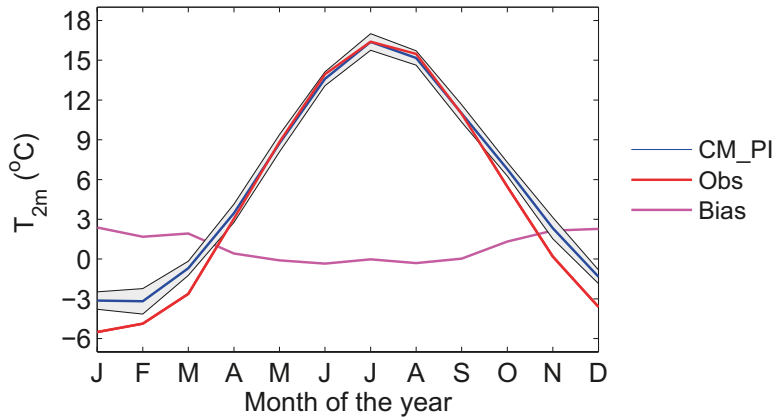


Figure 2-9. Monthly average T_{2m} (°C) in Uppsala in the pre-industrial CCSM4 simulation (blue) averaged over 1,000 model years and in the observations from Uppsala (red) averaged over the period 1751–1850 AD. For CCSM4, the uncertainty in the simulated monthly average T_{2m} is shown (see text; grey area). The bias in the monthly average T_{2m} in Uppsala in the pre-industrial CCSM4 simulation, i.e. the difference between the 1,000-year CCSM4 average and the observations from Uppsala, is also shown (magenta).

3 Results and discussion

The results of the climate and permafrost model simulations are presented in the following. To account for systematic errors in the simulated climate, the anomaly with respect to the pre-industrial climate is presented. The anomaly is thus defined as the difference between a specific simulation and the corresponding pre-industrial simulation performed with the same climate model. Forsmark T_{2m} is bias-corrected, as described in Section 2.8, to account for systematic errors in the simulated climate. Only bias-corrected Forsmark T_{2m} is presented in this section.

3.1 Equilibrium simulations for 17 ka AP and 54 ka AP

As described in Section 2.4.2, the climate in the future periods of minimum summer insolation at high northern latitudes at 17 ka and 54 ka AP was analysed in a set of simulations. For each future period (17 ka AP and 54 ka AP), seven LOVECLIM simulations with different atmospheric CO_2 concentration were performed. Further, one CCSM4 simulation was performed for each of the two future periods. All climate simulations performed are listed in Table 2-2.

3.1.1 Simulated global climate

LOVECLIM

The global annual average T_{2m} in the LC_PI ensemble is 14.9°C, which is c. 1.2°C higher than the IPCC estimate for the period 1800–1850 (IPCC 2007). The global annual average T_{2m} in the equilibrium simulations for 17 ka AP and 54 ka AP is lower than in the LC_PI ensemble for atmospheric CO_2 concentrations of 180–280 ppmv (Figure 3-1). To illustrate the effect of the insolation difference between the 17 and 54 ka AP periods and the pre-industrial period, the simulations with atmospheric CO_2 concentration of 280 ppmv (LC_17k_280 and LC_54k_280, Table 2-1) can be utilized. These simulations use the same atmospheric greenhouse gas concentrations (CO_2 , CH_4 and N_2O) as the LC_PI ensemble, but differ from the LC_PI ensemble in the orbital parameters that determine the latitudinal and seasonal distribution of insolation. Although the latitudinal and seasonal insolation distribution differs substantially between the 17 ka AP and 54 ka AP periods and the pre-industrial (Figure 2-1), the global annual average insolation difference is small (–0.23 and –0.16 respectively). This is reflected in the simulated global annual average T_{2m} , which is 0.12°C and 0.26°C lower in LC_17k_280 and LC_54k_280 than in the LC_PI ensemble.

As described in Section 1.1.3, (Pimenoff et al. 2011) employed the CLIMBER-2 model with SICOPOLIS to study the future evolution of climate in Olkiluoto, the site chosen for the Finnish repository for spent nuclear fuel. They simulated the coming 120 ka in four simulations with constant atmospheric CO_2 concentration of 280 ppmv and 400 ppmv, respectively. An ensemble of two simulations was produced for each CO_2 concentration. To compare the results of the present study to their results, anomalies with respect to the respective simulated pre-industrial climate are determined. The annual global average near-surface temperature anomaly is c. –0.5°C and c. –1°C at 17 ka AP and 54 ka AP respectively in their simulation with a constant atmospheric CO_2 concentration of 280 ppmv, see Figure 26 in Pimenoff et al. (2011). These temperatures are significantly colder than the global annual average temperature anomalies simulated with LOVECLIM which are –0.12°C and –0.26°C at 17ka AP and 54 ka AP respectively (Figure 3-1). This difference is associated with global cooling due to growth of Northern Hemisphere ice sheets in the CLIMBER-2 simulations. This process is not included in the LOVECLIM simulations. The annual global average anomaly is c. +1°C and c. +0.75°C at 17 ka AP and 54 ka AP respectively in the CLIMBER-2 simulations with a constant atmospheric CO_2 concentration of 400 ppmv. These temperatures are closer to the global annual average temperature anomalies simulated here with LOVECLIM of +0.88°C and +0.70°C at 17ka AP and 54 ka AP respectively (Figure 3-1). The better agreement is associated with substantially less influence of Northern Hemisphere ice sheet growth in the CLIMBER-2 simulations with atmospheric CO_2 concentration of 400 ppmv.

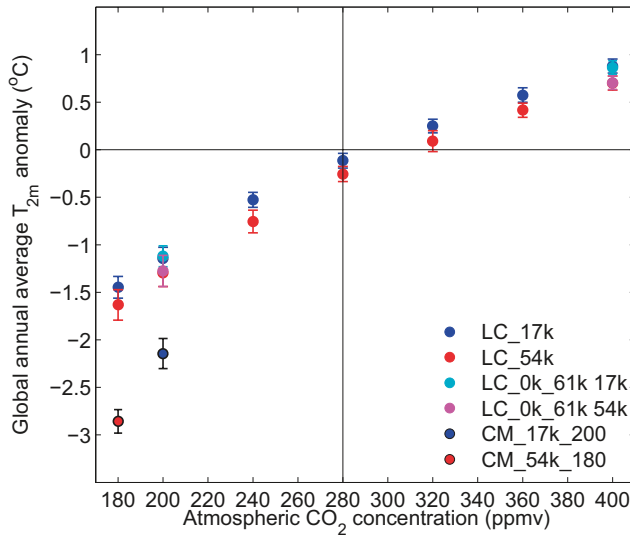


Figure 3-1. Global annual average T_{2m} ($^{\circ}\text{C}$) anomaly with respect to the respective simulated pre-industrial climate for LOVECLIM and CCSM4 equilibrium simulations for 17 ka AP (blue circles) and 54 ka AP (red circles). Global annual average T_{2m} ($^{\circ}\text{C}$) anomaly with respect to the LC_PI ensemble for the LOVECLIM transient simulations, discussed in Section 3.2, is also displayed (cyan and magenta circles). The pre-industrial atmospheric CO_2 concentration is indicated with a vertical line. The climate simulations are described in Section 2.4 and listed in Table 2-2.

Influence of insolation distribution difference

To illustrate the effect of the difference in the latitudinal and seasonal distribution of insolation between the 17 ka AP and 54 ka AP periods and the pre-industrial (Figure 2-1), the zonal average T_{2m} anomaly w r t the LC_PI ensemble is shown in Figure 3-2. T_{2m} is reduced in high northern latitudes in the LC_17k_280 and LC_54k_280 simulations in all months of the year, with the strongest reductions in winter for LC_17k_280 and in autumn and winter for LC_54k_280. Insolation at these latitudes is reduced in spring at 17 ka AP and in spring and summer in 54 ka AP (Figure 2-1), why these results indicate climate system feedbacks on the insolation distribution difference. T_{2m} is reduced also in high southern latitudes in both simulations as a result of reduced austral spring and summer insolation. Although the insolation anomaly is weaker in the northern than in the southern high latitudes, the maximum Northern Hemisphere T_{2m} anomaly is of the same order as, or stronger than, in the Southern Hemisphere. This inter-hemispheric difference is associated with a stronger surface albedo (Figure 3-3) due to sea ice expansion in the northern high latitudes.

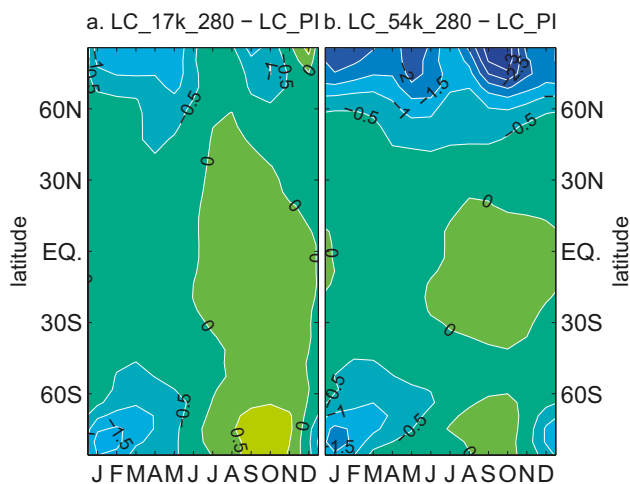


Figure 3-2. Zonal monthly average T_{2m} ($^{\circ}\text{C}$) in LOVECLIM simulations with atmospheric CO_2 concentration 280 ppmv. (a.) LC_17k_280 minus LC_PI and (b.) LC_54k_280 minus LC_PI .

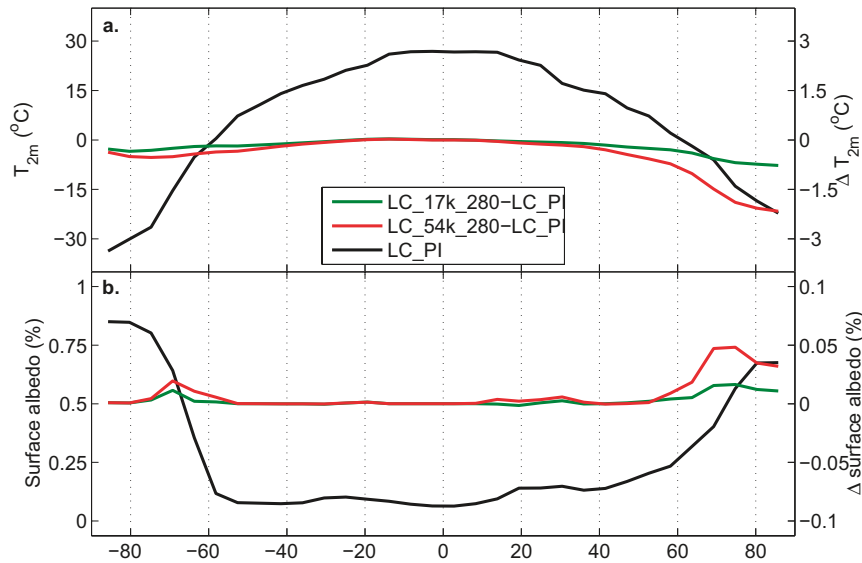


Figure 3-3. Annual zonal average of (a.) T_{2m} ($^{\circ}\text{C}$) and (b.) surface albedo (%) in the LC_PI ensemble (black line). The differences (right axis), Δ , LC_17k_280 minus LC_PI (green line) and LC_54k_280 minus LC_PI (red line) are also shown.

Annual average T_{2m}

The combined effect of the atmospheric CO_2 and insolation distribution differences between the 17 ka AP and 54 ka AP periods and the pre-industrial period on near-surface temperature as simulated with LOVECLIM is illustrated in Figure 3-4. The annual average T_{2m} in the LC_PI ensemble is also displayed in Figure 3-4. Northern high latitude cooling occurs in response to the insolation distribution differences, as illustrated by the LC_17k_280 and LC_54k_280 simulations. As discussed above, this effect is stronger in the 54 ka AP period due to a stronger high latitude insolation anomaly (compare left and right panels in Figure 3-4). As expected, a globally colder climate results from substantially decreased atmospheric CO_2 concentrations and a globally warmer climate results from substantially increased atmospheric CO_2 concentrations. The spatial pattern of this component includes a strong Arctic, and to a lesser extent Antarctic, cooling. This pattern, usually termed polar amplification, bears resemblance to the warming simulated in future climate projections (Meehl et al. 2007).

Oceanic circulation

The effect of the atmospheric CO_2 and insolation distribution differences between the 17 ka AP and 54 ka AP periods and the pre-industrial period on the Atlantic meridional overturning circulation as simulated with LOVECLIM is illustrated in Figure 3-5. The maximum overturning strength at 27°N is c.15 Sv in LC_PI, which can be compared to recent observations of the overturning at 26.5°N of 18 Sv (Cunningham et al. 2007). The strength of the overturning cell is not significantly different in the LOVECLIM simulations with an atmospheric CO_2 concentration of 280 ppmv or more than in the LC_PI ensemble. A weakening, and to some extent northward shift, of the maximum overturning strength in the North Atlantic is however simulated in the LC_17k_180 and LC_54k_180 simulations.

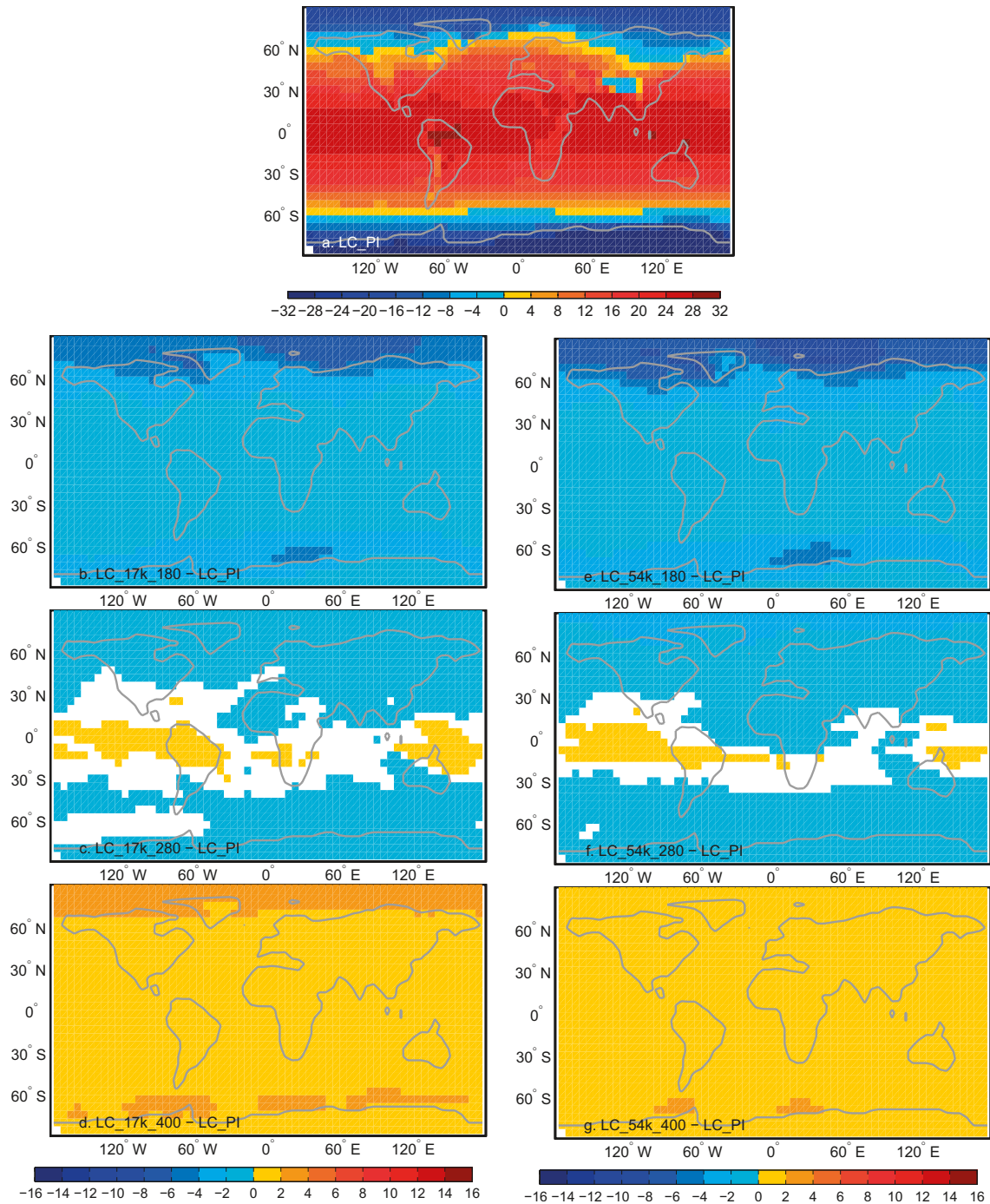


Figure 3-4. (a.) Annual average T_{2m} ($^{\circ}\text{C}$) in the LC_PI ensemble average (averaged over the period 1751–1850; upper panel). The difference between the (b.) LC_17k_180, (c.) LC_17k_280 and (d.) LC_17k_400 simulations and the PI ensemble average. The difference between the (e.) LC_54k_180, (f.) LC_54k_280 and (g.) LC_54k_400 simulations and the PI ensemble average. The LC_17k and LC_54k results are averaged over model years 1,001–3,000 as in Figure 3-12. Note that the LC_PI data is **not** bias-corrected. Only differences that are statistically significant at the 5% level are shown.

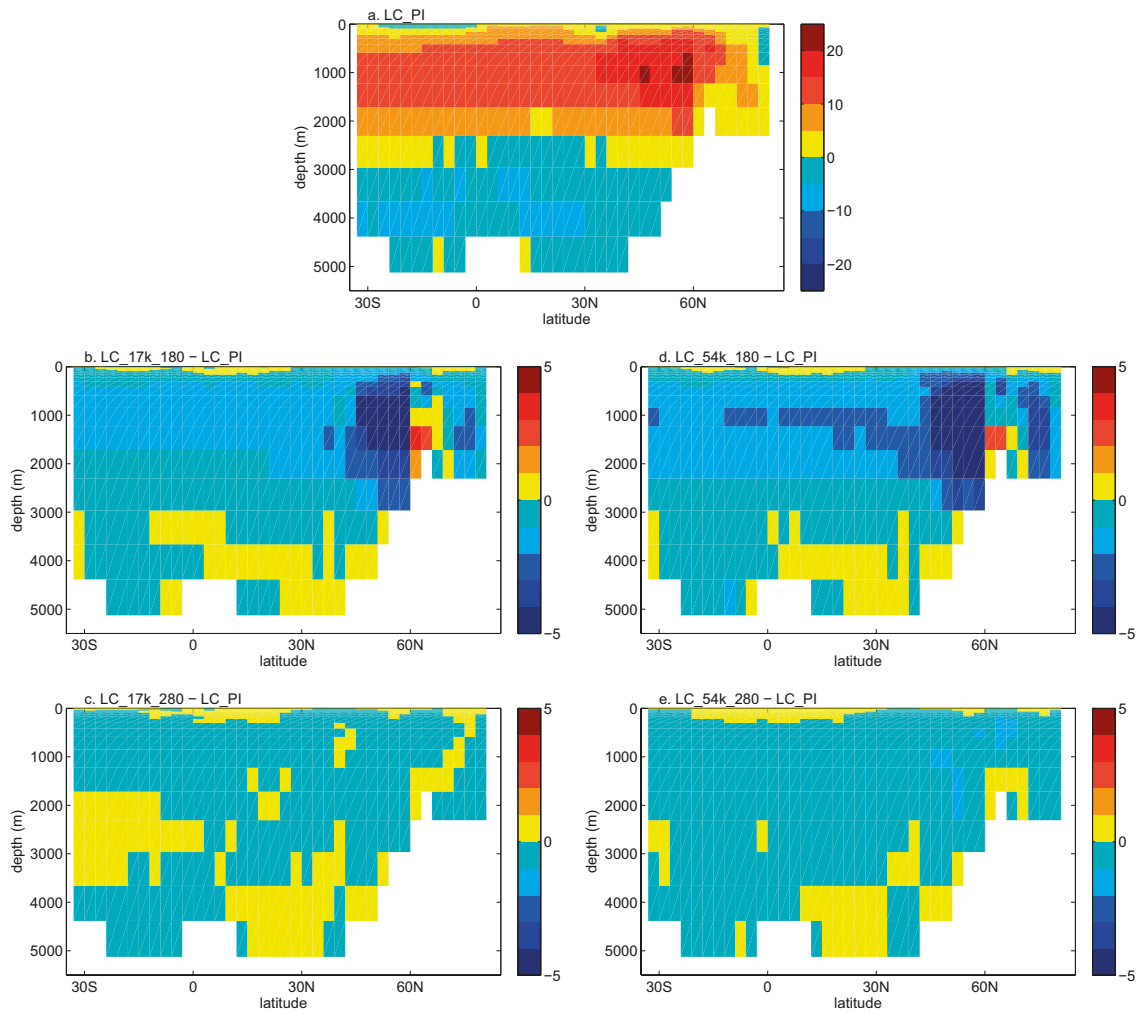


Figure 3-5. The annual average Atlantic meridional overturning circulation (Sv) in (a.) the LC_PI ensemble average. The difference (b.) LC_17k_180 minus LC_PI, (c.) LC_17k_280 minus LC_PI, (d.) LC_54k_180 minus LC_PI and (e.) LC_54k_280 minus LC_PI.

Annual cycle in T_{2m}

The effect of the atmospheric CO_2 and insolation distribution differences between the 17 ka AP and 54 ka AP periods and the pre-industrial period on the zonal monthly average T_{2m} is illustrated here with the LC_17k_200 and LC_54k_180 simulations. These are chosen for comparison to the CCSM4 simulations which were performed with the same forcing conditions (see Section 2.4). The zonal monthly average T_{2m} anomaly w r t the LC_PI ensemble is shown in Figure 3-6. T_{2m} is reduced in high northern latitudes in all months of the year with maximum cooling in September-May. The latitude-month distribution of the anomalies is similar to that simulated with only the insolation difference (compare Figure 3-2), but with a strengthening of the Arctic amplification.

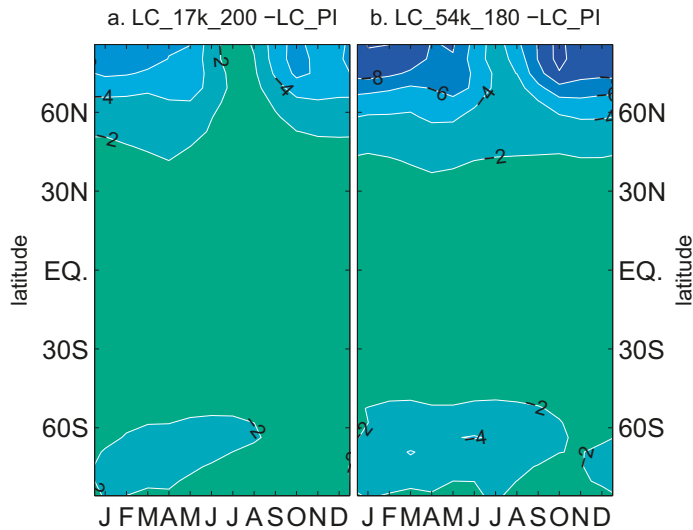


Figure 3-6. Zonal monthly average T_{2m} . ($^{\circ}\text{C}$) (a.) LC_17k_200 minus LC_PI and (b.) LC_54k_180 minus LC_PI.

CCSM4

Due to the computational cost of the CCSM4 simulations, each simulation was only run for a total of 1,590 and 1,660 model years for CM_17k_200 and CM_54k_180 respectively. The last 300 model years of each simulation is used for the present analysis. To assess the remaining drift in the simulated climate, the linear trend in annual global average T_{2m} and abyssal ocean temperature (displayed in Figure 3-7 and Figure 3-8) is determined for the last 300 model years following Brandefelt and Otto-Bliesner (2009). The linear trend in annual global average T_{2m} is -0.042°C and -0.051°C per century in the CM_17k_200 and CM_54k_180 simulations, respectively. The linear trend in annual global average abyssal ocean (below 2,000 meters depth) temperature is -0.056°C and -0.063°C per century in the CM_17k_200 and CM_54k_180 simulations, respectively. These trends are 3–5 times larger than in the LC_PI simulation (-0.011°C in T_{2m} and -0.020°C in abyssal ocean potential temperature), which indicates that the simulated climate has not fully reached a new quasi-equilibrium in the CM_17k_200 and CM_54k_180 simulations.

The global annual average T_{2m} in the CM_PI simulation is 13.5°C , which is c. 0.2°C lower than the IPCC estimate for the period 1800–1850 (IPCC 2007). The global annual average T_{2m} is lower than in CM_PI in both CCSM4 simulations due to the combination of low atmospheric CO_2 concentrations of 180 ppmv and 200 ppmv respectively and changes in the insolation distribution (Figure 3-1). For CCSM4, it is not possible to determine the individual importance of the changed forcing conditions, atmospheric CO_2 concentration and insolation distribution, since no simulations with changes in only insolation were performed.

In agreement with the low equilibrium climate sensitivity (ECS) of LOVECLIM as compared to CCSM4, discussed in Section 2.2, the global annual average T_{2m} anomaly with respect to the PI simulation is almost twice as large in the CCSM4 simulations as compared to the LOVECLIM simulations.

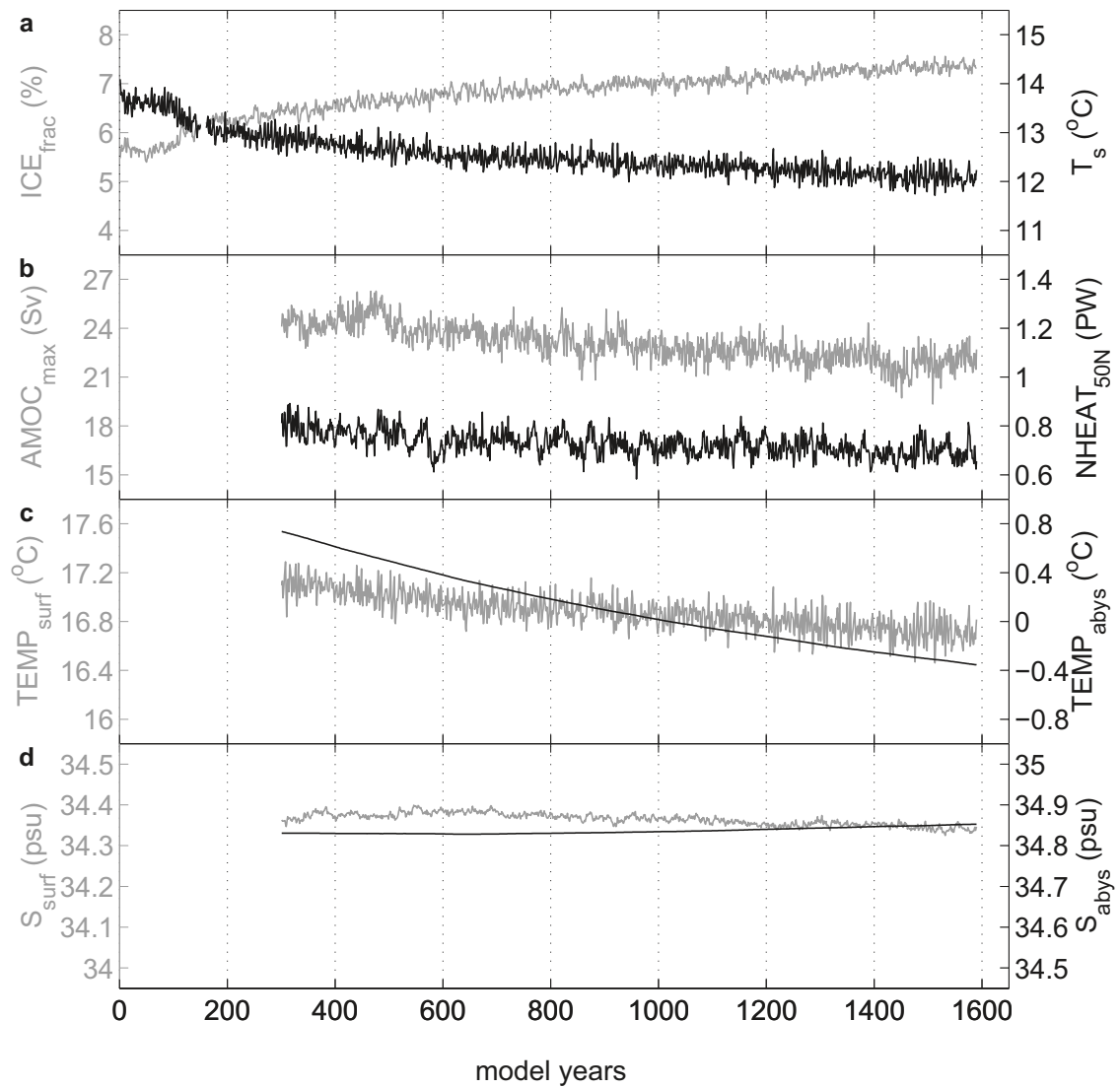


Figure 3-7. Global annual averages in the CCSM4 simulation CM_17k_200. (a.) T_{2m} ($^{\circ}\text{C}$) and sea ice concentration (%), (b.) maximum AMOC streamfunction (Sv) and northward heat transport at 50°N (PW), (c.) surface (above 200 meters depth) and abyssal (below 2,000 meters depth) ocean potential temperature ($^{\circ}\text{C}$) and (d.) surface (above 200 meters depth) and abyssal (below 2,000 meters depth) ocean salinity (psu). Data from the ocean model was not saved for model years 1–300.

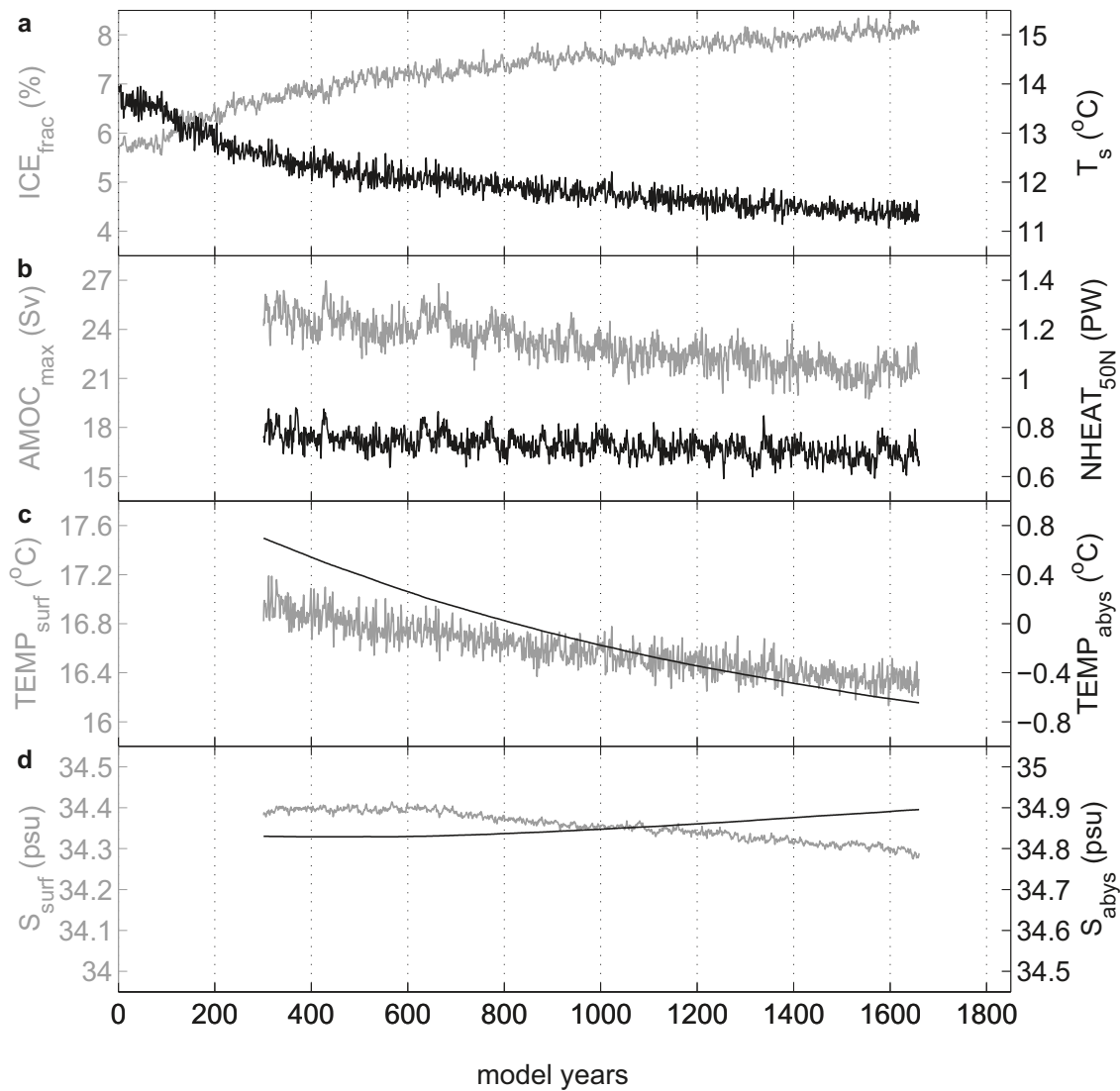


Figure 3-8. Global annual averages in the CCSM4 simulation CM_54k_180. (a.) Sea ice concentration (%) and T_{2m} ($^{\circ}\text{C}$), (b.) maximum AMOC streamfunction(Sv) and northward heat transport at 50°N (PW), (c.) surface (above 200 meters depth) and abyssal (below 2,000 meters depth) ocean potential temperature ($^{\circ}\text{C}$) and (d.) surface (above 200 meters depth) and abyssal (below 2,000 meters depth) ocean salinity (psu). Data from the ocean model was not saved for model years 1–300.

Annual average T_{2m}

The annual average T_{2m} in both CM_17k_200 and CM_54k_180 is significantly lower than in the CM_PI simulation at all locations (Figure 3-9). The strongest cooling is found in northern high latitudes and over the Southern Ocean. This polar amplification pattern bears resemblance to the warming simulated in future climate projections (Meehl et al. 2007).

As indicated in the global annual average results, the CCSM4 simulations give a substantially colder climate than the LOVECLIM simulations under the same orbital forcing conditions and atmospheric CO_2 concentrations. This difference is most pronounced in northern high latitudes. The regional pattern of the anomaly w r t the respective PI simulation differs between the CCSM4 and LOVECLIM simulations (compare Figure 3-4e. and Figure 3-9c.). The strongest cooling occurs in Barents Sea and Alaska in LC_54k_180 and in Alaska, Norwegian and Barents Seas in CM_54k_180. This inter-model-difference is associated with the coupled dynamics of the atmosphere, ocean and sea ice, a topic that is outside the scope of the present study.

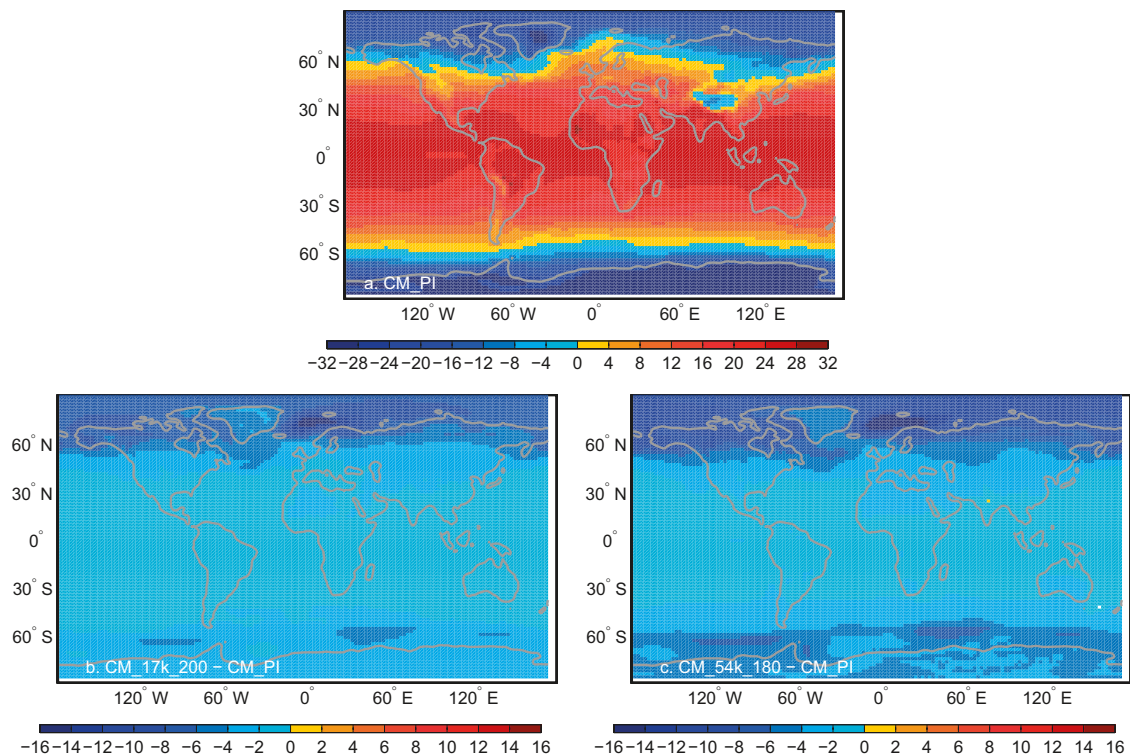


Figure 3-9. (a.) Annual average T_{2m} ($^{\circ}\text{C}$) in the CM_PI simulation. The difference between the (b.) CM_17k_200 and (c.) CM_54k_180 simulations and CM_PI . The results are averaged over the last 300 model years for each simulation. Note that the CM_PI data is not bias-corrected. The differences are statistically significant at the 5% level in both simulations.

Oceanic circulation

The effect of the atmospheric CO_2 and insolation distribution differences between the 17 ka AP and 54 ka AP periods and the pre-industrial period on the Atlantic meridional overturning circulation as simulated with CCSM4 is illustrated in Figure 3-10. There is a decrease in maximum AMOC strength over time in all the CCSM4 simulations. To compare the long-term decrease in the different simulations, 300-year averages of maximum AMOC strength were determined for model years 301–600 and 1291–1590 for the CM_PI , CM_17k_200 and CM_54k_180 simulations. The time intervals were chosen such that data exist from all three simulations. For model years 301–600, the maximum AMOC strength is quite similar (24.5, 24.3 and 24.4 Sv in the CM_PI , CM_17k_200 and CM_54k_180 simulations respectively). After another c. 1,000 model years, the maximum AMOC strength has decreased faster in the cold CM_17k_200 and CM_54k_180 simulations than in CM_PI . For model years 1,291–1,590, the maximum AMOC strength is 23.2, 22.0 and 21.6 Sv in the CM_PI , CM_17k_200 and CM_54k_180 simulations respectively.

For the pre-industrial climate simulations, LC_PI and CM_PI give similar maximum strengths for the AMOC, with c. 21 Sv in LC_PI and c. 23 Sv in CM_PI . The simulated circulation is also similar in the two models, with the maximum more confined to the North Atlantic in LC_PI than in CM_PI . In CCSM4 the response to the differences in forcing conditions between the future periods 17 ka AP and 54 ka AP is a weakening of clock-wise upper ocean circulation in the North Atlantic associated with the sea ice expansion. This weakening is also found in the LOVECLIM simulations as compared to LC_PI (see Figure 3-5). For CCSM4, the counter-clockwise bottom circulation is strengthened. This strengthening is not simulated with LOVECLIM.

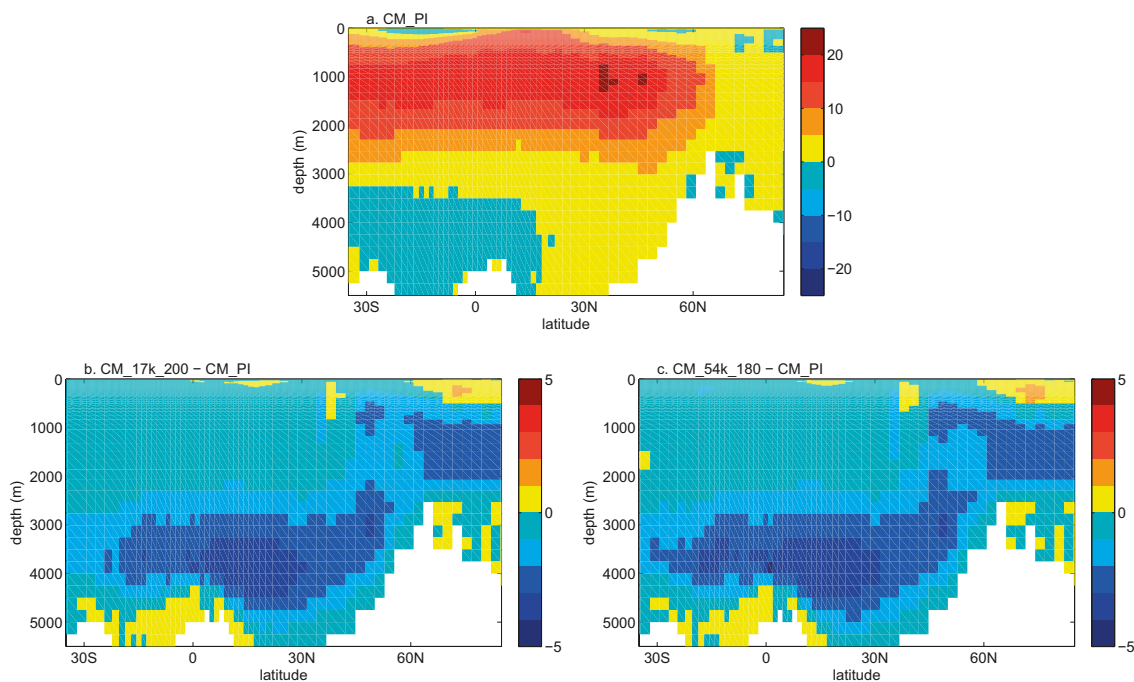


Figure 3-10. The annual average Atlantic meridional overturning circulation (Sv) in the CM_PI simulation (a.). The anomaly w r t the CM_PI ensemble for (b.) CM_17k_200, and (c.) CM_54k_180. The results are averaged over model years 1,291–1,590 for each simulation.

Annual cycle in T_{2m}

For comparison to the LOVECLIM simulations, the zonal monthly average T_{2m} anomaly w r t CM_PI is shown in Figure 3-11 for the CM_17k_200 and CM_54k_180 simulations. T_{2m} is reduced in high northern latitudes in all months of the year with maximum cooling in September-May. The latitude-month distribution of the anomalies is similar to that simulated with LOVECLIM (compare Figure 3-6).

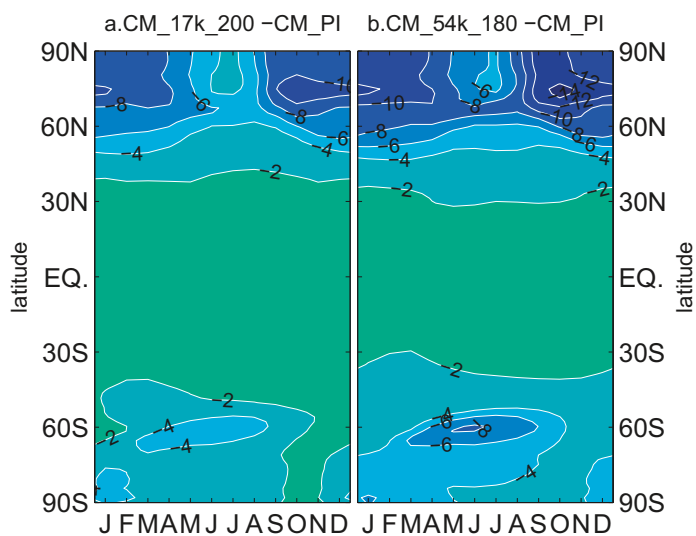


Figure 3-11. Zonal monthly average T_{2m} ($^{\circ}\text{C}$) anomaly w r t CM_PI for the CCSM4 equilibrium simulations CM_17k_200 (left panel) and CM_54k_180 (right panel).

3.1.2 Simulated Forsmark climate

LOVECLIM

Annual average T_{2m} in Forsmark in the set of LOVECLIM simulations with constant forcing and boundary conditions is displayed in Figure 3-12 as a function of the atmospheric CO_2 concentration. In accordance with the global average T_{2m} (Figure 3-1), the annual average T_{2m} in the Forsmark region decreases with decreasing atmospheric CO_2 concentration. Furthermore, for a given atmospheric CO_2 concentration, the annual average T_{2m} in Forsmark is colder in the 54 ka AP than the 17 ka AP simulated climate as a result of decreased summer insolation (Figure 2-1).

The results presented here can be compared to the CLIMBER-2 – SICOPOLIS simulations described in Section 1.1.3 (Pimenoff et al. 2011). Fennoscandian T_{2m} is c. $-5.9^\circ C$ to $-2.3^\circ C$ and c. $-6.8^\circ C$ to $-4.1^\circ C$ at 17 ka AP and 54 ka AP respectively in their simulations with a constant atmospheric CO_2 concentration of 280 ppmv (see their Figure 26). Pimenoff et al. (2011) also perform a statistical downscaling of the coarse resolution CLIMBER-2 – SICOPOLIS results for Oliklouto. Downscaled Oliklouto T_{2m} is c. $-10^\circ C$ and c. $-1.0^\circ C$ to $-7.1^\circ C$ at 17 ka AP and 54 ka AP respectively in their simulations with a constant atmospheric CO_2 concentration of 280 ppmv (see their Figure 27). The low temperature (and uncertainty) is associated with the proximity of the Fennoscandian ice sheet to the site in these simulations. These temperatures are significantly colder than the Forsmark T_{2m} simulated here with LOVECLIM of $+4.3^\circ C$ and $+3.9^\circ C$ at 17ka AP and 54 ka AP respectively (Figure 3-12). This difference is associated with global cooling due to growth of Northern Hemisphere ice sheets in the CLIMBER-2 simulations with atmospheric CO_2 concentration of 280 ppmv. This process is not included in the LOVECLIM simulations.

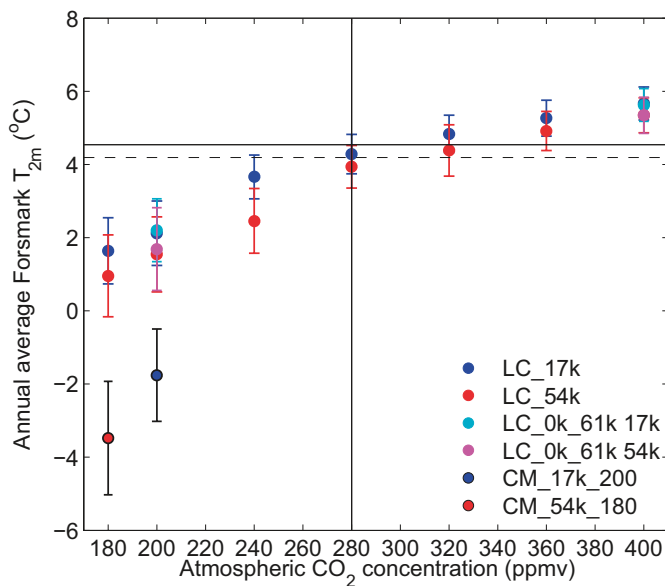


Figure 3-12. Annual average bias-corrected T_{2m} ($^\circ C$) in Forsmark in the LOVECLIM and CCSM4 simulations with constant forcing and boundary conditions for orbital years 17 ka AP (blue circles) and 54 ka AP (red circles). Annual average bias-corrected T_{2m} for the LOVECLIM transient simulations, discussed in Section 3.2, is also displayed (cyan and magenta circles). T_{2m} is shown as a function of the atmospheric CO_2 concentration. The standard deviation of the annual average bias-corrected T_{2m} in Forsmark is indicated as error bars. The annual average bias-corrected T_{2m} in Forsmark in the LC_PI ensemble ($+4.54^\circ C$; horizontal black line) and in CM_PI ($+4.19^\circ C$; horizontal black dashed line) is indicated. The pre-industrial atmospheric CO_2 concentration is indicated with a vertical line. The climate simulations are described in Section 2.4 and listed in Table 2-2.

Fennoscandian T_{2m} is c. 0.9–2.3°C and c. 0°C at 17 ka AP and 54 ka AP respectively in their simulations with a constant atmospheric CO₂ concentration of 400 ppmv (see their Figure 26). Downscaled Olkiluoto T_{2m} is c. +5.5–6°C and c. +5–6°C at 17 ka AP and 54 ka AP respectively in their simulations with a constant atmospheric CO₂ concentration of 400 ppmv (see their Figure 28). We speculate that the Fennoscandian temperature is lower than Olkiluoto temperature partly due to the inclusion of ice sheet covered areas which do not influence Olkiluoto temperature. The downscaled Olkiluoto T_{2m} is close to the Forsmark T_{2m} simulated here with LOVECLIM of +5.7°C and +5.3°C at 17 ka AP and 54 ka AP respectively (Figure 3-12). The improved agreement for the simulations with high atmospheric CO₂ concentration is associated with substantially less influence of Northern Hemisphere ice sheet growth in these CLIMBER-2 – SICOPOLIS simulations than for the case with low atmospheric CO₂ concentration.

Intra-centennial variability

To investigate the full potential of permafrost development in Forsmark, the potential importance of intra-centennial variability for the climate in Forsmark was analysed. In order to make a pessimistic choice for the analysis of permafrost development, the coldest simulations were chosen for this analysis. Thus, the simulations with atmospheric CO₂ concentration of 180 ppmv and 200 ppmv were extended to a total length of 6,000 model years both for the 17 ka AP and 54 ka AP period.

The annual average T_{2m} in Forsmark exhibits variability on annual, decadal and centennial timescales (Figure 3-13). The variability on inter-centennial timescales is significant for the simulations with 180–240 ppmv atmospheric CO₂ in which episodes of a few centuries occur with ~1°C colder or warmer than average T_{2m} . Further, the amplitude of the variations is stronger in the 54ka AP simulations than in the 17 ka AP simulations. This variability is associated with variability in the Atlantic meridional overturning circulation, as shown in Figure 3-9. The maximum AMOC stream-function below 500 meters depth in the LC_54k_180 and LC_54k_280 simulations is displayed. To illustrate the surface climate variations associated with these variations in the oceanic circulation, the annual average T_{2m} in a period of high maximum AMOC stream function (model years 1681–1780; indicated with a red bar in Figure 3-9) is compared to a period of low AMOC (model years 1481–1580; indicated with a blue bar in Figure 3-9). The largest T_{2m} differences occur in the Nordic and Barents Seas (Figure 3-15) and are associated with differences in surface albedo and sea ice extent (not shown). In the period of high maximum AMOC stream function, oceanic convection occurs in the Labrador Sea and in the Nordic Seas (not shown). In the period of low maximum AMOC stream function, oceanic convection does not occur in the Labrador and it is more shifted to the south in the Nordic Seas. This is in line with results by Schulz et al. (2007) who found low-frequency oscillations of the AMOC in an earlier version of the ECBilt-CLIO model (i.e. the atmospheric, oceanic and sea ice components of LOVECLIM).

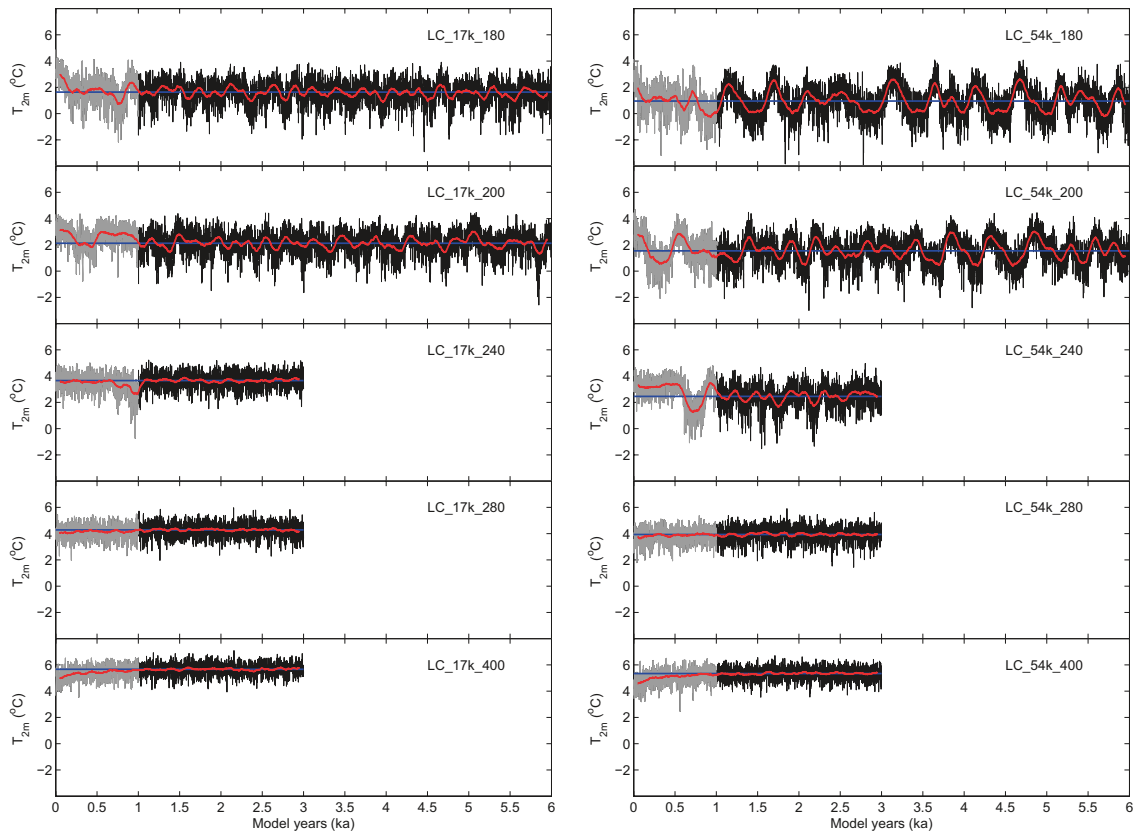


Figure 3-13. Annual average bias-corrected T_{2m} ($^{\circ}\text{C}$) in Forsmark in the 6,000 year LOVECLIM simulations for orbital year 17 ka AP and 54 ka AP with atmospheric CO_2 concentration of 180–400 ppmv. The simulation name, which gives the orbital year and atmospheric CO_2 concentration, is displayed in each panel. A 100-year running average is also displayed for each simulation (red curve). The annual average over the last 2,000–5,000 years of each simulation is also displayed (blue line). The results for the first 1,000 model years are shown in grey to indicate the equilibration period.

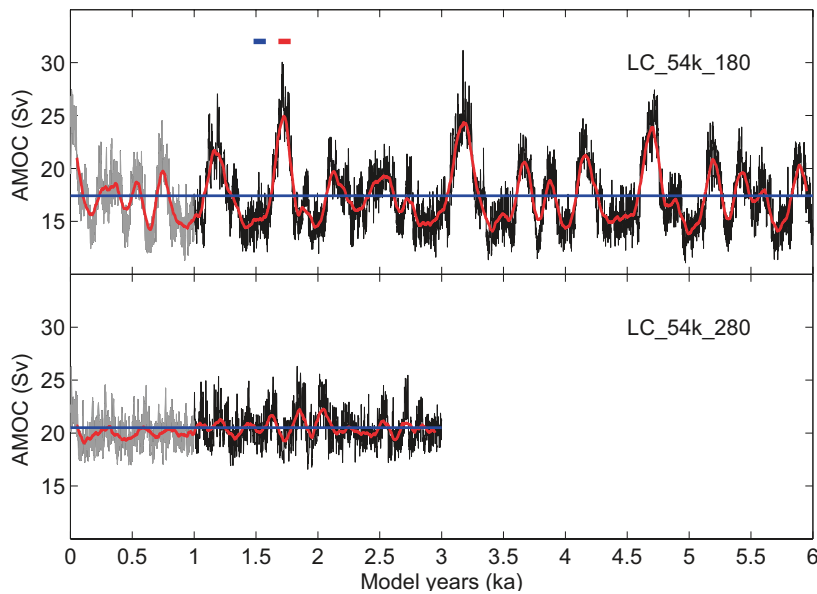


Figure 3-14. Annual average maximum AMOC strength (Sv) below 500 meters depth in the LC_54k_180 and LC_54k_280 simulations. A 100 model year period of low (blue bar) and high (red bar) maximum AMOC strength is indicated in the upper panel. The results for the first 1,000 model years are shown in grey to indicate the equilibration period.

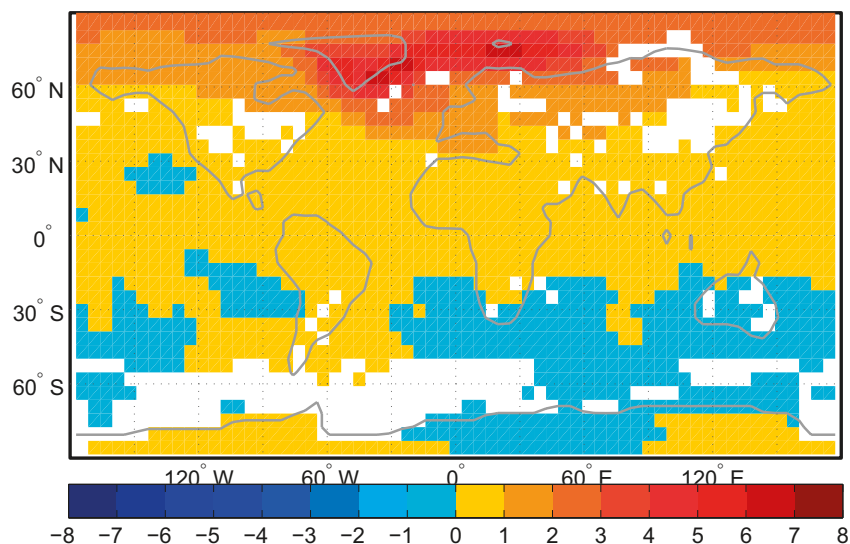


Figure 3-15. Difference in annual average T_{2m} ($^{\circ}\text{C}$) between a high AMOC strength period (indicated with a red bar in upper panel of Figure 3-14) and a low AMOC strength period (indicated with a blue bar in upper panel of Figure 3-14) in the LC_54k_180 simulation. Only differences that are statistically significant at the 5% level are shown.

CCSM4

Annual average bias-corrected T_{2m} in Forsmark in this set of simulations is displayed in Figure 3-12 as a function of the atmospheric CO_2 concentration. The figure also includes the data from the constant-forcing LOVECLIM simulations, as previously displayed in Figure 3-12. Annual average Forsmark temperature differs substantially between the CCSM4 and LOVECLIM simulations. For orbital year 17 ka AP and atmospheric CO_2 concentration of 200 ppmv annual average Forsmark T_{2m} is -0.86°C in the CCSM4 simulation as compared to 2.1°C in the LOVECLIM simulation. For orbital year 54 ka AP and atmospheric CO_2 concentration of 180 ppmv annual average Forsmark T_{2m} is -2.96°C in the CCSM4 simulation as compared to 0.96°C in the LOVECLIM simulation. The two CCSM4 simulations are thus 3.9°C and 4.4°C colder than the corresponding LOVECLIM simulations.

Annual cycle in T_{2m}

Not only the annual average T_{2m} , but also the annual cycle in T_{2m} is of importance to the permafrost development (Section 2.5). The monthly mean Forsmark T_{2m} is displayed in Figure 3-16 for the LOVECLIM and CCSM4 equilibrium simulations with atmospheric CO_2 concentration less or equal to the pre-industrial 280 ppmv. The annual cycle of the T_{2m} anomaly, displayed in Figure 3-17, is similar in the two CCSM4 simulations with the strongest cooling in winter (December–April) and the weakest cooling in summer and autumn (May–November). The annual cycle in Forsmark T_{2m} anomaly is similar to the zonal average T_{2m} annual cycle at the latitude of Forsmark (Figure 3-17), although Forsmark experiences stronger winter cooling and reduced autumn cooling as compared to the zonal average. The difference between the zonal average and Forsmark T_{2m} annual cycle anomaly is explained by differences in the large-scale atmospheric and oceanic circulation. The zonal average T_{2m} annual cycle at the latitude of Forsmark is similar in LOVECLIM and CCSM4 (Figure 3-17). In LOVECLIM, the annual cycle in Forsmark T_{2m} anomaly is similar to the zonal average T_{2m} annual cycle at the latitude of Forsmark. The differences between the Forsmark T_{2m} anomaly simulated with LOVECLIM and CCSM4 illustrate the inter-model differences associated with modelling of climates that are significantly different from the present.

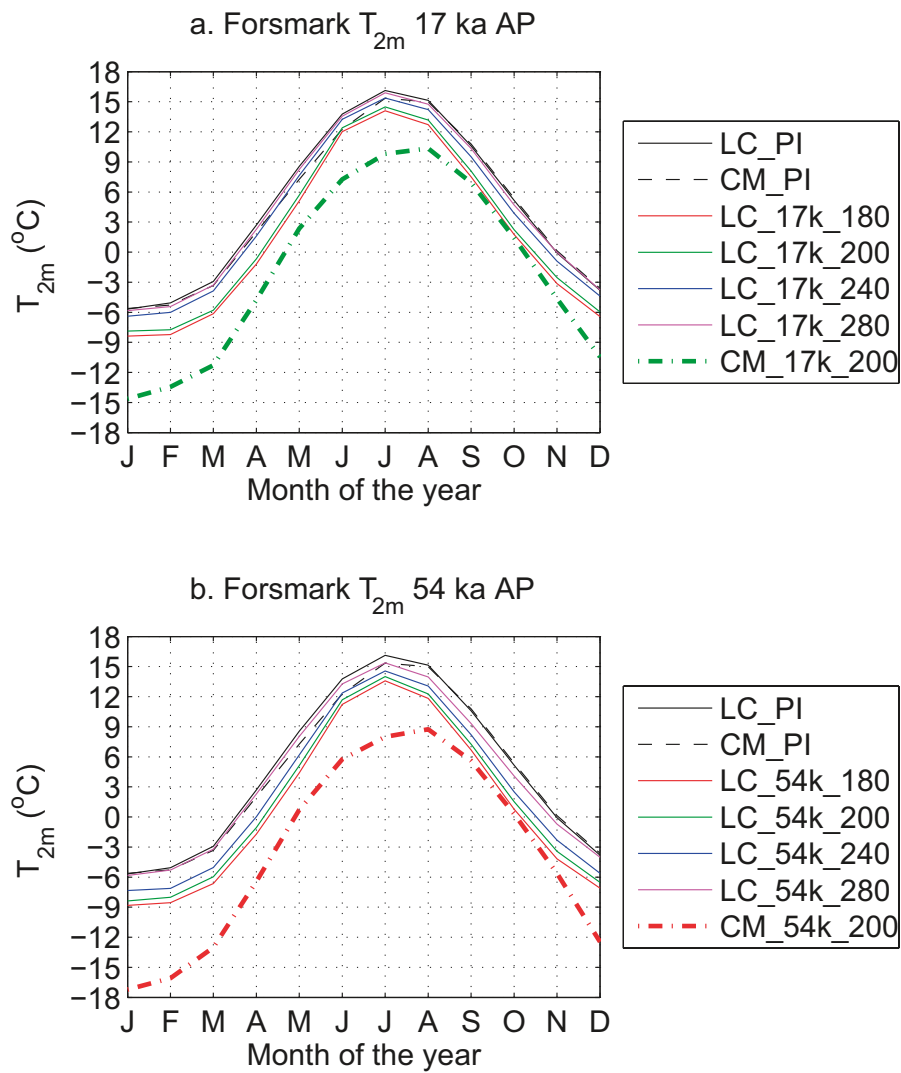


Figure 3-16. Monthly mean Forsmark T_{2m} (°C) the LOVECLIM and CCSM4 equilibrium simulations with atmospheric CO_2 concentration of 180–280 ppmv. (a.) Orbital year 17 ka AP and (b.) 54 ka AP. The pre-industrial simulations LC_PI and CM_PI are also included for comparison.

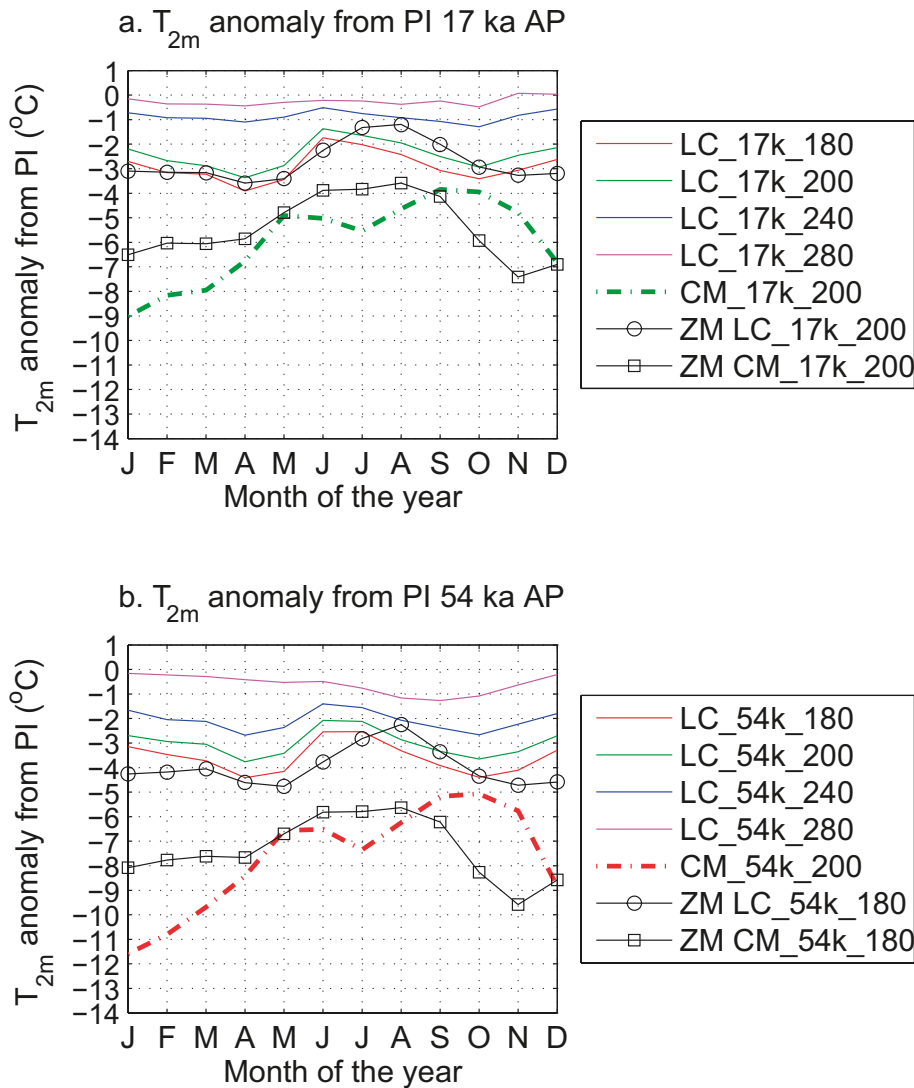


Figure 3-17. Monthly mean Forsmark T_{2m} (°C) anomaly w r t the respective pre-industrial simulation for the LOVECLIM and CCSM4 equilibrium simulations with atmospheric CO_2 concentration of 180–280 ppmv. (a.) Orbital year 17 ka AP and (b.) 54 ka AP. The zonal mean T_{2m} anomaly at the latitude of Forsmark (60.41°N; black lines with circles/squares) is also displayed for the simulations that were set up with the same forcing conditions in both models.

3.1.3 Sensitivity to atmospheric CH_4 concentration

As described in Section 2.3.2, all EMIC simulations for the future climate were unintentionally performed with an atmospheric CH_4 concentration of 650 ppbv, rather than the 19th century concentration of 760 ppbv. Furthermore, the future atmospheric CH_4 concentration is not known. To investigate the uncertainty in the results associated with the atmospheric CH_4 concentration, a set of sensitivity simulations were performed (listed in Table 3-1). Equilibrium simulations for orbital year 17 ka AP and 54 ka AP with atmospheric CH_4 concentration of 385 ppbv (representing a glacial climate in ice core data) and 760 ppbv (representing the 19th century concentration) were performed.

The bias-corrected annual average T_{2m} in Forsmark in these simulations is compared to the original simulations with atmospheric CH_4 concentration of 650 ppbv (Table 3-2). The use of an atmospheric CH_4 concentration of 650 ppbv rather than 760 ppbv leads to a difference in the annual average bias-corrected Forsmark T_{2m} of 0.06–0.07°C. Therefore it is concluded that this error does not significantly influence the annual average bias-corrected Forsmark T_{2m} in this model. The glacial-interglacial range of CH_4 concentrations (385–760 ppbv) leads to a difference in the annual average bias-corrected Forsmark T_{2m} of 0.34°C for orbital year 54 ka AP and an atmospheric CO_2 concentra-

Table 3-1. Sensitivity simulations performed with LOVECLIM.

Simulation label	Orbital year (ka AP)	Atmospheric CO ₂ concentration (ppmv)	Atmospheric CH ₄ concentration (ppbv)	Climate model	Simulation type
LC_17k_180_760, LC_17k_280_760	17	180, 280	760	LOVECLIM	Equilibrium
LC_54k_180_760	54	180	760	LOVECLIM	Equilibrium
LC_54k_180_385	54	180	385	LOVECLIM	Equilibrium

Table 3-2. Annual average bias-corrected T_{2m} in Forsmark in LOVECLIM simulations.

Simulation label	Annual average bias-corrected T _{2m} in Forsmark (°C)
LC_17k_180	1.64
LC_17k_180_760	1.71
LC_17k_280	4.28
LC_17k_280_760	4.34
LC_54k_180	0.96
LC_54k_180_385	0.69
LC_54k_180_760	1.03

tion of 180 ppmv. These results indicate that T_{2m} is relatively insensitive to such a significant reduction in the CH₄ concentration. The comparison was, however, performed with one specific climate model and for one specific set of other forcing and boundary conditions. To account for uncertainty in the climate system response to a significant reduction of the atmospheric CH₄ concentration, it is assumed here that a reduction from an inter-glacial concentration to a glacial concentration could potentially lower the annual average T_{2m} by 0.5°C.

3.2 Transient EMIC simulations

As described in Section 2.4.2, a set of transient EMIC simulations of the next 60 ka were performed.

3.2.1 Simulated global climate

The global annual average T_{2m} anomaly with respect to the LC_PI ensemble in the transient LOVECLIM simulations is displayed in Figure 3-18. Note that the simulated T_{2m} illustrates an evolution under the unrealistic assumptions of constant low atmospheric CO₂ concentration and constant glacier and ice sheet volume and extent. Given the present-day higher atmospheric CO₂ concentration, and its anticipated slow decay following a future cease in carbon emissions, the simulated future air temperature for the initial several thousands of years or more are lower than expected in LC_0k-61k_200, and should therefore not be regarded as realistic. Similarly, depending on future carbon emissions and the decay rate of atmospheric CO₂, the simulated future air temperature in LC_0k-61k_400 may be higher than expected beyond c. 10 ka AP. Furthermore, the response of glaciers and ice sheets to the expected increasing temperatures in the next few thousand years may lead to higher global average temperatures than simulated for this period in LC_0k-61k_400. Similarly, the response of glaciers and ice sheets to the expected decreasing temperatures beyond the point when atmospheric CO₂ concentration has decreased to pre-industrial values may lead to lower T_{2m} than that simulated.

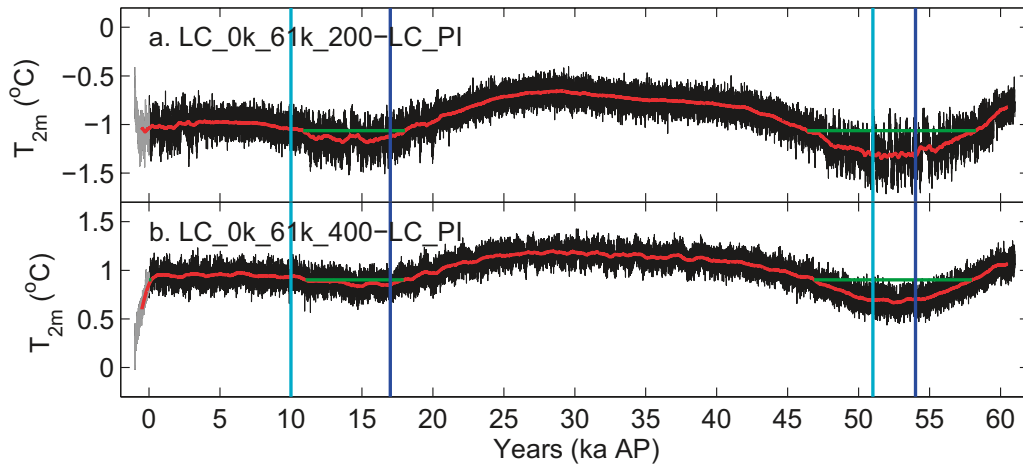


Figure 3-18. Global annual average T_{2m} anomaly ($^{\circ}\text{C}$) in the transient LOVECLIM simulations for the LC_0k-61k_200 simulation (a) and the LC_0k-61k_400 (b). The anomaly as compared to the LC_PI ensemble average is shown. A 1,000-year running average is also shown (red line). The results for the first 1,000 model years are shown in grey to indicate the equilibration period. T_{2m} minima are indicated with green horizontal lines. Further, obliquity minima (cyan lines) and June insolation at 60°N minima (blue lines) are indicated. Note that the simulated T_{2m} illustrates an evolution under the unrealistic assumptions of constant low atmospheric CO_2 concentration and constant glacier and ice sheet volume and extent. Given the present-day higher atmospheric CO_2 concentration, and it's anticipated slow decay following a future cease in carbon emissions, the simulated future air temperature for the initial several thousands of years or more in LC_0k-61k_200 are lower than expected, and should therefore not be regarded as realistic (see Section 3.2.1 for discussion).

Due to the slow orbital variation, the insolation distribution is not significantly altered in a 2 ka period centred at 17 ka AP and 54 ka AP respectively. Therefore, the global annual average T_{2m} anomaly for a 2,000 year period around 17 ka AP and 54 ka AP respectively agrees within $\pm 0.02^{\circ}\text{C}$ with the corresponding LOVECLIM simulations with constant atmospheric CO_2 concentration and orbital forcing (not shown). As noted in Section 3.1.2, multi-centennial variability is larger for colder climates, i.e. for low atmospheric CO_2 concentrations as compared to high atmospheric CO_2 concentrations and for insolation minima as compared to maxima.

The approximate timing of minima in the time series is determined based on the 1,000-year running average T_{2m} anomaly ($T_{2m_runave_anomaly}$). A cold year (y) is identified when

$$T_{2m_runave_anomaly}(y) < (M - 0.5S).$$

Here, M is the average $T_{2m_runave_anomaly}$ over years 0–60 ka AP and S is the standard deviation of $T_{2m_runave_anomaly}$ for the same years. Based on this criterion, temperature minima are found at c. 10.9–18.0 ka AP and 46.4–58.3 ka AP for low (200 ppmv) atmospheric CO_2 concentration and at c. 11.0–18.0 ka AP and 46.9–58.0 ka AP for high (400 ppmv) atmospheric CO_2 concentration (green lines in Figure 3-18). These global annual average T_{2m} minima occur in the period from the obliquity minima (10 ka AP and 51 ka AP; Figure 1-3; cyan lines in Figure 3-18) and the minima in June insolation at 60°N (17 ka AP and 54 ka AP; Figure 1-3; blue lines in Figure 3-18). The timing of the global minima does not agree with the results of the CLIMBER-2 – SICOPOLIS simulations described in Section 1.1.3 (Pimenoff et al. 2011). In their simulations, minima in the global annual average temperature lag behind the minima in June insolation at 60°N (see their Figure 26). We hypothesize that the timing of global annual average T_{2m} minima is delayed due to build up of ice sheets in the CLIMBER-2 – SICOPOLIS simulations (a process that is not modelled in the present LOVECLIM simulations).

3.2.2 Simulated Forsmark climate

Annual average Forsmark T_{2m} in the transient LOVECLIM simulations is displayed in Figure 3-19. The annual average T_{2m} for a 2,000 year period around 17 ka AP and 54 ka AP respectively agrees within $\pm 0.15^\circ\text{C}$ ($\pm 0.04^\circ\text{C}$) with the T_{2m} in the corresponding LOVECLIM simulations with constant atmospheric CO_2 concentration and orbital forcing (Figure 3-12) for atmospheric CO_2 concentration of 200 ppmv (400 ppmv).

The approximate timing of minima in the time series is determined as described in Section 3.2.1. Based on this criterion, minima are found prior to c. 2.0 ka AP, at c.11.8–17.8 ka AP and 46.8–58.1 ka AP for low (200 ppmv) atmospheric CO_2 concentration and at c. 9.6–9.7 ka AP, 11.8–17.8 ka AP and 46.8–58.1 ka AP for high (400 ppmv) atmospheric CO_2 concentration (green lines in Figure 3-19). These Forsmark T_{2m} minima broadly coincide with the global annual average T_{2m} minima, i.e. in the period from the obliquity minima (10 ka AP and 51 ka AP; Figure 1-3; cyan lines in Figure 3-18) and the minima in June insolation at 60°N (17 ka AP and 54 ka AP; Figure 1-3; blue lines in Figure 3-18). As noted for the global annual average T_{2m} , the timing of the Forsmark minima does not agree with the results of the CLIMBER-2 – SICOPOLIS simulations described in Section 1.1.3 (Pimenoff et al. 2011) for the same reason.

There is a significant correlation between the simulated near-surface temperature in Forsmark and the summer insolation at 60°N (Figure 1-3), whilst the obliquity minimum at 10 ka AP does not produce cold temperatures in Forsmark. Minima in the annual average T_{2m} in Forsmark occur at times of minimum summer insolation at high northern latitudes.

In addition to the long term variation associated with the orbital forcing, the transient LOVECLIM simulations exhibit variability on annual, decadal and centennial timescales in Forsmark T_{2m} (Figure 3-19). Specifically, periods of a few centuries occur with c. 1°C colder/warmer than average T_{2m} in the LC_0k-61k_200 simulation. Such internal variability is simulated during periods of colder climate, i.e. the periods of minimum summer insolation at 60°N . Such centennial variability is not found in the warmer climate simulation LC_0k-60k_400.

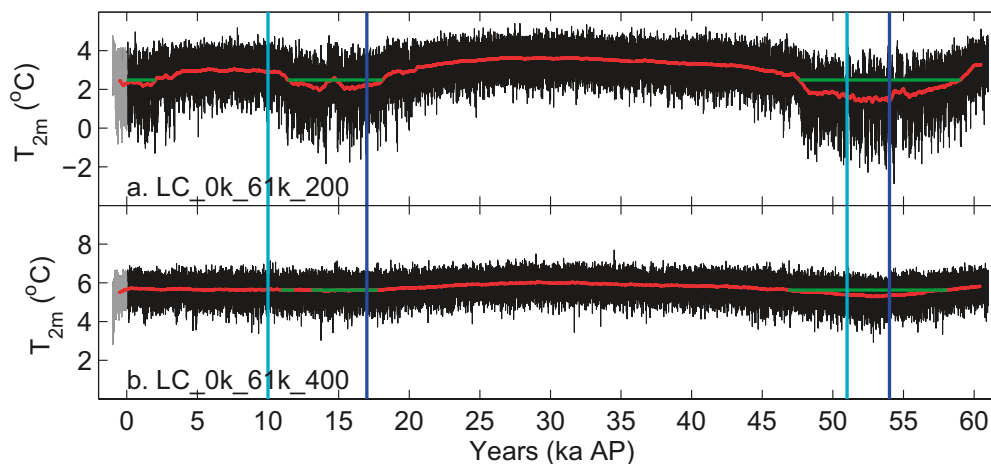


Figure 3-19. Annual average bias-corrected T_{2m} ($^\circ\text{C}$) in the Forsmark region in the transient LOVECLIM simulations (a.) 0k-61k_200. (b.), LC_0k-61k_400. A running 1,000-year average is also displayed for each simulation (red curve). The results for the first 1,000 model years is shown in grey to indicate the equilibration period. T_{2m} minima are indicated with green horizontal lines. Further, obliquity minima (cyan lines) and June insolation at 60°N minima (blue lines) are indicated. Note that the simulated T_{2m} illustrates an evolution under the unrealistic assumptions of constant low atmospheric CO_2 concentration and constant glacier and ice sheet volume and extent. Given the present-day higher atmospheric CO_2 concentration, and it's anticipated slow decay following a future cease in carbon emissions, the simulated future air temperature for the initial several thousands of years or more in LC_0k-61k_200 are lower than expected, and should therefore not be regarded as realistic (see Section 3.2.1 for discussion).

3.3 Uncertainty in climate model results

To assess the potential of permafrost in Forsmark in the coming 60 ka AP, the uncertainty in the climate model results must first be assessed. Models of the Earth's climate system are designed to simulate the dynamics of the system. The complexity of climate system dynamics is however partly unresolved, both in terms of incomplete knowledge of some processes and in terms of insufficient resources to numerically resolve small-scale processes in the models. Further uncertainty in the results of such models exists due to the nonlinear nature of the climate system. To assess the uncertainty in the bias-corrected T_{2m} in Forsmark used as input to the permafrost model, a number of sources of uncertainty have been identified. The sources and magnitudes of the uncertainties are described in the following. Uncertainties are given in integer °C, rounded up to avoid underestimation.

Inter-model differences and internal variability. Climate or earth system models use different formulations and different numerical resolution. Furthermore, the results are associated with internal variability due to the nonlinear nature of the system. This uncertainty is illustrated by the difference between the LOVECLIM and CCSM4 simulations performed within the present study (Figure 3-12). However, to fully assess this uncertainty, a multi-model inter-comparison study would be necessary. Since no such study exists for the periods of interest here, other multi-model comparison studies are here utilized to estimate this uncertainty.

Lind and Kjellström (2008) analyzed the climate change signal for Sweden in scenarios for the 21st century included in CMIP3 and used in the fourth assessment report by the Intergovernmental Panel on Climate Change (IPCC 2007) They showed that the range of regional near-surface winter temperature response in southern Sweden associated with inter-model differences and internal variability is c. 3°C for low carbon emission scenarios and c. 5°C for high emission scenarios (their Table 4.2). The range of summer temperature response in southern Sweden is c. 3°C for low carbon emission scenarios and c. 6°C for high emission scenarios (their Table 4.2).

Bakker et al. (2012) compared simulations with eight different climate and earth system models of the last inter-glacial (130 ka BP–115 ka BP) temperature evolution. They found July temperature anomalies compared to the pre-industrial at Northern Hemisphere high and mid-latitudes of +0.3 to +3.7°C for the warmest interval around 130–120 ka BP (their Table 2). January temperature anomalies for the same interval were –5.8 to +1.2°C. For the coldest interval around 117 ka BP to 115 ka BP they found July temperature anomalies compared to the pre-industrial at Northern Hemisphere high and mid-latitudes of c. –4.3 to –1.8°C (their Figure 2). January temperature anomalies for the same interval were c. –7 to +1°C. The results presented by Bakker et al. (2012) indicate that uncertainty range at Northern Hemisphere high and mid-latitudes is larger in winter than in summer and larger for cold climates than for warm climates. This is in agreement with the results presented here, with a stronger inter-model difference for winter than summer Forsmark T_{2m} (Figure 3-17).

The studies by Lind and Kjellström (2008) and Bakker et al. (2012) do not include information on the uncertainty range for all months or seasons, why an annual average range cannot be properly determined. An annual average uncertainty range is therefore here determined based only on the summer and winter or July and January ranges given, recognising that this procedure introduces errors. The uncertainty range presented by Bakker et al. (2012) for their coldest period were here used as representative also for the coldest climates simulated in the present study, i.e. with low atmospheric CO₂ concentrations. The annual average uncertainty range was estimated to c. 5.3°C, taken as the average of the uncertainty range of c. 2.5°C for July and c. 8°C for January. This number is in agreement with the southern Sweden annual average uncertainty range of c. 5.5°C, calculated using only summer and winter temperature, for high future emission scenarios.

The Forsmark T_{2m} difference between the LOVECLIM and CCSM4 simulations for an atmospheric CO₂ concentration of 180 ppmv is c.3–4°C in July and c. 7–8.5°C in January. This uncertainty is similar to that found for the coldest period in Bakker et al. (2012). Further, the Forsmark and zonal-mean T_{2m} anomalies compared to the pre-industrial climate in these simulations (Figure 3-17) are similar to anomalies for the coldest period presented by Bakker et al. (2012). Therefore, the annual average T_{2m} uncertainty calculated for the coldest period in Bakker et al. (2012) was utilized in the present study to estimate the uncertainty in the coldest simulated climates with an atmospheric CO₂ concentration of 180 ppmv. The uncertainty in annual average Forsmark T_{2m} is thus set to 6°C for the simulations with 180 ppmv CO₂.

The uncertainty range is larger for climates that are radically different from the present. To account for this dependency the uncertainty in annual average Forsmark T_{2m} due to inter-model differences and internal variability was taken to decrease linearly as a function of the CO_2 concentration from 6°C for the simulations with substantially changed forcing conditions (atmospheric CO_2 concentration of 180 ppmv) to 1°C for the simulations with pre-industrial atmospheric CO_2 concentration of 280 ppmv.

Atmospheric greenhouse gas concentrations (except CO_2). As described in Sections 2.3.2 and 3.1.3, the future atmospheric concentrations of the major greenhouse gases CH_4 and N_2O are uncertain. The importance of the future atmospheric CH_4 concentration was analysed in Section 3.1.3 in a set of sensitivity simulations and concluded to be maximum 0.5°C for the annual average bias-corrected Forsmark T_{2m} . The atmospheric N_2O concentration is assumed to have equal or smaller influence on global climate than the atmospheric CH_4 concentration, the total uncertainty due to this source is taken to be c. 1°C.

Atmospheric aerosol concentrations. Aerosols are an integral part of the atmospheric hydrological cycle and the atmosphere's radiation budget, with many possible feedback mechanisms that are not yet fully understood (e.g. Stevens and Boucher 2012). Since future projections of the atmospheric aerosol burden only exist for the coming few centuries, atmospheric aerosol concentrations are not varied in the present study. The uncertainty associated with feedback mechanisms associated with aerosols can be regarded as included in the uncertainty due to inter-model differences. Due to the uncertainty in the feedback mechanisms it is not possible to estimate the uncertainty in climate modelling results due to uncertainties in future atmospheric aerosol concentration.

Glacier and ice sheet dynamics. The simulations presented here include the coupled dynamics of the atmosphere, oceans, sea ice, land surface and vegetation (LOVECLIM) or the carbon-nitrogen cycle (CCSM4). The dynamics of glaciers and ice sheets, which plays an important role in the global climate evolution between warmer and colder climate states is however not included. To assess the possible importance of this, the results presented here are compared to Pimenoff et al. (2011) as described in Section 3.1.2. Due to growth of a Fennoscandian ice sheet in their simulations with a constant atmospheric CO_2 concentration of 280 ppmv Pimenoff et al. (2011) find substantially colder near-surface temperatures in Fennoscandia at 17 ka AP and 54 ka AP than in the present study. The difference between (statistically down-scaled) Olkiluoto near-surface temperature and (bias-corrected, spatially interpolated) Forsmark T_{2m} is c. 5°C both for 17 ka AP and 54 ka AP. A direct comparison is not possible, due to different resolutions and the use of statistical downscaling in their study. Further, an unrealistically low atmospheric CO_2 concentration of 280 ppmv (Archer et al. 2009) is assumed for the next 10 ka in Pimenoff et al. (2011) why ice sheet growth is likely to initiate too early in their simulations. Nevertheless, glacier and ice sheet dynamics may influence Earth's climate at 17 ka AP and, even more so, at 54 ka AP. Other studies of future climate evolution are described in Section 1.1.3 and summarised in Table 1-1. Although the results differ substantially among these studies, a general conclusion is that glacial inception may occur in the coming 100 ka once the atmospheric CO_2 concentration falls below 270–290 ppmv. Since the atmospheric CO_2 concentration is likely to exceed 280 ppmv for the next 10 ka (Archer et al. 2009), ice sheet growth is assumed here to initiate after these first 10 ka. Ice sheet growth is a slow process, therefore the uncertainty in Forsmark T_{2m} due to these processes is assumed to be 2°C (rather than 5°C as indicated by Pimenoff et al. (2011)) at 17 ka AP. The uncertainty at 54 ka AP is assumed to be 5°C.

As described in Section 2.2.1, the equilibrium climate sensitivity of LOVECLIM is low as compared to the IPCC AR4 and CMIP5 AOGCMs. Thus, the temperature response to a change in the CO_2 concentration is lower in this model than in most AOGCMs. The annual average bias-corrected Forsmark T_{2m} simulated with this model for 17 ka AP and 54 ka AP is therefore taken here as an upper limit for atmospheric CO_2 concentrations less than the pre-industrial. The uncertainties listed above were applied to the annual average bias-corrected Forsmark T_{2m} from the LOVECLIM equilibrium simulations, assuming that they all result in cooling. This assumption was made since the primary task of this study was to explore the potential for cold climate conditions that may result in frozen ground in Forsmark. The resulting minimum annual average bias-corrected Forsmark T_{2m} is listed in Table 3-3 (17 ka AP) and Table 3-4 (54 ka AP). These estimates are discussed in relation to the results of the permafrost modelling in Section 4.

Table 3-3. The minimum annual average bias-corrected Forsmark T_{2m} when all uncertainties are taken into account for LOVECLIM simulations for orbital year 17 ka AP.

Atmospheric CO ₂ concentration (ppmv)	180	200	240	280	320
Annual average bias-corrected Forsmark T_{2m} (°C)	1.6	2.1	3.7	4.3	4.8
T_{2m} uncertainty due to inter-model differences and internal variability	-6	-5	-3	-1	-1
T_{2m} uncertainty due to future atm. CH ₄ and N ₂ O concentration uncertainty	-1	-1	-1	-1	-1
T_{2m} uncertainty due to future glacier and ice sheet development uncertainty	-2	-2	-2	-2	-2
Minimum annual average bias-corrected Forsmark T_{2m} (°C)	-7.4	-5.9	-2.3	0.3	0.8

Table 3-4. The minimum annual average bias-corrected Forsmark T_{2m} when all uncertainties are taken into account for LOVECLIM simulations for orbital year 54 ka AP.

Atmospheric CO ₂ concentration (ppmv)	180	200	240	280	320
Annual average bias-corrected Forsmark T_{2m} (°C)	1.0	1.5	2.5	3.9	4.4
T_{2m} uncertainty due to inter-model differences and internal variability	-6	-5	-3	-1	-1
T_{2m} uncertainty due to future atm. CH ₄ and N ₂ O concentration uncertainty	-1	-1	-1	-1	-1
T_{2m} uncertainty due to future glacier and ice sheet development uncertainty	-5	-5	-5	-5	-5
Minimum annual average bias-corrected Forsmark T_{2m} (°C)	-11	-9.5	-6.5	-3.1	-2.6

3.4 Permafrost modelling

The coldest climate conditions in Forsmark were obtained in the LC_54k_180 simulation, which combines the low summer insolation at high northern latitudes at 54 ka AP with a low glacial atmospheric CO₂ concentration of 180 ppmv. The results of this simulation were used as input to a reference case for the permafrost model simulations. The annual cycle in bias-corrected Forsmark T_{2m} in this simulation is displayed in Figure 3-20.

To assess the importance of the uncertainty in the climate modelling results discussed in Section 3.3 for the potential for permafrost in Forsmark, a number of sensitivity simulations were performed with the permafrost model. These are described in Section 3.4.3.

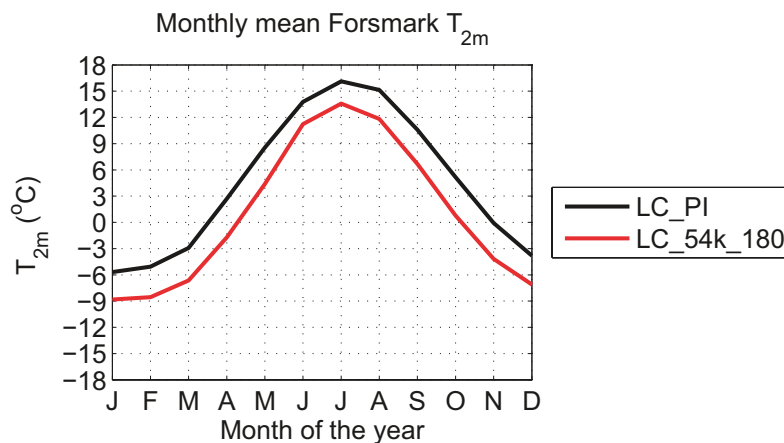


Figure 3-20. Monthly mean bias-corrected Forsmark T_{2m} (°C) in the LC_54k_180 simulation used as input to the permafrost modelling reference case. The LC_PI ensemble mean is also displayed for comparison.

3.4.1 Initialization and initial state

The initial state for the permafrost simulations was obtained from the initial state described in Section 2.4 by simulating the evolution of ground temperatures using the monthly average bias-corrected T_{2m} from the LOVECLIM simulation LC_54k_180 (Figure 3-20) until ground temperature has reached equilibrium. This simulation, as well as the other simulations performed with the permafrost model within this study, was run for 10,000 model years. Fast equilibration of the ground temperature in the first c. 1,000 model years is followed by a slow (less than $0.0005^{\circ}\text{C}/\text{year}$) decrease in ground temperature.

3.4.2 The 54 ka AP period

As expected from the annual average Forsmark T_{2m} in the LC_54k_180 simulation of $+0.96^{\circ}\text{C}$, the ground temperature showed no development of permafrost and perennially frozen ground within the model domain for this climate forcing case. In this case, the minimum annual average temperature at the ground surface was $+4.4^{\circ}\text{C}$ at the SFR repository location and $+3.6^{\circ}\text{C}$ within the 15 km long permafrost model domain.

3.4.3 Sensitivity to Forsmark T_{2m}

To account for the uncertainties in the future Forsmark T_{2m} described in Section 3.3 a suite of 7 sensitivity simulations were performed with the permafrost model. In these experiments the annual average Forsmark T_{2m} was lowered by 2 to 8°C as compared to the reference case. The sensitivity experiments were initiated from the reference case and the annual average Forsmark T_{2m} was gradually decreased at a rate of approximately $0.009^{\circ}\text{C}/\text{year}$ until the T_{2m} had been lowered by the pre-defined amount (2 to 8°C). The decrease rate was determined based on the decrease found in the evolution from relatively warm to relatively cold periods in the last 5,000 model years of the LC_54k_180 simulation (Figure 3-13). After the lowering of the annual average air temperature, the air temperature was kept constant until the end of the simulation. Each simulation was run for a total of 10,000 model years.

The amplitude and shape of the annual cycle of T_{2m} varies with the annual average T_{2m} . To account for this variation in the sensitivity experiments, a linear regression between the monthly average and annual average T_{2m} as determined for each month of the year using data from the LC_54k_180 time series. The regression coefficients were thus used to determine the resulting annual cycle in Forsmark T_{2m} for each sensitivity experiment displayed in Figure 3-21.

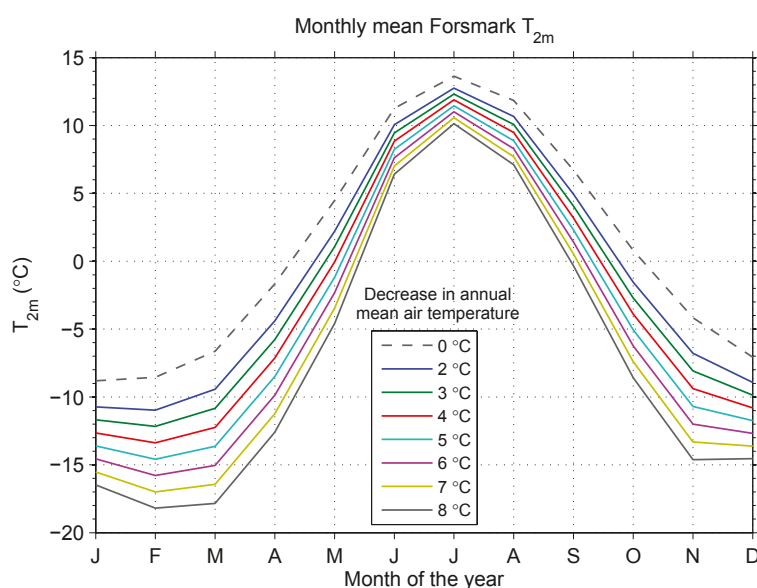


Figure 3-21. Monthly mean bias-corrected Forsmark T_{2m} ($^{\circ}\text{C}$) in the LC_54k_180 simulation (dashed line) and in the sensitivity experiments (solid lines) performed with the permafrost model.

For subsequent analysis of repository safety, not conducted in the present study, not only the 0°C isotherm is of interest, but also the development and vertical distribution of lower bedrock temperatures. Therefore, the evolution of the maximum depth of the 0, -3 and -5°C isotherms over the SFR repository and within the entire model domain for cases with the air temperature decreased by 2 to 8°C is shown in Figure 3-22, Figure 3-23 and Figure 3-24.

The existing SFR 1 and planned SFR 3 repositories are located at c. 60 m and 115 m depth. In Table 3-5 and Table 3-6 the time needed for the 0°C, -3°C and -5°C isotherms to reach 60 m and 110 m depth over the repository and within the whole model domain is presented.

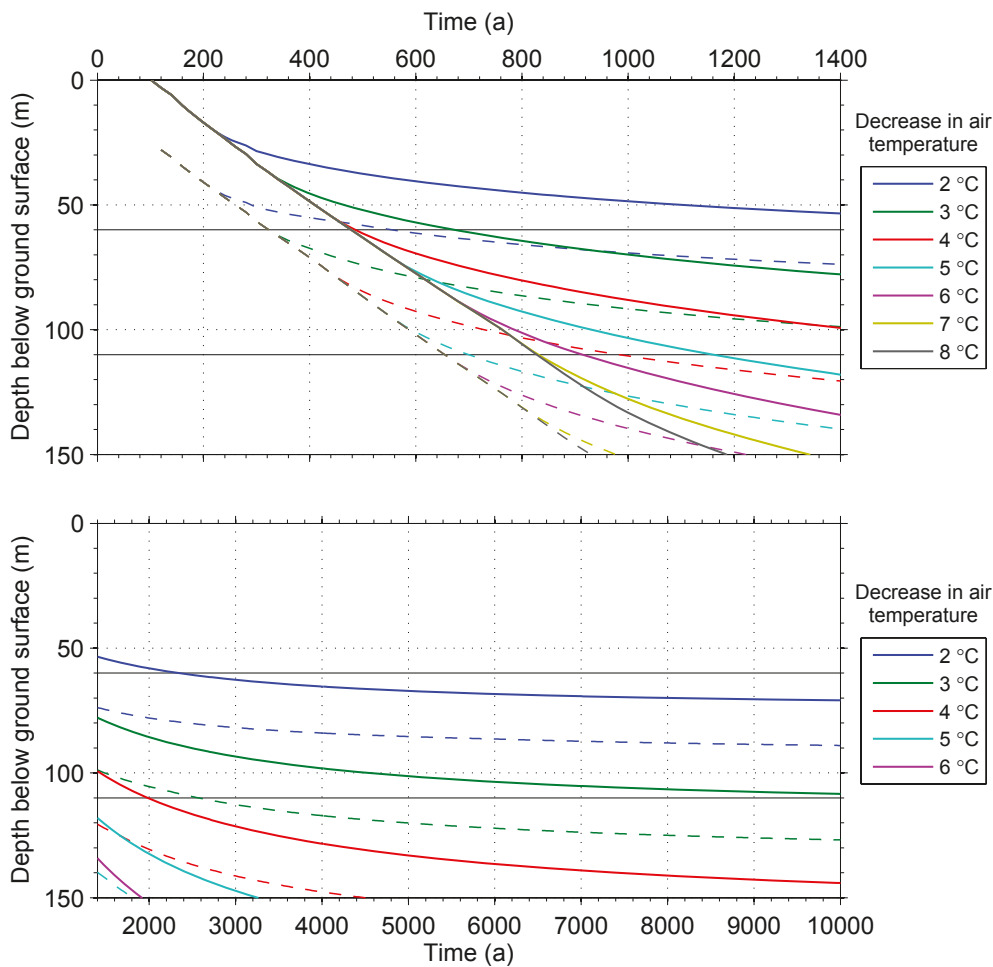


Figure 3-22. Evolution of maximum depth(m) of 0°C isotherm over the repository (solid lines) and within the whole model domain (dashed lines) when the annual average air temperature from the LOVECLIM simulation LC_54k_180 was lowered by 2, 3, 4, 5, 6, 7 and 8°C. Note that the reference case using the LC_54k_180 air temperature does not result in ground temperatures below 0°C.

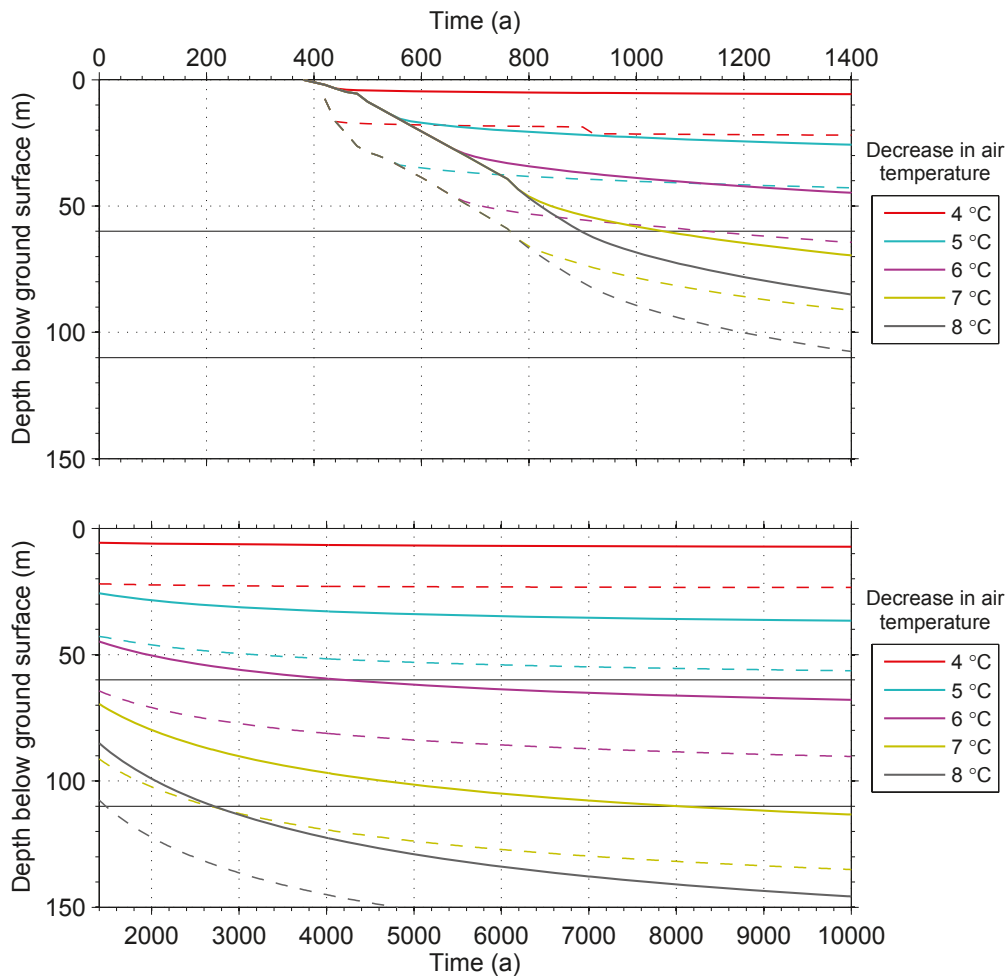


Figure 3-23. Evolution of the maximum depth (m) of the -3°C isotherm over the repository (solid lines) and within the whole model domain (dashed lines) when the average air temperature from the LOVECLIM simulation LC_54k_180 was lowered by 4, 5, 6, 7 and 8°C . Only simulations that result in ground temperatures of -3°C or below are included in the figure.

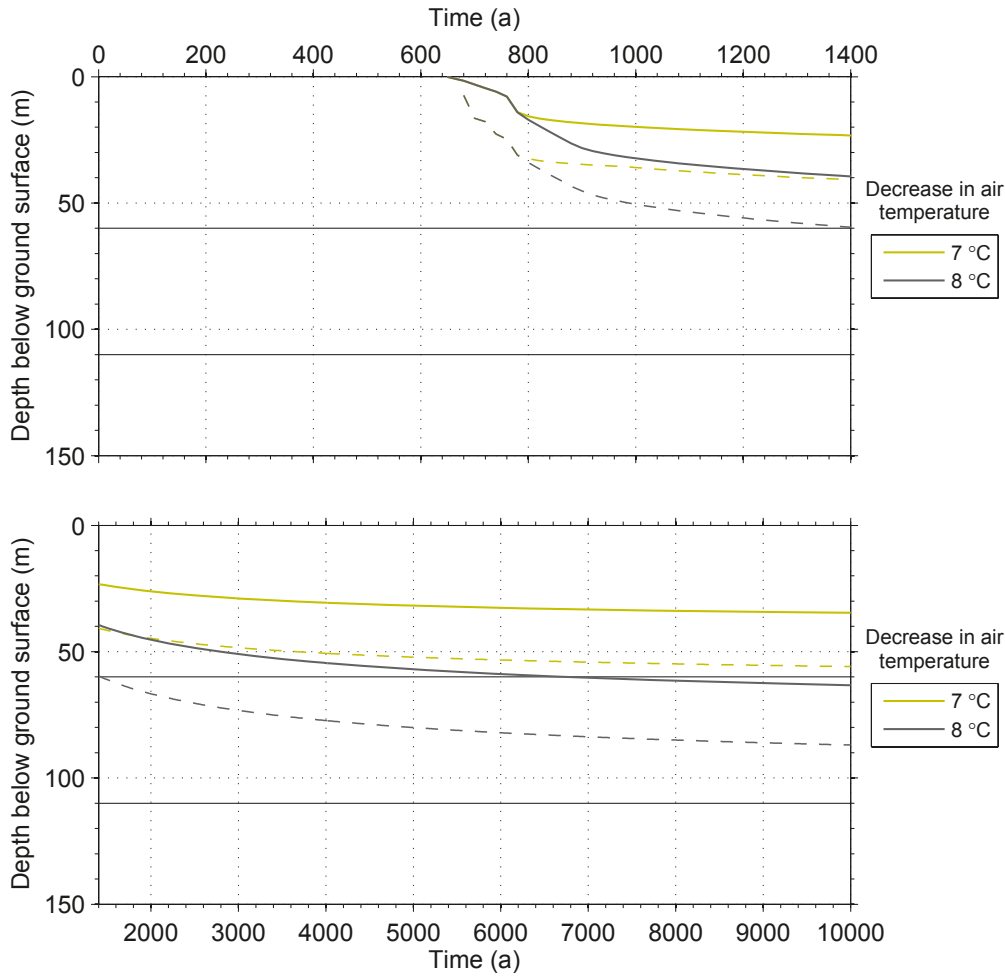


Figure 3-24. Evolution of the maximum depth (m) of -5°C isotherm over the repository (solid lines) and within the whole model domain (dashed lines) when the average air temperature from the LOVECLIM simulation LC_54k_180 was lowered by 7 and 8°C . Only simulations that result in ground temperatures of -5°C or below are included in the figure.

Table 3-5. Duration (years) for the 0 , -3 and -5°C isotherms to reach 60 m depth over the repository and within the full model domain when the average air temperature from the data of LOVECLIM simulation LC_54k_180 was lowered by 2, 3, 4, 5, 6, 7 and 8°C . Empty places in the table show that the specific isotherm does not reach 60 m depth for that climate situation. Note that the reference case using the LC_54k_180 air temperature does not result in ground temperatures below 0°C , why it is not included in the table.

Decrease in annual average air temperature ($^{\circ}\text{C}$)	Within the model domain			Over the repository		
	0°C isotherm	-3°C isotherm	-5°C isotherm	0°C isotherm	-3°C isotherm	-5°C isotherm
2	540			2,340		
3	320			660		
4	320			480		
5	320			460		
6	320	1,120		460	4,180	
7	320	760		460	1,040	
8	320	760	1,420	460	880	6,740

Table 3-6. Duration (years) for the 0, –3 and –5°C isotherms to reach 110 m depth over the repository and within the full model domain when the average air temperature from the data of LOVECLIM simulation LC_54k_180 was lowered by 2, 3, 4, 5, 6, 7 and 8°C. Empty places in the table show that the specific isotherm does not reach 60 m depth for that climate situation. Note that the reference case using the LC_54k_180 air temperature does not result in ground temperatures below 0°C, why it is not included in the table.

Decrease in annual average air temperature (°C)	Within the model domain			Over the repository		
	0°C isotherm	–3°C isotherm	–5°C isotherm	0°C isotherm	–3°C isotherm	–5°C isotherm
2						
3	2,560					
4	980			1,980		
5	680			1,160		
6	640			900		
7	640	2,660		820	8,020	
8	640	1,460		820	2,700	

3.4.4 Sensitivity to model formulation

The sensitivity of the results to the improvements made in the new version of the permafrost model was investigated. Thus, the results of the new version of the permafrost model, described in Section 2.5, were compared to experiments with identical forcing and boundary conditions performed with the old version of the model (described by Hartikainen et al. 2010).

Figure 3-25 shows the time evolution of the depth of the 0°C isotherm in the experiments with the new and the old version of the model. The new version, which includes an improved description of the influence of the annual temperature cycle on permafrost growth and thawing, simulates faster growth of permafrost and deeper equilibrium depths for the 0°C isotherm. The effect is larger for shallow depths than for deeper depths. For example, in the experiments with 2°C decrease in air temperature as compared to the reference case, the equilibrium depth of the 0°C isotherm in the new model results is more than twice the depth in the old model version. In the experiment with 8°C decrease in air temperature as compared to the reference case on the other hand, the 0°C isotherm in the new model results is only c. 7 % deeper than in the old model version. Since the new version of the permafrost model describes the coupling between the air temperature and the bedrock in greater detail it is reasonable to believe that this version gives more reliable results. Therefore the results of this model version were used in the analysis in the present study. This choice further reduces the risk of using too shallow isotherm depths used to analyse the potential for permafrost in Forsmark.

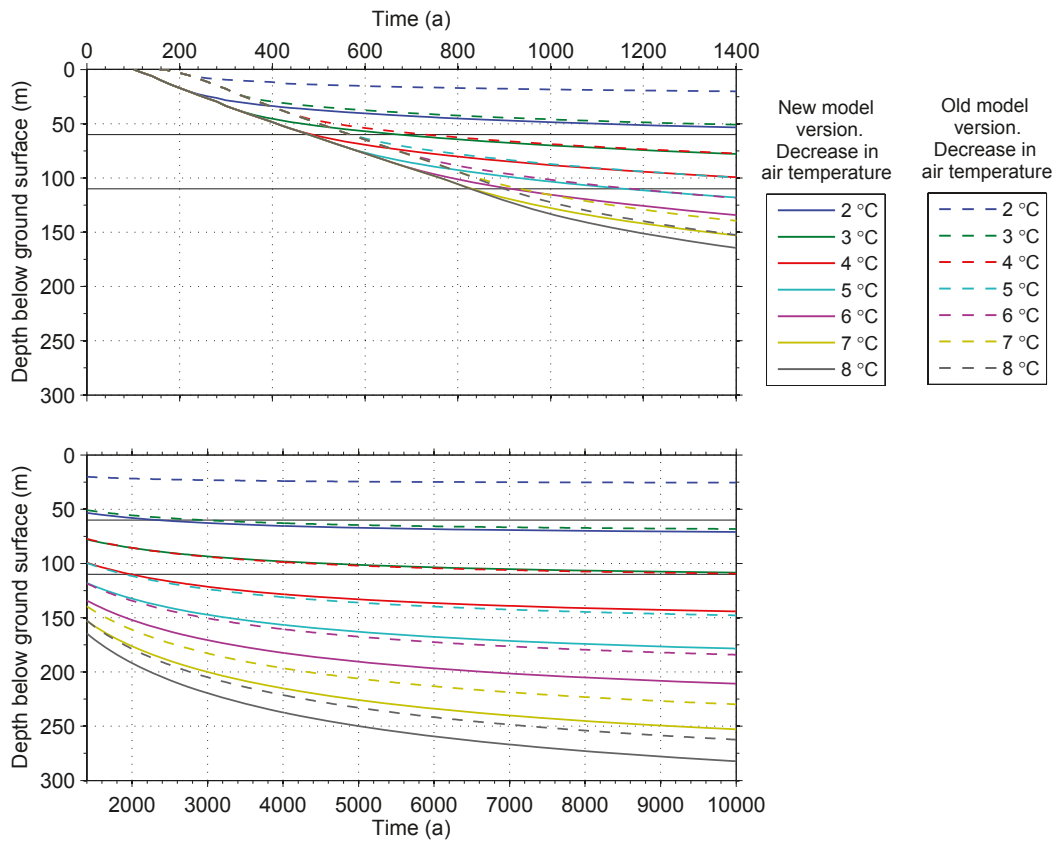


Figure 3-25. Evolution of maximum depth of the 0°C isotherm over the SFR repository when the annual average air temperature from the LOVECLIM simulation LC_54k_180 was lowered by 2, 3, 4, 5, 6, 7 and 8°C. The results from the new version of the model, described in Section 2.5, is given as solid lines and the results from the old version of the model, described by Hartikainen et al. (2010), is given as dashed lines.

4 Potential for permafrost – synthesis

The purpose of this study is to analyse the potential for cold climate and permafrost development in south-central Sweden, specifically in the region surrounding Forsmark, in the coming 60 ka. The results of the permafrost modelling described in Section 3.4 is summarised in Figure 4-1 which shows the maximum depth of the 0°C, -3°C and -5°C isotherms at the SFR repository location after 10,000 years of permafrost model integration as a function of the annual average Forsmark T_{2m} simulated for a cold climate period 54 ka AP. The permafrost modelling results are given here as a function of the annual average T_{2m} in Forsmark rather than the decrease as compared to the annual average T_{2m} in the reference case. Since the annual average T_{2m} in the LC_54k_180 simulation is +1.0°C, this means that a 1°C decrease as compared to the LC_54k_180 Forsmark T_{2m} is equal to an annual average Forsmark T_{2m} of 0°C.

It can be concluded that an annual average T_{2m} of c. -4.7°C and c. -5.9°C is required for the -3°C isotherm to reach the SFR 1 and SFR 3 depth respectively. It takes c. 4,000 years and c. 8,000 years for the -3°C isotherm to reach the SFR 1 and SFR 3 depth for an annual average T_{2m} of c. -5°C and c. -6°C respectively. To determine if the -3°C isotherm can reach these depths in the next 60 ka comparison to the minimum annual average Forsmark T_{2m} when all uncertainties in the climate modelling results is taken into account is performed (Table 3-3 and Table 3-4). For orbital year 17 ka AP it is concluded that an atmospheric CO₂ concentration of c. 210 ppmv or less is required to get annual average Forsmark T_{2m} below c. -5°C. For orbital year 54 ka AP it is concluded that an atmospheric CO₂ concentration of c. 250 ppmv or less is required to get annual average Forsmark T_{2m} below c. -5°C. Based on the discussion on the future atmospheric CO₂ concentration in Section 2.3.2, it is concluded that an atmospheric CO₂ concentration of c. 250 ppmv or less at 54 ka AP cannot be excluded. Based on the same discussion it is concluded that it is not likely that the atmospheric CO₂ concentration is c. 210 ppmv or less at 17 ka AP. To reach such low concentrations would require that (human and natural) carbon emissions to the atmosphere end in the near future such that natural processes can decrease the concentration to a pre-industrial value of 180–290 ppmv in the next 10 ka. After this the processes that produce the natural glacial-inter-glacial CO₂ variations seen in ice core data are required to reduce the concentration further by c. 70 ppmv in c. 7 ka. The required decrease rate of 10 ppmv per ka is almost twice the rapid decrease rate seen in ice core data for the last glacial inception around 100 ka BP.

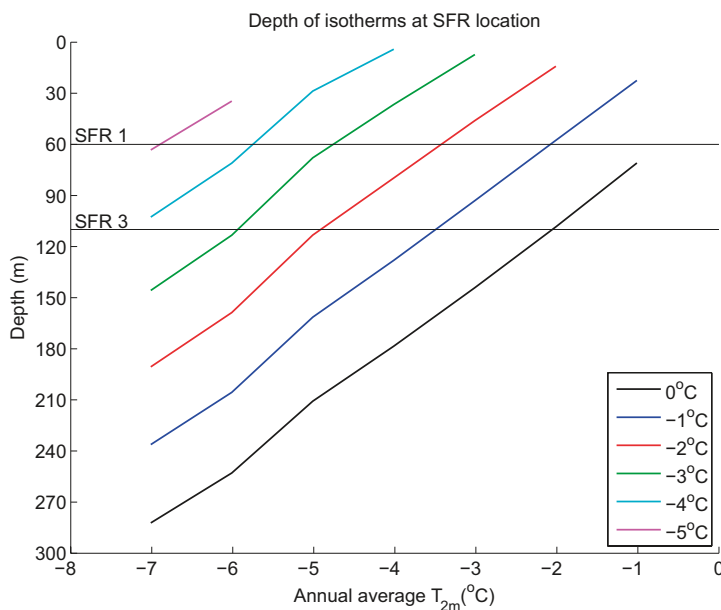


Figure 4-1. Depth (m) of the 0, -1, -2, -3, -4° and -5°C isotherm as a function of the annual average Forsmark T_{2m} . The depths of the existing SFR 1 repository (c. 60 m) and planned SFR 3 repository (c. 110 m) are indicated with black lines.

For comparison, it can be concluded that an annual average T_{2m} of c. -1°C and c. -2°C is required for the 0°C isotherm to reach the SFR 1 and SFR 3 depth respectively (Figure 3-22). It takes c. 2,000 years and c. 10,000 years for the 0°C isotherm to reach the SFR 1 and SFR 3 depth for an annual average T_{2m} of c. -1°C and c. -2°C respectively. To determine if the 0°C isotherm can reach these depths in the next 60 ka comparison to the minimum annual average Forsmark T_{2m} when all uncertainties in the climate modelling results is taken into account is performed (Table 3-3 and Table 3-4). For orbital year 17 ka AP it is concluded that an atmospheric CO_2 concentration of c. 260 ppmv or less is required to get annual average Forsmark T_{2m} below c. -1°C . Although unlikely, this atmospheric CO_2 concentration cannot be excluded. For orbital year 54 ka AP it is concluded that an annual average Forsmark T_{2m} below c. -1°C or -2°C cannot be excluded even for atmospheric CO_2 concentrations above 280 ppmv.

5 Summary and conclusions

This study was performed in order to analyse the potential for frozen ground and permafrost in the next 60 ka in south-central Sweden, more specifically in the Forsmark region. The results are planned to be used in safety assessments for nuclear waste repositories. Specifically, the potential for cold ground temperatures required to freeze the concrete barriers in the existing and planned repositories for low- and intermediate-level short-lived radioactive waste, SFR 1 and SFR 3. These repositories are (planned to be) located at a depth of c. 60 m and c. 110 m respectively.

In this study, all known uncertainties in future climate evolution are taken into account and discussed. The future climate evolution is uncertain due to

- Uncertainties in the evolution of the main forcing conditions (atmospheric greenhouse gas and aerosol concentrations).
- Inter-model differences in climate model projections and internal climate variability.
- Uncertainties in the evolution of glaciers and ice sheets.

Since the air temperature is the main factor that determines the ground surface temperature (Hartikainen et al. 2010), the large uncertainty in the future climate evolution results in a large uncertainty in future ground surface temperatures at the repository location in Forsmark. Therefore, all uncertainties in the modelled Forsmark air temperature are taken into account in a systematic way. Further, climate and surface conditions that promote permafrost growth are assumed, i.e. dry climate conditions and a dry ground surface.

Under the assumptions made in this study, it is concluded that ground temperature of 0°C cannot be excluded at c. 60 m and c. 110 m depth at 17 ka AP or at 54 ka AP. Under the assumptions made in this study, it is further concluded that it is very unlikely to get ground temperature of –3°C at c. 60 m and c. 110 m depth at 17 ka AP, but that this possibility cannot be excluded at 54 ka AP. The main reason for the different conclusions for the two time periods is the expected slow decrease in atmospheric CO₂ concentration.

Perspective

In the present study, the potential for cold climate conditions in the next 60 ka was assessed based on simulations with two different climate models. The earth system models used were run at relatively low spatial resolution. The method used to determine local temperature in Forsmark based on data from these models, i.e. spatial interpolation and bias correction, underestimates climate variability and may introduce systematic errors in the results. Such errors may be reduced using more sophisticated methods such as statistical or dynamical downscaling as discussed in Section 2.7. However, since Forsmark is located in an area of low topographic relief, a relatively small systematic error is expected. Therefore, inter-model differences in global Earth system simulations (Section 3.3) are much more important. As concluded by Racherla et al. (2012), the most important factor for climate change studies is the skill of the global model rather than the method used for downscaling.

Important components of the Earth system, most notably the global carbon cycle and ice sheet and glacier dynamics, were not included in the simulations presented here due to computational costs. The exclusion of these processes, essential to glacial – interglacial climate cycles, introduces large uncertainties in the results (Section 3.3). In the present study these uncertainties were estimated from other studies. To improve on the estimated future climate and climate uncertainty, inclusion of these processes in the modelling is necessary. Due to the large inter-model differences in the future earth system evolution, both in simulations of the carbon cycle (Section 2.3.2) and ice sheet and glacier dynamics (Section 1.1.3), an inter-model comparison project is needed to improve the estimations of future climate and climate uncertainty.

Acknowledgements

We thank Dr Anders Moberg at Stockholm University for providing us with the NORDKLIM data for Uppsala and Stockholm. We also thank the reviewers, Dr Marie-France Loutre, Université Catholique de Louvain (UCL), Belgium and Dr. Guido Vettoretti, University of Toronto, Canada, for valuable comments on the manuscript. UCL is acknowledged for sharing the LOVECLIM version 1.2 model. Further, the United States National Center for Atmospheric Research (NCAR) is acknowledged for sharing the Community Climate System Model version 4 (CCSM4). The CCSM project is supported by the National Science Foundation and the Office of Science (BER) of the U.S. Department of Energy. The Parallel Computing Centre (PDC) at the Royal Institute of Technology (KTH) in Stockholm, Sweden and the National Super-computer Centre in Linköping, Sweden are acknowledged for access to computing facilities. The Knut and Alice Wallenberg Foundation is acknowledged for funding of the Ekman computing resource at PDC.

References

SKB's (Svensk Kärnbränslehantering AB) publications can be found at www.skb.se/publications.

- Archer D, 2005.** Fate of fossil fuel CO₂ in geologic time. *Journal of Geophysical Research* 110, C09S05. doi: 10.1029/2004JC002625.
- Archer D, Ganopolski A, 2005.** A movable trigger: fossil fuel CO₂ and the onset of the next glaciation. *Geochemistry, Geophysics, Geosystems* 6. doi: 10.1029/2004GC000891.
- Archer D, Eby M, Brovkin V, Ridgwell A, Cao L, Mikolajewicz U, Caldeira K, Matsumoto K, Munhoven G, Montenegro A, Tokos K, 2009.** Atmospheric lifetime of fossil fuel carbon dioxide. *Annual Review of Earth and Planetary Sciences* 37, 117–134.
- Bakker P, Stone E J, Charbit S, Gröger M, Krebs-Kanzow U, Ritz S P, Varma V, Khon S, Lunt D J, Mikolajewicz U, Prange M, Renssen H, Schneider B, Schulz M, 2012.** Last interglacial temperature evolution – a model inter-comparison. *Climate of the Past Discussions* 8, 4663–4699.
- Berger A L, 1978.** Long-term variations of daily insolation and Quaternary climatic changes. *Journal of the Atmospheric Sciences* 35, 2362–2367.
- Berger A, Loutre M F, 1991.** Insolation values for the climate of the last 10 million years. *Quaternary Science Reviews* 10, 297–317.
- Berger A, Loutre M F, 2002.** An exceptionally long interglacial ahead? *Science* 297, 1287–1288.
- Berger A, Loutre M F, 2010.** Modeling the 100-kyr glacial–interglacial cycles. *Global and Planetary Change* 72, 275–281.
- Bitz C M, Shell K M, Gent P R, Bailey D A, Danabasoglu G, Armour K C, Holland M M, Kiehl J T, 2012.** Climate sensitivity of the community climate system model, version 4. *Journal of Climate* 25, 3053–3070.
- Brandefelt J, Otto-Bliesner B L, 2009.** Equilibration and variability in a Last Glacial Maximum climate simulation with CCSM3. *Geophysical Research Letters* 36. doi:10.1029/2009GL040364.
- Brandefelt J, Kjellström E, Näslund J-O, Strandberg G, Voelker A H L, Wohlfarth B, 2011.** A coupled climate model simulation of Marine Isotope Stage 3 stadial climate. *Climate of the Past* 7, 649–670.
- Brovkin V, Ganopolski A, Svirezhev Y, 1997.** A continuous climate-vegetation classification for use in climate-biosphere studies. *Ecological Modelling* 101, 251–261.
- Cochelin A-S B, Mysak L A, Wang Z, 2006.** Simulation of long-term future climate changes with the green McGill paleoclimate model: the next glacial inception. *Climatic Change* 79, 381–401.
- Collins W D, Bitz C M, Blackmon M L, Bonan G B, Bretherton C S, Carton J A, Chang P, Doney S C, Hack J J, Henderson T B, Kiehl J T, Large W G, McKenna D S, Santer B S, Smith R D, 2006.** The community climate system model version 3 (CCSM3). *Journal of Climate* 19, 2122–2143.
- Committee on Stabilization Targets for Atmospheric Greenhouse Gas Concentrations, 2011.** *Climate stabilization targets: emissions, concentrations, and impacts over decades to millennia.* Washington, DC: National Academies Press.
- Crucifix M, Rougier J, 2009.** On the use of simple dynamical systems for climate predictions: a Bayesian prediction of the next glacial inception. *The European Physical Journal Special Topics* 174, 11–31.
- Cunningham S A, Kanzow T, Rayner D, Baringer M O, Johns W E, Marotzke J, Longworth H R, Grant E M, Hirschi J J-M, Beal L M, Meinen C S, Bryden H L, 2007.** Temporal variability of the Atlantic meridional overturning circulation at 26.5 degrees N. *Science* 317, 935–938.
- Danabasoglu G, Bates S C, Briegleb B P, Jayne S R, Jochum M, Large W G, Peacock S, Yeager S G, 2012.** The CCSM4 ocean component. *Journal of Climate* 25, 1361–1389.

- Driesschaert E, 2005.** Climate change over the next millennia using LOVECLIM , a new Earth system model including the polar ice sheets. PhD thesis. Université Catholique de Louvain, Louvain-de-Neuve, Belgium.
- Driesschaert E, Fichet T, Goosse H, Huybrechts P, Janssens I, Mouchet A, Munhoven G, Brovkin V, Weber S L, 2007.** Modeling the influence of Greenland ice sheet melting on the Atlantic meridional overturning circulation during the next millennia. *Geophysical Research Letters* 34, L10707. doi: 10.1029/2007GL029516.
- Drysdale R N, Hellstrom J C, Zanchetta G, Fallick A E, Sánchez Goñi M F, Couchoud I, McDonald J, Maas R, Lohmann G, Isola I, 2009.** Evidence for obliquity forcing of glacial termination II. *Science* 325, 1527–1531.
- Eby M, Zickfeld K, Montenegro A, Archer D, Meissner K J, Weaver A J, 2009.** Lifetime of anthropogenic climate change: millennial time scales of potential CO₂ and surface temperature perturbations. *Journal of Climate* 22, 2501–2511.
- Ganopolski A, Calov R, Claussen M, 2010.** Simulation of the last glacial cycle with a coupled climate ice-sheet model of intermediate complexity. *Climate of the Past* 6, 229–244.
- Gent P R, Danabasoglu G, Donner L J, Holland M M, Hunke E C, Jayne S R, Lawrence D M, Neale R B, Rasch P J, Vertenstein M, Worley P H, Yang Z-L, Zhang M, 2011.** The Community Climate System Model Version 4. *Journal of Climate* 24, 4973–4991.
- Goodrich L E, 1978.** Some results of a numerical study of ground thermal regimes. In *Proceedings of the Third International Conference on Permafrost*, Edmonton, Alberta, Canada, 10–13 July 1978. Ottawa: National Research Council of Canada, 30–34.
- Goosse H, Fichet T, 1999.** Importance of ice–ocean interactions for the global ocean circulation: a model study. *Journal of Geophysical Research* 104, 23337–23355.
- Goosse H, Brovkin V, Fichet T, Haarsma R, Huybrechts P, Jongma J, Mouchet A, Selten F, Barriat P-Y, Campin J-M, Deleersnijder E, Driesschaert E, Goelzer H, Janssens I, Loutre M-F, Morales Maqueda M A, Opsteegh T, Mathieu P-P, Munhoven G, Pettersson E J, Renssen H, Roche D M, Schaeffer M, Tartinville B, Timmermann A, Weber S L, 2010.** Description of the Earth system model of intermediate complexity LOVECLIM version 1.2. *Geoscientific Model Development* 3, 603–633.
- Hartikainen J, Kouhia R, Wallroth T, 2010.** Permafrost simulations at Forsmark using a numerical 2D thermo-hydro-chemical model. SKB TR-09-17, Svensk Kärnbränslehantering AB.
- Hunke E C, Lipscomb W H, 2008.** CICE: the Los Alamos sea ice model documentation and software user’s manual, Version 4.0, LA-CC-06-012. Los Alamos, NM: Los Alamos National Laboratory.
- Huybers P, Wunsch C, 2005.** Obliquity pacing of the late Pleistocene glacial terminations. *Nature* 434, 491–494.
- Imbrie J, Imbrie J Z, 1980.** Modeling the climatic response to orbital variations. *Science* 207, 943–953.
- Imbrie J, Berger A, Boyle E, Clemens S, Duffy A, Howard W R, Kukla G, Kutzbach J, Martinson D G, McIntyre A, Mix A C, Molfino B, Morley J J, Peterson L C, Pisias N G, Prell W L, Raymo M E, Shackleton N J, Toggweiler J R, 1993.** On the structure and origin of major glaciation cycles 2. The 100,000-year cycle. *Paleoceanography* 8, 699–735.
- IPCC, 2000.** Summary for policy makers: emissions scenarios. Special report, IPCC Working Group III. Geneva: Intergovernmental Panel on Climate Change.
- IPCC, 2007.** *Climate Change 2007: the physical science basis*. Cambridge: Cambridge University Press.
- Jochum M, Jahn A, Peacock S, Bailey D A, Fasullo J T, Kay J, Levis S, Otto-Bliesner B, 2012.** True to Milankovitch: glacial inception in the new Community Climate System Model. *Journal of Climate* 25, 2226–2239.
- Lambeck K, Esat T M, Potter E-K, 2002.** Links between climate and sea levels for the past three million years. *Nature* 419, 199–206.

- Lawrence D, Oleson K W, Flanner M G, Thornton P E, Swenson S C, Lawrence P J, Zeng X, Yang Z-L, Levis S, Sakaguchi K, Bonan G B, Slater A G, 2011.** Parameterization improvements and functional and structural advances in Version 4 of the Community Land Model. *Journal of Advances in Modeling Earth Systems* 3, M03001. doi:10.1029/2011MS000045.
- Lind P, Kjellström E, 2008.** Temperature and precipitation changes in Sweden: a wide range of model-based projections for the 21st century. Report RMC No. 113, Swedish Meteorological and Hydrological Institute.
- Lisiecki L E, Raymo M E, 2005.** A Pliocene-Pleistocene stack of 57 globally distributed benthic $\delta^{18}\text{O}$ records. *Paleoceanography* 20. doi: 10.1029/2004PA001071.
- Loutre M F, Berger A, 2000.** Future climatic changes: are we entering an exceptionally long interglacial? *Climatic Change* 46, 61–90.
- Lunardini V J, 1978.** Theory of n-factors and correlation of data. In *Proceedings of the Third International Conference on Permafrost*, Edmonton, Alberta, Canada, 10–13 July 1978. Ottawa: National Research Council of Canada, Vol 1, 40–46.
- Lüthi D, Le Floch M, Bereiter B, Blunier T, Barnola J-M, Siegenthaler U, Raynaud D, Jouzel J, Fischer H, Kawamura K, Stocker T F, 2008.** High-resolution carbon dioxide concentration record 650,000–800,000 years before present. *Nature* 453, 379–382.
- Matthews H D, Gillett N P, Stott P A, Zickfeld K, 2009.** The proportionality of global warming to cumulative carbon emissions. *Nature* 459, 829–832.
- Meehl G A, Stocker T F, Collins W D, Friedlingstein P, Gaye A T, Gregory J M, Kitoh A, Knutti R, Murphy J M, Noda A, Raper S C B, Watterson I G, Weaver A J, Zhao Z-C, 2007.** Global climate projections. In Solomon S, Qin D, Manning M, Chen Z, Marquis M, Averyt K B, Tignor M, Miller H L (eds). *Climate Change 2007: The Physical Science Basis. Contribution of Working Group I to the Fourth Assessment Report of the Intergovernmental Panel on Climate Change*. Chapter 10. Cambridge: Cambridge University Press.
- Mikolajewicz U, Gröger M, Maier-Reimer E, Schurgers G, Vizcaíno M, Winguth A M E, 2007.** Long-term effects of anthropogenic CO_2 emissions simulated with a complex earth system model. *Climate Dynamics* 28, 599–633.
- Mitchell T D, Jones P D, 2005.** An improved method of constructing a database of monthly climate observations and associated high-resolution grids. *International Journal of Climatology* 25, 693–712.
- Moss R H, Edmonds J A, Hibbard K A, Manning M R, Rose S K, van Vuuren D P, Carter T R, Emori S, Kainuma M, Kram T, Meehl G A, Mitchell J F B, Nakicenovic N, Riahi K, Smith S J, Stouffer R J, Thomson A M, Weyant J P, Wilbanks T J, 2010.** The next generation of scenarios for climate change research and assessment. *Nature* 463, 747–756.
- Mysak L A, 2008.** Glacial inception: past and future. *Atmosphere–Ocean* 46, 317–341.
- Neale R B, Richter J H, Jochum M, 2008.** The impact of convection on ENSO: from a delayed oscillator to a series of events. *Journal of Climate* 21, 5904–5924.
- Opsteegh B J D, Haarsma R J, Selten F M, Kattenberg A, 1998.** ECBILT: a dynamic alternative to mixed boundary conditions in ocean models. *Tellus A*, 348–367.
- Pausata F S R, Li C, Wettstein J J, Kageyama M, Nisancioglu K H, 2011.** The key role of topography in altering North Atlantic atmospheric circulation during the last glacial period. *Climate of the Past* 7, 1089–1101.
- Peltier W R, Solheim L P, 2004.** The climate of the Earth at Last Glacial Maximum: statistical equilibrium state and a mode of internal variability. *Quaternary Science Reviews* 23, 335–357.
- Pimenoff N, Venäläinen A, Järvinen H, 2011.** Climate scenarios for Olkiluoto on a time-scale of 120,000 years. Posiva 2011-04, Posiva Oy, Finland.
- Racherla P N, Shindell D T, Faluvegi G S, 2012.** The added value to global model projections of climate change by dynamical downscaling: a case study over the continental US using the GISS-ModelE2 and WRF models. *Journal of Geophysical Research* 117, D20118. doi:10.1029/2012JD018091.

- Randall D A, Wood R A and coauthors, 2007.** Climate models and their evaluation. In Solomon S, Qin D, Manning M, Chen Z, Marquis M, Averyt K B, Tignor M, Miller H L (eds). *Climate Change 2007: The Physical Science Basis. Contribution of Working Group I to the Fourth Assessment Report of the Intergovernmental Panel on Climate Change.* Chapter 10. Cambridge: Cambridge University Press, 589–662.
- Roche D M, Dokken T M, Goosse H, Renssen H, Weber S L, 2007.** Climate of the Last Glacial Maximum: sensitivity studies and model-data comparison with the LOVECLIM coupled model. *Climate of the Past* 3, 205–224.
- Schulz M, Prange M, Klocker A, 2007.** Low-frequency oscillations of the Atlantic Ocean meridional overturning circulation in a coupled climate model. *Climate of the Past* 3, 97–107.
- Shackleton N J, 2000.** The 100,000-year ice-age cycle identified and found to lag temperature, carbon dioxide, and orbital eccentricity. *Science* 289, 1897–1902.
- SKB, 2010.** Climate and climate-related issues for the safety assessment SR-Site. SKB TR-10-49, Svensk kärnbränslehantering AB.
- Smith R, Jones P, Briegleb B, Bryan F, Danabasoglu G, Dennis J, Dukowicz J, Eden C, Fox-Kemper B, Gent P, Hecht M, Jayne S, Jochum M, Large W, Lindsay K, Maltrud M, Norton N, Peacock S, Vertenstein M, Yeager S, 2010.** The Parallel Ocean Program (POP) reference manual. LAUR-10-01853, Los Alamos National Laboratory, Los Alamos, NM.
- Smith R S, Gregory J, 2012.** The last glacial cycle: transient simulations with an AOGCM. *Climate Dynamics* 38, 1545–1559.
- Solomon S, Plattner G-K, Knutti R, Friedlingstein P, 2009.** Irreversible climate change due to carbon dioxide emissions. *Proceedings of the National Academy of Sciences of the United States of America* 106, 1704–1709.
- Stevens B, Boucher O, 2012.** Climate science: the aerosol effect. *Nature* 490, 40–41.
- Texier D, Degnan P, Loutre M-F, Paillard D, Thorne M, 2003.** Modelling sequential BIOSphere systems under CLIMate change for radioactive waste disposal. Project BIOCLIM. In *Proceedings of the 10th International High-Level Waste Management Conference, Las Vegas, Nevada, 30 March – 2 April 2003.*
- Tzedakis P C, Channell J E T, Hodell D A, Kleiven H F, Skinner L C, 2012a.** Determining the natural length of the current interglacial. *Nature Geoscience* 5, 1–4.
- Tzedakis P C, Wolff E W, Skinner L C, Brovkin V, Hodell D A, McManus J F, Raynaud D, 2012b.** Can we predict the duration of an interglacial? *Climate of the Past* 8, 1473–1485.
- Waelbroeck C, Labeyrie L, Michel E, Duplessy J C, McManus J F, Lambeck K, Balbon E, Labracherie M, 2002.** Sea-level and deep water temperature changes derived from benthic foraminifera isotopic records. *Quaternary Science Reviews* 21, 295–305.
- Vavrus S, Waliser D, 2008.** An improved parameterization for simulating arctic cloud amount in the CCSM3 climate model. *Journal of Climate* 21, 5673–5687.
- Vavrus S, Philippon-Berthier G, Kutzbach J E, Ruddiman W F, 2011.** The role of GCM resolution in simulating glacial inception. *The Holocene* 21, 819–830.
- Vettoretti G, Peltier W R, 2004.** Sensitivity of glacial inception to orbital and greenhouse gas climate forcing. *Quaternary Science Reviews* 23, 499–519.
- Vettoretti G, Peltier W R, 2011.** The impact of insolation, greenhouse gas forcing and ocean circulation changes on glacial inception. *The Holocene* 21, 803–817.
- Winograd I J, Coplen T B, Landwehr J M, Riggs A C, Ludwig K R, Szabo B J, Kolesar P T, Revesz K M, 1992.** Continuous 500,000-year climate record from vein calcite in Devils Hole, Nevada. *Science* 258, 255–260.
- Zickfeld K, Eby M, Matthews H D, Weaver A J, 2009.** Setting cumulative emissions targets to reduce the risk of dangerous climate change. *Proceedings of the National Academy of Sciences of the United States of America* 106, 16129–16134.
- Zickfeld K, Arora V K, Gillett N P, 2012.** Is the climate response to CO₂ emissions path dependent? *Geophysical Research Letters* 39. doi:10.1029/2011GL050205.

Deliverables and data format for input- and output data stored in data base at SKB

Project: Potential for cold climate conditions and permafrost in Forsmark in the next 60,000 years

Delivered: 20130531

From: Jenny Brandefelt, SKB

To: Jens-Ove Näslund, SKB

This data was delivered within the project Potential for cold climate conditions and permafrost in Forsmark in the next 60,000 years. The project is described in the following report: Brandefelt J, Zhang Q, Hartikainen J, Näslund J-O, 2013. Potential for cold climate conditions and permafrost in Forsmark in the next 60,000 years. SKB TR-13-04, Svensk Kärnbränslehantering AB.

Models

We used the Community Climate System Model version 4 (CCSM4; Gent et al. 2011) and the LOVECLIM 1.2 intermediate complexity model (Goosse et al. 2010). Further a 2D permafrost model was used (Hartikainen et al. 2010).

Climate model simulations

Two sets of simulations were performed.

In the first set, simulations with constant forcing and boundary conditions were performed for the periods around 17 ka AP and 54 ka AP. For each period, a set of seven LOVECLIM simulations and one CCSM4 simulation were performed with atmospheric CO₂ concentration in the range 180–400 ppmv.

In the second set, two simulations with constant atmospheric CO₂ concentration were performed with LOVECLIM. In these simulations the latitudinal and seasonal insolation distribution is varied based on the known future variations in the orbital parameters.

Permafrost model simulations

Two sets of simulations were performed.

In the first set, the new version of the permafrost model, described in Section 2.5 in TR-13-05, was used to simulate permafrost development based on the coldest climate simulated with LOVECLIM.

For comparison to earlier results, the version of the model used in SR-Site and described by Hartikainen et al. (2010), was used. In this second set of simulations the permafrost development based on the coldest climate simulated with LOVECLIM was also determined and compared to the results from the new version of the model.

Time periods

The climate model simulations were run for between 1,500 and 6,000 model years to reach equilibrium and to generate data for analysis of averages and variability. The last 300 model years of the CCSM4 simulations and model years 1,001–3,000 of the LOVECLIM simulations were used in the analysis and as input to the permafrost model.

Climate models

Data needed to reproduce results

The data needed to restart or rerun the CCSM4 and LOVECLIM simulations are saved as NetCDF in directories ccsm4/ and loveclim/.

Resulting data

The monthly and annual average T_{2m} , as well as a long list of atmospheric and surface variables, for the 300 model years (CCSM4) and 2,000 model years (LOVECLIM) are saved at the grid used by each model. These are delivered in NetCDF format.

Time series of monthly mean bias-corrected T_{2m} interpolated to Forsmark is also saved for the complete length of the climate simulations.

Permafrost model

Data needed to reproduce results

The data needed to restart or rerun the permafrost model simulations are saved in XXX format in the directory permafrostmodel/.

Resulting data

Annual average bedrock temperature from the complete length of the permafrost simulations is saved.

Figures

All figures in TR-13-04 are saved as image files (.eps) in figures/. Specific fields, time series etc from CCSM3 and RCA3 used to make the figures are also saved in figure_data/.

Glossary

This appendix contains a glossary of abbreviations used in the report

AMOC	Atlantic Meridional Overturning Circulation.
AOGCM	Atmosphere Ocean General Circulation Model
AP	after present
CCSM4	Community Climate System Model version 4 (http://www.cesm.ucar.edu/).
CMIP3	Climate Model Intercomparison Project 3
CMPI5	Climate Model Intercomparison Project 5
CRU	Climate Research Unit
EMIC	Earth system Model of Intermediate Complexity
ECS	Equilibrium Climate Sensitivity
ESM	Earth System Model
GIA	Glacial Isostatic Adjustment
IPCC	Intergovernmental Panel on Climate Change
ka	1,000 years
NCAR	National Centre for Atmospheric Research
PI	Pre-Industrial
Pg	Peta gram (10^{15} gram)
ppmv/ppbv	Unit for concentration of e.g. gases in air (1 ppm = 1 part per million/billion)
SAT	Surface Air Temperature
SFR	Repository for short-lived nuclear waste in Forsmark, Sweden
SRES	Special Report on Emission Scenarios (by the IPCC)
Sv	Sverdrup (unit for flux of water, 1Sv = 1 km ³ /s)
T _{2m}	Air temperature at 2-meters height